Moment method for polyatomic gases:
from modelling to numerical simulations

Von der Fakultät für Mathematik und Naturwissenschaften der RWTH Aachen University zur Erlangung des akademischen Grades eines Doktors der Naturwissenschaften genehmigte Dissertation

vorgelegt von

Vladimir Đorđić, M.Sc.

aus Uzovnica, Serbia

Berichter: Univ.-Prof. Dr. rer. nat. Manuel Torrilhon
Assoc. Prof. Dr. Milana Pavić-Čolić

Tag der mündlichen Prüfung: 11. December 2025

I hereby declare that I have created this work completely on my own and used no other sources or tools than the ones listed, and that I have marked any citations accordingly.

Hiermit versichere ich, dass ich die vorliegende Arbeit selbständig verfasst und keine anderen als die angegebenen Quellen und Hilfsmittel benutzt sowie Zitate kenntlich gemacht habe.

$Aachen, 19th December 2025$
Vladimir Đorđić

Contents

Abstract

This thesis presents models for polyatomic gases at both mesoscopic and macroscopic levels. At the mesoscopic level, the Boltzmann equation with a polyatomic collision operator is used, and new collision kernels are proposed allowing flexibility to match specific gas properties. At the macroscopic level, moment equations—specifically the 14- and 17-moment systems—are used to model flows in the transition regime. The collision operator is evaluated to obtain transport coefficients, and a data-driven approach is used to fit model parameters to reproduce experimental values for viscosity, bulk-to-shear viscosity ratio, and the Prandtl number.

To validate the models, numerical simulations of heat conduction in polyatomic gases are performed using a finite element method within the FEniCS framework. Regularized version of the 17-moment system with entropy-stable boundary conditions is developed, and its linear, steady-state form is implemented. The simulations demonstrate mesh convergence and reveal that, for small Knudsen numbers, non-equilibrium temperatures converge, consistent with previous results for polyatomic gases. The impact of bulk viscosity is also examined, showing that it primarily affects the dynamical pressure, while the total temperature profile remains stable.

Überblick

In dieser Arbeit werden Modelle für polyatomare Gase sowohl auf mesoskopischer als auch auf makroskopischer Ebene vorgestellt. Auf der mesoskopischen Ebene wird die Boltzmann-Gleichung mit einem polyatomaren Kollisionsoperator verwendet, und es werden neue Kollisionskerne vorgeschlagen, die eine flexible Anpassung an spezifische Gaseigenschaften ermöglichen. Auf der makroskopischen Ebene werden Impulsgleichungen - insbesondere die 14- und 17-Momentensysteme - zur Modellierung von Strömungen im Übergangsbereich verwendet. Der Kollisionsoperator wird ausgewertet, um Transportkoeffizienten zu erhalten, und ein datengesteuerter Ansatz wird zur Anpassung der Modellparameter verwendet, um experimentelle Werte für die Viskosität, das Verhältnis von Schütt- zu Scherviskosität und die Prandtl-Zahl zu reproduzieren.

Zur Validierung der Modelle werden numerische Simulationen der Wärmeleitung in polyatomaren Gasen mit einer Finite-Elemente-Methode im Rahmen von FEniCS durchgeführt. Eine regulierte Version des 17-Momente-Systems mit entropiestabilen Randbedingungen wird entwickelt und seine lineare, stationäre Form wird implementiert. Die Simulationen zeigen die Konvergenz des Netzes und zeigen, dass für kleine Knudsenzahlen die Nicht-Gleichgewichtstemperaturen konvergieren, was mit früheren Ergebnissen für polyatomare Gase übereinstimmt. Die Auswirkungen der Volumenviskosität werden ebenfalls untersucht und es zeigt sich, dass sie in erster Linie den dynamischen Druck beeinflusst, während das Gesamttemperaturprofil stabil bleibt.

Acknowledgements

I would like to express my gratitude to Professor Dr. Manuel Torrilhon for giving me the opportunity to work on this topic. I learned a lot from him during my Ph.D. program, and each time we discussed it, he motivated me to continue working on the topic.

I would also like to thank Dr. Milana Čolić. She introduced me to the topic during my master's studies in Novi Sad. She also supervised me during my Ph.D. studies, which, unfortunately, could not be official due to administrative challenges. Thank you for your help, motivation, and knowledge.

During my Ph.D. studies, I interacted with colleagues from the ACoM Institute and the EDDY group. Thank you all for the discussions, help, support, and time we shared in and outside the office.

Here in Aachen, I also got to meet people at the Serbian Orthodox Church. I am very grateful for that. Thank you for your prayers, encouragement, and help.

I am very grateful to my family for their support and patience while I finished this thesis.

This work has been funded by the Deutsche Forschungsgemeinschaft (DFG, German Research Foundation) - project no. 320021702/GRK2326 - Energy, Entropy, and Dissipative Dynamics (EDDy).

Chapter 1

Introduction

The central idea of kinetic theory is to statistically describe state of a gas. Rather than tracking individual molecules and solving Newton's equations for each one, the kinetic theory introduces the distribution function $f(t, x, v)$, where $t \geq 0$ is time, $x \in \mathbb{R}^3$ is the position vector, and $v \in \mathbb{R}^3$ is the particle velocity. The quantity $f(t, x, v)\,\mathrm{d}x\,\mathrm{d}v$ represents the number of particles within a phase-space volume centered at (x, v) at time t. This concept, developed independently by Ludwig Boltzmann and James Clerk Maxwell, leads to the Boltzmann equation, in which particle collisions are modeled by a collision operator.

This thesis focuses on *polyatomic* gases. Due to their internal molecular structure, an additional internal variable $I \geq 0$ is introduced to represent internal state of a molecule. Here, internal energy is modeled as a continuous variable [8], though discrete models are also available in the literature, such as in [29].

The physical laws during the collision (such as conservation laws of momentum and energy) shape the structure of the Boltzmann collision operator, which was first generalized to polyatomic gases in [8]. Regarding the collision kernel, one of the earliest practical models was the hard-sphere model only in the velocity variable, which yields reasonable predictions for viscosity but fails to capture the correct Prandtl number [30]. Motivated by analytical results on well-posedness for the space homogeneous Boltzmann equation, new collision kernels were proposed in [23]. In this thesis, we adopt this collision kernel and combine it with frozen collisions, which are the collisions that do not change the internal energy [19]. This formulation is referred to as the *initial model*. We also introduce an *extended model* of the collision kernel, designed to enhance flexibility in predicting first-order transport coefficients [21]. Both models include adjustable parameters intended to recover the physical behavior of gases, akin to the role of parameters in the hard-sphere model. These kernels will be employed with Grad's

method to derive moment equations for polyatomic gases.

Grad's method constructs a system of partial differential equations by integrating the distribution function over velocity and microscopic internal energy space [25]. This yields macroscopic quantities such as density, momentum, stress, and heat flux—known as the *moments* of the distribution function. In this work, we consider different moment systems, including the 14-moment and 17-moment models, presented in Chapter 3. The choice of moment set depends on the complexity of the physical phenomena under study; for instance, highly non-equilibrium flows require a greater number of moments for accurate modeling. Furthermore, first-order transport coefficients are computed, and they depend on both the chosen moment system and the collision kernel. Comparison with experimental data, which may be used to determine the model parameters, are carried out in Chapter 4.

In general, the moment method yields a nonlinear system of partial differential equations. For numerical solutions, techniques such as the Discontinuous Galerkin method are often used. However, in this thesis, we focus on a steady-state, linearized, and regularized version of the 17-moment system in a two-dimensional setting, as outlined in Chapter 5. We derive the regularized 17-moment equations and impose boundary conditions based on the Maxwell accommodation model. The resulting system is solved using the finite element method for various geometries and mesh refinements. In particular, we demonstrate second-order convergence toward the analytical solution in a double-disk domain. Finally, we simulate various heat flow scenarios for polyatomic gases, as presented in Chapter 6.

The results contained in this thesis are based on the following articles:

V. Djordjić, M. Pavić-Čolić, and N. Spasojević. Polytropic gas modelling at kinetic and macroscopic levels. *Kinet. Relat. Models*, 14(3):483–522, 2021.

V. Djordjić, M. Pavić-Čolić, and M. Torrilhon. Consistent, Explicit and Accessible Boltzmann Collision Operator for Polyatomic Gases. *Phys. Rev. E*, 104:025309, 2021.

V. Djordjić, G. Oblapenko, M. Pavić-Čolić, and M. Torrilhon. Boltzmann collision operator for polyatomic gases in agreement with experimental data and DSMC method. *Continuum Mech. Thermodyn.*, 35:103–119, 2023.

V. Djordjić, M. Pavić-Čolić, and M. Torrilhon. 14- and 17-moment systems for polytropic gases - comparison regarding transport coefficients. *AIP Conference Proceedings*, 2996(1):040011, 02 2024.

Chapter 2

Boltzmann equation

2.1 Boltzmann equation for monatomic gases

For monatomic gases, the state of a molecule at time $t \geq 0$ is described by its position in space $x \in \mathbb{R}^d$ and its velocity $v \in \mathbb{R}^d$, where d denotes the dimension of the vector space. Let z be the total number of particles in the volume Z. According to Newton's second law, the motion of particle α is governed by

$$\frac{\mathrm{d}x_\alpha}{\mathrm{d}t} = v_\alpha, \quad m\frac{\mathrm{d}v_\alpha}{\mathrm{d}t} = F_\alpha, \quad \alpha = 1, \ldots, z,$$

where F_α is the total force acting on particle α. Under standard atmospheric pressure of 102325 Pa and temperature 273.15 K, one cubic meter contains approximately $z \sim 2.68 \times 10^{25}$ atoms. Solving a system of $2dz$ ordinary differential equations is computationally expensive [14]. Another challenge is specifying initial conditions $x_\alpha(0)$ and $v_\alpha(0)$. To circumvent this, kinetic theory introduces the distribution function $f(t, x, v)$, which statistically describes the gas. For instance, $f(t, x, v)\mathrm{d}v$ represents the number of atoms with velocities in the interval $[v, v + \mathrm{d}v]$ at time t and position x. Integrating over all velocities yields the number density

$$n(t, x) = \int_{\mathbb{R}^d} f(t, x, v)\, \mathrm{d}v.$$

The equation that governs the evolution of the distribution function was introduced by Ludwig Boltzmann[1] in 1872 [12].

[1] Ludwig Boltzmann (1844–1906), Austrian physicist and mathematician

In the absence of collisions, f remains constant along particle trajectories,

$$\frac{\mathrm{d}f}{\mathrm{d}t} = 0. \tag{2.1.1}$$

Since $x = x(t)$ and $v = v(t)$, the total derivative becomes

$$\frac{\mathrm{d}f}{\mathrm{d}t} = \partial_t f + \nabla_x f \cdot \frac{\mathrm{d}x}{\mathrm{d}t} + \nabla_v f \cdot \frac{\mathrm{d}v}{\mathrm{d}t} = 0. \tag{2.1.2}$$

Assuming the system is isolated, external forces vanish ($\frac{\mathrm{d}v}{\mathrm{d}t} = (1/m)F_{\text{ext}} = 0$), and (2.1.2) simplifies to the transport equation

$$\partial_t f + v \cdot \nabla_x f = 0. \tag{2.1.3}$$

The solution to (2.1.3) remains constant along the characteristics $x = vt + C$, yielding

$$\frac{\mathrm{d}x}{\mathrm{d}t} = v, \quad \frac{\mathrm{d}v}{\mathrm{d}t} = 0,$$

which implies $f(t, x, v) = f(0, x - vt, v)$.

To fully capture gas dynamics, interactions—mainly collisions—must be considered. Since collisions affect velocities, they influence the evolution of f and result in introducing the collision operator $Q(f)$ on the right-hand side of (2.1.3)

$$\partial_t f + v \cdot \nabla_x f = Q(f). \tag{2.1.4}$$

Because of a collision, a particle can change its velocity to v, counted as gain of atoms with velocity v; or an atom with velocity v can change its velocity to v' which corresponds to a loss of atoms with velocity v. Following this idea, under certain assumptions, the collision operator can be split into the gain part $Q^+(f)$ and loss part $Q^-(f)$,

$$Q(f) = Q^+(f) + Q^-(f). \tag{2.1.5}$$

Kinetic theory involves several assumptions affecting the collision operator [45]. In this thesis, we assume:

A1 The gas is dilute enough. Typically, if we deal with a three-dimensional gas of z hard spheres of radius r, this would mean

$$zr^3 \ll 1, zr^2 \backsimeq 1.$$

A2 Only binary collisions are considered.

A3 Collisions are localized in time and space.

A4 Collisions are micro-reversible; the reverse process follows the same path.

A5 Molecular chaos: pre-collisional velocities are uncorrelated.

Assumption A3 implies the collision operator acts only on velocity variable,

$$\frac{\mathrm{d}f}{\mathrm{d}t} = Q(f(t,x,\cdot))(v).$$

From A2, the two-particle distribution function $f_2(t,x,v,v_*)$ is introduced, with

$$f_2(t,x,v,v_*) = f(t,x,v)f(t,x,v_*)$$

by A5. Let $p\left((v',v'_*) \to (v,v_*)\right)$ denote the probability that particles with velocities v' and v'_* become v and v_* after collision.

The gain term becomes

$$Q^+(f)(v) = \int_{\mathbb{R}^{3d}} f_2(t,x,v',v'_*)p((v',v'_*) \to (v,v_*))\mathrm{d}v'\mathrm{d}v'_*\mathrm{d}v_*,$$

and the loss term

$$Q^-(f)(v) = \int_{\mathbb{R}^{3d}} f_2(t,x,v,v_*)p((v,v_*) \to (v',v'_*))\mathrm{d}v'\mathrm{d}v'_*\mathrm{d}v_*.$$

By A4 (micro-reversibility), the transition probabilities are equal, yielding

$$Q(f,f)(v) = \int_{\mathbb{R}^{3d}} \left(f'f'_* - ff_*\right) p((v',v'_*) \to (v,v_*))\mathrm{d}v'\mathrm{d}v'_*\mathrm{d}v_*, \tag{2.1.6}$$

with shorthand notation

$$\begin{aligned} f' &:= f(t,x,v'), f'_* := f(t,x,v'_*), \\ f &:= f(t,x,v), f_* := f(t,x,v_*). \end{aligned} \tag{2.1.7}$$

However, not all collisions are admissible. We assume that the collision conserves momentum and energy of the colliding particles,

$$mv' + mv'_* = mv + mv_*, \tag{2.1.8}$$

$$\frac{m}{2}|v'|^2 + \frac{m}{2}|v'_*|^2 = \frac{m}{2}|v|^2 + \frac{m}{2}|v_*|^2. \tag{2.1.9}$$

Thus, the transition probability function becomes

$$p((v',v'_*) \to (v,v_*)) = B(v,v_*,v',v'_*) \cdot \delta_{\{mv'+mv'_*=mv+mv_*\}} \cdot \delta_{\left\{\frac{m}{2}|v'|^2+\frac{m}{2}|v'_*|^2=\frac{m}{2}|v|^2+\frac{m}{2}|v_*|^2\right\}},$$

where δ_z is the Kronecker delta

$$\delta_z = \begin{cases} 1 & \text{if } z \text{ is true,} \\ 0 & \text{if } z \text{ is false,} \end{cases} \tag{2.1.10}$$

and $B(v, v_*, v', v'_*)$ is the non-negative collision kernel.

To simplify the domain of integration, express pre-collision velocities in terms of post-collision ones. Define the center-of-mass and relative velocities

$$V := \frac{v + v_*}{2}, \quad u := v - v_*, \tag{2.1.11}$$

$$V' := \frac{v' + v'_*}{2}, \quad u' := v' - v'_*. \tag{2.1.12}$$

Then,

$$v' = V' + \frac{u'}{2}, \quad v'_* = V' - \frac{u'}{2}. \tag{2.1.13}$$

Using conservation laws (2.1.8) and (2.1.9)

$$V = V', \quad |u| = |u'|. \tag{2.1.14}$$

Thus, V is unchanged and u' lies on a sphere of radius $|u|$. In 2D, this is illustrated in Figure 2.1. Introduce a unit vector $\sigma \in S^{d-1}$ to parametrize u' as $u' = |u|\sigma$. Thus,

$$\begin{aligned} v' &= \frac{v + v_*}{2} + \frac{1}{2}|v - v_*|\sigma, \\ v'_* &= \frac{v + v_*}{2} - \frac{1}{2}|v - v_*|\sigma. \end{aligned} \tag{2.1.15}$$

The collision operator now reads

$$\begin{aligned} Q(f, f)(v) = \int_{\mathbb{R}^d \times \mathbb{S}^{d-1}} &\left[f(t, x, v') f(t, x, v'_*) - f(t, x, v) f(t, x, v_*) \right] \\ &\times B\left(|v - v_*|, \frac{v - v_*}{|v - v_*|} \cdot \sigma \right) \mathrm{d}\sigma \mathrm{d}v_*. \end{aligned} \tag{2.1.16}$$

Here, Galilean invariance implies that the collision kernel depends on the relative speed and the angle between u and u'.

2.2 Boltzmann equation for polyatomic gases

2.2.1 Specific challenges in polyatomic gas modelling

A polyatomic molecule possesses an internal structure that allows it to move with more degrees of freedom. Compared to the monatomic case, where all of the atom's energy is

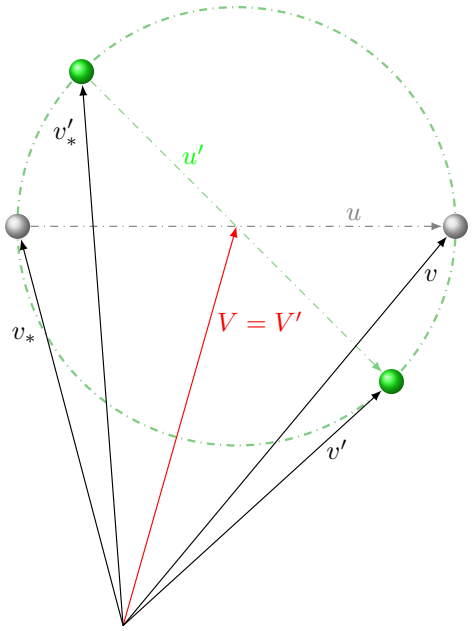

Figure 2.1: The magnitude of the relative velocity and the center-of-mass velocity remain unchanged during a collision, i.e., $|u| = |u'|$ and $V = V'$.

stored in translational motion, a polyatomic molecule exhibit additional rotational and vibrational degrees of freedom. The rotational degrees of freedom correspond to the molecule's ability to rotate around axes perpendicular to the direction of the molecular bond. The vibrational degrees of freedom, on the other hand, represent oscillations along the direction of the molecular bond.

Both types of motion contribute to the macroscopic internal energy $e(T)$, which is generally a nonlinear function of temperature. The internal energy e is related to the specific heat capacity at constant volume c_v by

$$\frac{\mathrm{d}e(T)}{\mathrm{d}T} = c_v(T), \tag{2.2.1}$$

expressed in units of $\mathrm{kg} \cdot \mathrm{J/K}$.

A polyatomic gas with constant c_v is called a polytropic or calorically perfect gas. In that case,

$$e(T) = c_v T, \tag{2.2.2}$$

with the normalization $e(T_0) = 0$ [27].

Here, values of c_v will be extracted from experimental data provided by the National Institute of Standards and Technology [1]. In general, however, the assumption of con-

stant c_v is not valid for polyatomic gases [1]. Nevertheless, there exist temperature intervals in which the experimental values of c_v remain approximately constant [32].

Alternatively, the constant value of c_v can be expressed in terms of the number of additional degrees of freedom $\delta > 0$

$$c_v = \frac{3+\delta}{2}\frac{k}{m}, \tag{2.2.3}$$

where k is Boltzmann's constant and m is the mass of a molecule. Note that δ is not necessarily an integer. Then, δ can be inferred from experimental values of c_v as

$$\delta = 2\frac{m}{k}c_v - 3, \tag{2.2.4}$$

applicable within temperature ranges where c_v is approximately constant, for instance if its relative change is below 5% over a significant temperature range that starts with the room temperature of 300K [21].

Incorporating the nonlinear behavior of c_v (2.2.2) presents a specific challenge for modelling.

One way to resolve it is to introduce an additional continuous variable to account for the internal energy arising from rotational and vibrational degrees of freedom [8, 15]. This variable is referred to as the microscopic internal energy $I \geq 0$. The state of a molecule is then described by its velocity v and internal energy I. The internal energy I becomes an independent variable in the distribution function $f(t, x, v, I)$, where $f(t, x, v, I)\,\mathrm{d}v\,\mathrm{d}I\,\mathrm{d}x$ represents the number of molecules in the phase-space volume element $\mathrm{d}x\,\mathrm{d}v\,\mathrm{d}I$, centered at the point (x, v, I) at time $t \geq 0$.

The evolution of the distribution function f is governed by the Boltzmann equation

$$\partial_t f + v \cdot \nabla_x f = Q(f, f)(v, I), \tag{2.2.5}$$

where $Q(f, f)(v, I)$ is the collision operator for polyatomic gases.

In what follows, we present the polyatomic collision operator in the continuous internal energy framework using the Borgnakke-Larsen procedure.

2.2.2 Microscopic dynamics of polyatomic gases

As in the monatomic case, collisions and their parametrization play a crucial role in the structure of the collision operator. Let us consider the collision of two polyatomic molecules of mass m, having the states (v', I') and (v'_*, I'_*) before the collision. After the

collision, their states become (v, I) and (v_*, I_*), respectively. We consider collisions in which both momentum and total energy E are conserved

$$mv+mv_* = mv'+mv'_*, \qquad \frac{m}{2}|v|^2+I+\frac{m}{2}|v_*|^2+I_* = \frac{m}{2}|v'|^2+I'+\frac{m}{2}|v'_*|^2+I'_*. \quad (2.2.6)$$

Introducing the center-of-mass velocity $V = \frac{v+v_*}{2}$ and relative velocity $u = v - v_*$, the conservation laws (2.2.6) become

$$V = V', \quad E = \frac{m}{4}|u|^2 + I + I_* = \frac{m}{4}|u'|^2 + I' + I'_*. \quad (2.2.7)$$

Similar to the monatomic case, the center-of-mass velocity is conserved. However, the magnitude of the relative velocity is not. The objective is to express the pre-collisional states (v', I'), (v'_*, I'_*) in terms of the post-collisional variables (v, I), (v_*, I_*). Since we need to determine $2d+2$ variables in $d+1$ equations, $d+1$ parameters are introduced. The direction of the post-collisional relative velocity is represented by $\sigma \in S^{d-1}$. The remaining two parameters are introduced through the Borgnakke-Larsen procedure [7], which involves two scalars $R, r \in [0, 1]$ such that

$$\frac{m}{4}|u'|^2 = RE, \quad I' + I'_* = (1-R)E, \quad I' = r(1-R)E, \quad I'_* = (1-r)(1-R)E. \quad (2.2.8)$$

In other words, total energy E is split into a kinetic part RE, and an internal part $(1-R)E$, which is then further divided between the two molecules using the variable r.

From (2.2.8), we obtain

$$|u'| = 2\sqrt{\frac{RE}{m}}, \quad (2.2.9)$$

which, together with (2.1.13), yields

$$v' = \frac{v+v_*}{2}+\sqrt{\frac{RE}{m}}\,\sigma, \quad v'_* = \frac{v+v_*}{2}-\sqrt{\frac{RE}{m}}\,\sigma, \quad I' = r(1-R)E, \quad I'_* = (1-r)(1-R)E. \quad (2.2.10)$$

2.2.3 Collision operator for polyatomic gases

In this section, we present the Boltzmann collision operator for polyatomic gases in the non-weighted setting [8].

For polyatomic gases, the collision operator has the following form, for $d = 3$,

$$Q(f,f)(v,I) = \int_{[0,1]^2\times S^2\times[0,\infty)\times\mathbb{R}^3} \left(f'f'_* \left(\frac{II_*}{I'I'_*}\right)^{\delta/2-1} - ff_* \right) \times \mathcal{B}H_\delta(r,R)\,\mathrm{d}R\,\mathrm{d}r\,\mathrm{d}\sigma\,\mathrm{d}I_*\,\mathrm{d}v_*, \quad (2.2.11)$$

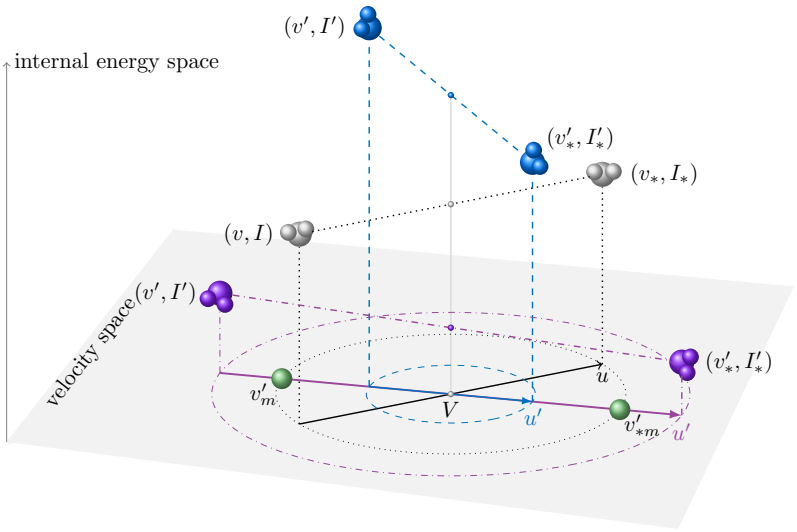

Figure 2.2: Illustration of different post-collisional scenarios. First, the post-collisional states (v, I) and (v_*, I_*) are fixed (in gray). Then the parameters σ, R, and r are selected. For the blue molecules, $R = 0.1$, indicating more energy transferred into internal modes. For the purple ones, $R = 0.8$, implying that more kinetic energy is retained. Figure from [23].

with standard notation, $f' = f(t, x, v', I')$, $f'_* = f(t, x, v'_*, I'_*)$, and $f_* = f(t, x, v_*, I_*)$. Note that the pre-collisional values are given by (2.2.10).

The function

$$H_\delta(r, R) = (r(1-r))^{\delta/2-1} (1-R)^{\delta-1} \sqrt{R}, \tag{2.2.12}$$

ensures the correct weak form of the collision operator, as discussed in the next section. It contains the Jacobian of the transformation from the pre-collisional to the post-collisional quantities.

The parameter $\delta > 0$ ensures the correct caloric equation of state, given by the relation (2.2.3). Therefore, the distribution function is renormalized with the factor $I^{\delta/2-1}$.

The function $\mathcal{B} \geq 0$ is the collision kernel that satisfies

$$\begin{aligned} \mathcal{B} := \mathcal{B}(v, v_*, I, I_*, R, r, \sigma) &= \mathcal{B}(v', v'_*, I', I'_*, R', r', \sigma') \\ &= \mathcal{B}(v_*, v, I_*, I, R, 1-r, -\sigma). \end{aligned} \tag{2.2.13}$$

2.2.4 Properties of the collision operator

The goal of this section is to explore the properties of the polyatomic collision operator (2.2.11).

Lemma 2.2.1. *For any $\delta > 0$, the following measure*

$$\mathrm{d}A = \mathcal{B}H_\delta(r,R) I^{\delta/2-1} I_*^{\delta/2-1} \,\mathrm{d}R\,\mathrm{d}r\,\mathrm{d}\sigma\,\mathrm{d}I_*\,\mathrm{d}v_*\,\mathrm{d}I\,\mathrm{d}v \tag{2.2.14}$$

is invariant with respect to the changes

$$(v, v_*, I, I_*, R, r, \sigma) \leftrightarrow (v', v_*', I', I_*', R', r', \sigma'), \tag{2.2.15}$$

$$(v, v_*, I, I_*, R, r, \sigma) \leftrightarrow (v_*, v, I_*, I, R, 1-r, -\sigma). \tag{2.2.16}$$

Lemma 2.2.2 (The weak form of the collision operator $Q(f,f)$)**.** *For any test function $\chi(v,I)$ that makes the following expressions meaningful, the collision operator* (2.2.11) *takes the following weak form*

$$\begin{aligned}\int_{\mathbb{R}^3\times[0,\infty)} & Q(f,f)(v,I)\,\chi(v,I)\,\mathrm{d}I\,\mathrm{d}v \\ &= \frac{1}{2}\int_{\mathbb{R}^6\times[0,\infty)^2\times[0,1]^2\times S^2} f f_* \left(\chi(v',I') + \chi(v_*',I_*') - \chi(v,I) - \chi(v_*,I_*)\right) \\ &\qquad\qquad \times \mathcal{B}H_\delta(r,R)\,\mathrm{d}R\,\mathrm{d}r\,\mathrm{d}\sigma\,\mathrm{d}I_*\,\mathrm{d}v_*\,\mathrm{d}I\,\mathrm{d}v. \end{aligned} \tag{2.2.17}$$

Proof. After integration of the collision operator (2.2.11) against a test function $\chi(v,I)$ with respect to v and I variables, one performs changes of variables (2.2.15) and (2.2.16). Using invariance properties of the measure $\mathrm{d}A$ (2.2.14) stated in Lemma 2.2.1, results in

$$\begin{aligned}&\int_{\mathbb{R}^3\times[0,\infty)} Q(f,f)(v,I)\chi(v,I)\mathrm{d}I\,\mathrm{d}v \\ &= \int_{\mathbb{R}^6\times[0,\infty)^2\times[0,1]^2\times S^2} \frac{f f_*}{(I I_*)^{\delta/2-1}} \left(\chi(v',I') - \chi(v,I)\right)\mathrm{d}A \\ &= \int_{\mathbb{R}^6\times[0,\infty)^2\times[0,1]^2\times S^2} \frac{f f_*}{(I I_*)^{\delta/2-1}} \left(\chi(v_*',I_*') - \chi(v_*,I_*)\right)\mathrm{d}A,\end{aligned} \tag{2.2.18}$$

which yields the desired estimate (2.2.17). □

As a consequence of the previous lemma, for some test function $\chi(v,I)$, the weak form of the collision operator may vanish. Such functions are called collision invariants. From the collision laws (2.2.10), it follows that choosing $\chi(v,I)$ as m, mv, or $m\frac{|v|^2}{2} + I$

leads to a vanishing weak form. Moreover, any linear combination of the following functions is also a collision invariant [30],

$$\begin{pmatrix} m \\ mv \\ \frac{m}{2}|v|^2 + I \end{pmatrix}.$$

Our next goal is to formulate the H-theorem for the collision operator (2.2.11). To that end, we first define the entropy production,

$$D(f) = \int_{\mathbb{R}^3 \times [0,\infty)} Q(f,f)(v,I) \log(f(v,I) I^{-\delta/2+1}) \, \mathrm{d}I \mathrm{d}v, \tag{2.2.19}$$

and then study its properties in the following theorem.

Theorem 2.2.1 (H-theorem)**.** *Let the collision kernel $\mathcal{B}$ be positive almost everywhere, and let $f \geq 0$ be such that the collision operator $Q(f,f)$ and the entropy production $D(f)$ are well defined. Then the following properties hold,*

i. Entropy production is non-positive, that is

$$D(f) \leq 0. \tag{2.2.20}$$

ii. The three following properties are equivalent

(1) $D(f) = 0$,

(2) $Q(f,f) = 0$ *for all* $v \in \mathbb{R}^3,\ I \in [0,\infty)$,

(3) There exists $n \geq 0$, $U \in \mathbb{R}^3$, *and* $T > 0$, *such that*

$$f_E(v,I) = \frac{n}{Z(T)} \left(\frac{m}{2\pi k T}\right)^{\frac{3}{2}} I^{\delta/2-1} \, e^{-\frac{1}{kT}\left(\frac{m}{2}|v-U|^2 + I\right)}, \tag{2.2.21}$$

where $Z(T)$ is a partition (normalization) function

$$Z(T) = \int_{[0,\infty)} I^{\delta/2-1} e^{-\frac{I}{kT}} \mathrm{d}I = (kT)^{\delta/2} \Gamma(\delta/2),$$

with Γ representing the Gamma function.

The proof is given in [8]. The H-Theorem is equivalent to the second law of thermodynamics and implies that the gas attains a state of maximum entropy, corresponding to the Maxwellian equilibrium distribution function (2.2.21).

2.2.5 Frozen collision operator

Frozen collisions are collisions in which the two colliding molecules exchange only their kinetic energy, meaning that $I = I'$ and $I_* = I'_*$. This implies that $|u| = |u'|$, and therefore, the Borgnakke-Larsen procedure is not needed. Instead, a standard parametrization is used, as in the monatomic case (2.1.15),

$$v' = V + \frac{|u|}{2}\sigma, \quad v'_* = V - \frac{|u|}{2}\sigma. \tag{2.2.22}$$

With this, the resulting frozen collision operator takes the form [19, 4]

$$Q^{(\text{frozen})}(f,f)(v,I) = \int_{\mathbb{R}^3\times[0,\infty)\times S^2} \left(f'f'_*\big|_{\substack{I'=I \\ I'_*=I_*}} - ff_* \right) \overline{B}\,\mathrm{d}\sigma\,\mathrm{d}v_*\,\mathrm{d}I_*, \tag{2.2.23}$$

where $\overline{B} := \overline{B}(v, v_*, I, I_*, \sigma)$ is the collision kernel for frozen collisions, which satisfies monatomic-like micro-reversibility, i.e. $\overline{B}(v, v_*, I, I_*, \sigma) = \overline{B}(v', v'_*, I, I_*, \sigma') = \overline{B}(v_*, v, I_*, I, -\sigma)$.

Moreover, the case of frozen collisions is equivalent to $R = R'$ and $r' = r$, so the frozen collision operator can be seen as a classical non-frozen operator (2.2.11) with a Dirac delta measure $\delta_{R=R'}\delta_{r=r'}$ and scaled with H_δ.

In the further analysis, we will combine the frozen collision operator (2.2.23) and the non-frozen one (2.2.11),

$$Q(f,f) = \omega Q(f,f)^{(\text{non frozen})} + (1-\omega)Q^{(\text{frozen})}(f,f), \tag{2.2.24}$$

which is a convex combination with parameter $0 \le \omega \le 1$.

Chapter 3

Moment method

Moment method is an approximation technique to solve the Boltzmann equation. Moments are quantities that are reproduced from the distribution function $f(t, x, v, I)$ by multiplying it with different test functions and integrating over the phase space (v, I). Taking a general polynomial, we define the convective moment as

$$u^{(a,b)}_{i_1 i_2 \ldots i_n} = \int_{\mathbb{R}^3 \times [0,\infty)} |v|^{2a} I^b v_{i_1} v_{i_2} .. v_{i_n} f \mathrm{d}v \mathrm{d}I, \tag{3.0.1}$$

where a and b are integers and $i_1, i_2 .... i_n \in \{1, 2, 3\}$.

Similarly, non-convective moments are defined as

$$\rho^{(a,b)}_{i_1 i_2 \ldots i_n} = \int_{\mathbb{R}^3 \times [0,\infty)} |c|^{2a} I^b c_{i_1} c_{i_2} .. c_{i_n} f \mathrm{d}c \mathrm{d}I \tag{3.0.2}$$

where $c = v - U$ is the peculiar velocity with respect to the macroscopic gas velocity U.

After multiplying the Boltzmann equation with the test function $m|v|^{2a} I^b v_{i_1} v_{i_2} .. v_{i_n}$ and integrating with respect to v and I, one gets

$$\begin{aligned} \partial_t \int_{\mathbb{R}^3 \times [0,\infty)} m|v|^{2a} I^b v_{i_1} v_{i_2} .. v_{i_n} f \mathrm{d}v \mathrm{d}I + \partial_{x_i} \int_{\mathbb{R}^3 \times [0,\infty)} m|v|^{2a} I^b v_{i_1} v_{i_2} .. v_{i_n} v_i f \mathrm{d}v \mathrm{d}I \\ = \int_{\mathbb{R}^3 \times [0,\infty)} Q(f,f) m|v|^{2a} I^b v_{i_1} v_{i_2} .. v_{i_n} f \mathrm{d}v \mathrm{d}I, \end{aligned} \tag{3.0.3}$$

that can be rewritten as the transition equation

$$\partial_t u^{(a,b)}_{i_1 i_2 \ldots i_n} + \partial_{x_i} u^{(a,b)}_{i_1 i_2 \ldots i_n i} = P^{(a,b)}_{i_1 i_2 \ldots i_n}. \tag{3.0.4}$$

Here, $P^{(a,b)}_{i_1 i_2 \dots i_n}$ denotes the production terms, which are computed using the test function $m|v|^{2a} I^b v_{i_1} v_{i_2} \dots v_{i_n}$ in the weak form of the collision operator $Q(f, f)$. These production terms vanish when the test function is a linear combination of the collision invariants. In all other cases, additional calculations are required.

By choosing a specific set of test functions, one can derive a hierarchy of moment equations. If this set does not include an equation for the evolution of the flux $u^{(a,b,c)}_{i_1 i_2 \dots i_n i}$, then the system is not closed. To close the moment system, higher-order fluxes must be expressed as functions of lower-order moments, such as $u^{(a,b)}_{i_1 i_2 \dots i_n}$. This closure is typically achieved by integrating an explicit form of the distribution function.

An important practical question arises: which moments should be selected and used? As we will see, this choice often depends on the specific problem under consideration.

In general, moment equations are inherently nonlinear. This nonlinearity can be understood by examining the physical meaning of the moments themselves.

3.1 Moments in kinetic theory

In contrast to microscopic quantities or the distribution function—which cannot be measured directly—macroscopic (physical) quantities are often accessible through experiments. These macroscopic quantities are obtained as moments of the distribution function, as detailed in this section.

Using convective or non-convective moments, physical quantities are defined as follows. The density ρ is defined as

$$u^{(0,0)} = \rho = \int_{\mathbb{R}^3 \times [0,\infty)} m f \mathrm{d}v \mathrm{d}I. \tag{3.1.1}$$

For the test function mv_i, one gets momentum of the gas ρU_i

$$u^{(0,0)}_i = \rho U_i = \int_{\mathbb{R}^3 \times [0,\infty)} m v_i f \mathrm{d}v \mathrm{d}I. \tag{3.1.2}$$

Considering the peculiar velocity $c = v - U$, from the definition of density ρ and momentum ρU_i, the non-convective moment is

$$\rho^{(0,0)}_i = \int_{\mathbb{R}^3 \times [0,\infty)} m c_i f \mathrm{d}v \mathrm{d}I = \int_{\mathbb{R}^3 \times [0,\infty)} m(v_i - U_i) f \mathrm{d}v \mathrm{d}I = 0. \tag{3.1.3}$$

Taking $v_i v_j$ as the test function,

$$u_{ij}^{(0,0)} = \int_{\mathbb{R}^3\times[0,\infty)} m v_i v_j f \mathrm{d}v\mathrm{d}I = \int_{\mathbb{R}^3\times[0,\infty)} m(c_i+U_i)(c_j+U_j) f \mathrm{d}v\mathrm{d}I \tag{3.1.4}$$

$$= \int_{\mathbb{R}^3\times[0,\infty)} m c_i c_j f \mathrm{d}v\mathrm{d}I + \rho U_i U_j. \tag{3.1.5}$$

The stress tensor p_{ij} is defined by

$$p_{ij} = \rho_{ij}^{(0,0)} = \int_{\mathbb{R}^3\times[0,\infty)} m c_i c_j f \mathrm{d}v\mathrm{d}I. \tag{3.1.6}$$

The stress tensor can be split into its trace-free part σ_{ij} and its trace $\mathscr{P}$ that is also called the non-equilibrium pressure,

$$p_{ij} = \sigma_{ij} + \delta_{ij}\mathscr{P}, \tag{3.1.7}$$

with

$$\sigma_{ij} = \int_{\mathbb{R}^3\times[0,\infty)} m c_{\langle i} c_{j\rangle} f \mathrm{d}c\mathrm{d}I, \quad \mathscr{P} = \frac{1}{3}\int_{\mathbb{R}^3\times[0,\infty)} m|c|^2 f \mathrm{d}c\mathrm{d}I. \tag{3.1.8}$$

Here the index notation with the Einstein convention is used and the trace free part of 2nd order tensor A_{ij} is

$$A_{\langle ij\rangle} = \frac{1}{2}(A_{ij}+A_{ji}) - \frac{1}{3}\delta_{ij}A_{ll}, \tag{3.1.9}$$

The non-equilibrium pressure $\mathscr{P}$ can be further split into hydrodynamical pressure p and dynamical pressure Π

$$\mathscr{P} = p + \Pi. \tag{3.1.10}$$

The flux of stress tensor is calculated from

$$u_{ijk}^{(0,0)} = \int_{\mathbb{R}^3\times[0,\infty)} m v_i v_j v_k \mathrm{d}v\mathrm{d}I = \rho U_i U_j U_k + p_{ijk} + 3U_{(i}p_{jl)}, \tag{3.1.11}$$

where

$$\rho_{ijk}^{(0,0)} = p_{ijk} = \int_{\mathbb{R}^3\times[0,\infty)} m c_i c_j c_k \mathrm{d}v\mathrm{d}I, \tag{3.1.12}$$

and the following notation is used,

$$A_{(ijk)} = \frac{1}{3}(A_{ij}+A_{jk}+A_{ik}).$$

The total energy is obtained by

$$\frac{1}{2}\rho^{(1,0)} + \frac{1}{m}\rho^{(0,1)} = \int_{\mathbb{R}^3\times[0,\infty)} \left(\frac{m}{2}|v|^2 + I\right) f \mathrm{d}v\mathrm{d}I = \int_{\mathbb{R}^3\times[0,\infty)} \left(\frac{m}{2}|c+U|^2 + I\right) f \mathrm{d}v\mathrm{d}I$$

$$= \int_{\mathbb{R}^3\times[0,\infty)} \left(\frac{m}{2}|c|^2 + I\right) f \mathrm{d}v\mathrm{d}I + \frac{1}{2}\rho|U|^2,$$

where the internal energy of gas is

$$\rho e = \int_{\mathbb{R}^3\times[0,\infty)} \left(\frac{m}{2}|c|^2 + I\right) f \mathrm{d}c\mathrm{d}I = \frac{3+\delta}{2}\rho\frac{k}{m}T. \tag{3.1.13}$$

The internal energy of the gas can be further split into two parts

$$\rho e_K = \int_{\mathbb{R}^3\times[0,\infty)} \frac{m}{2}|c|^2 f \mathrm{d}c\mathrm{d}I = \frac{3}{2}\rho\frac{k}{m}T_{tr}, \quad \rho e_I = \int_{\mathbb{R}^3\times[0,\infty)} I f \mathrm{d}c\mathrm{d}I = \frac{\delta}{2}\rho\frac{k}{m}T_{int}. \tag{3.1.14}$$

On this way, the two non-equilibrium temperatures θ_{tr} and θ_{int} are defined with the total temperature θ,

$$\theta_{tr} = \frac{k}{m}T_{tr}, \quad \theta_{int} = \frac{k}{m}T_{int}, \quad \theta = \frac{k}{m}T, \quad \frac{3}{2}\theta_{tr} + \frac{\delta}{2}\theta_{int} = \frac{3+\delta}{2}\theta. \tag{3.1.15}$$

They relate to the dynamical pressure as follows

$$\Pi = \rho(\theta_{tr} - \theta) = \frac{\delta}{3}\rho(\theta - \theta_{int}) = -\frac{\delta}{\delta+3}\rho(\theta_{int} - \theta_{tr}).$$

Now it is clear that, in the equilibrium, dynamical pressure vanishes and the two non-equilibrium temperatures coincide.

The energy flux is defined by

$$\int_{\mathbb{R}^3\times[0,\infty)} \left(\frac{m}{2}|v|^2 + I\right) v_i f \mathrm{d}v\mathrm{d}I = \int_{\mathbb{R}^3\times[0,\infty)} \left(\frac{m}{2}|c+U|^2 + I\right)(c_i + U_i) f \mathrm{d}v\mathrm{d}I \tag{3.1.16}$$

$$= \int_{\mathbb{R}^3\times[0,\infty)} \left(\frac{m}{2}|c|^2 + I\right) c_i f \mathrm{d}c\mathrm{d}I + \left(\frac{1}{2}\rho|U|^2 + \rho e\right) U_i + U_j p_{ij}, \tag{3.1.17}$$

where total internal energy flux $q^{(tot)}$ is

$$q_i^{(tot)} = \int_{\mathbb{R}^3\times[0,\infty)} \left(\frac{m}{2}|c|^2 + I\right) c_i f \mathrm{d}c\mathrm{d}I. \tag{3.1.18}$$

We can split the total heat flux on the translational part q and the internal part s

$$q_i = \int_{\mathbb{R}^3\times[0,\infty)} \frac{m}{2}|c|^2 c_i f \mathrm{d}c\mathrm{d}I, \quad s_i = \int_{\mathbb{R}^3\times[0,\infty)} I c_i f \mathrm{d}c\mathrm{d}I. \tag{3.1.19}$$

In this thesis, we will also need higher order fluxes defined by

$$\frac{1}{2}u_{ik}^{(1,0)} = \int_{\mathbb{R}^3\times[0,\infty]} \frac{m}{2}|v|^2 v_i v_k \mathrm{d}v\mathrm{d}I = \int_{\mathbb{R}^3\times[0,\infty)} \frac{m}{2}|c+U|^2 (c_i + U_i)(c_k + U_k) \mathrm{d}v\mathrm{d}I. \tag{3.1.20}$$

Since

$$\frac{m}{2}|c+U|^2(c_i+U_i)(c_k+U_k) = \frac{m}{2}|c|^2c_ic_k + mc_ic_jc_kU_j + \frac{m}{2}|U|^2c_ic_k$$
$$+\frac{m}{2}|c|^2v_ic_k + mc_jU_iU_jc_k + \frac{m}{2}|U|^2U_ic_k + \frac{m}{2}|c+U|^2(c_i+U_i)U_k,$$

and flux of the translational heat flux is defined

$$q_{ik} = \int_{\mathbb{R}^3\times[0,\infty)} \frac{m}{2}|c|^2c_ic_kf\mathrm{d}c\mathrm{d}v,$$

flux $u_{ik}^{(1,0)}$ can be expressed as

$$\frac{1}{2}u_{ik}^{(1,0)} = q_{ik} + U_jp_{ijk} + \frac{1}{2}|U|^2p_{ik} + q_kU_i + p_{jk}U_iU_k + q_iU_k + p_{ij}U_jU_k \tag{3.1.21}$$
$$+\left(\frac{\rho}{2}|U|^2 + \rho e_K\right)U_iU_k. \tag{3.1.22}$$

In similar way, flux of the internal heat flux is defined as

$$\frac{1}{m}u_{ik}^{(0,1)} = \int_{\mathbb{R}^3\times[0,\infty)} I(c_i+U_i)(c_k+U_k)\mathrm{d}v\mathrm{d}I = s_{ik} + s_iU_k + s_kU_i + \rho e_IU_iU_k, \tag{3.1.23}$$

where the non-convective flux is

$$\frac{1}{m}\rho_{ik}^{(0,1)} = s_{ik} = \int_{\mathbb{R}^3\times[0,\infty)} Ic_ic_k\mathrm{d}c\mathrm{d}I. \tag{3.1.24}$$

In the sequel, we study evolution of the moments presented in this section.

3.2 Conservation laws

Conservation laws of Euler represent system of 5 moments . Namely, $u^{(0,0)}, u_i^{(0,0)}$ and $u^{(1,0)} + u^{(0,1)}$ are studied. Using classical physical variables, the system has the form

$$\partial_t\rho + \partial_{x_i}\rho U_i = 0, \tag{3.2.1}$$
$$\partial_t\rho U_i + \partial_{x_j}\left(\rho U_iU_j + p_{ij}\right) = 0, \tag{3.2.2}$$
$$\partial_t\left(\frac{1}{2}\rho|U|^2 + \rho e\right) + \partial_{x_j}\left(\left(\frac{1}{2}\rho|U|^2 + \rho e\right)U_j + U_ip_{ij} + q_j^{(tot)}\right) = 0, \tag{3.2.3}$$

that represents the conservation of density, momentum and total energy. However, the system above is not closed because fluxes p_{ij} and $q_i^{(tot)}$ are not determined as functions of densities. One possible way to close this system is to use the maximum entropy

method. The maximum entropy method searches for the distribution function which maximizes the entropy h, defined as

$$h = -k \int_{\mathbb{R}^3 \times [0,\infty)} \log \left(f I^{-\delta/2+1} \right) \mathrm{d}v \mathrm{d}I, \tag{3.2.4}$$

and also simultaneously reconstructs 5-moment densities

$$\begin{pmatrix} \rho \\ 0_i \\ \frac{3+\delta}{2} \rho \frac{k}{m} T \end{pmatrix} = \int_{\mathbb{R}^3 \times [0,\infty)} \begin{pmatrix} m \\ m c_i \\ \frac{m}{2} |c|^2 + I \end{pmatrix} f(t,x,c,I) \mathrm{d}I \mathrm{d}c. \tag{3.2.5}$$

In fact, the function that maximizes the entropy with 5-moment constraints is the local Maxwell distribution.

Lemma 3.2.1 (Maximum entropy distribution)**.** *The distribution function that maximizes the entropy h defined with* (3.2.4) *such that conditions* (3.2.5) *are satisfied has the form*

$$f_E(v,I) = \frac{\rho}{m(kT)^{\delta/2}\Gamma(\delta/2)} \left(\frac{m}{2\pi k T} \right)^{\frac{3}{2}} I^{\delta/2-1} \, e^{-\frac{1}{kT}\left(\frac{m}{2}|v-U|^2 + I\right)}, \tag{3.2.6}$$

where U is the macroscopic velocity.

Proof. The classical procedure of the maximum entropy principle is as follows. Namely, first the Lagrange multipliers $\lambda^{(0)}$, $\lambda_i^{(1)}$, and $\mu^{(0)}$ are introduced, corresponding to the constraints (3.2.5). Then, the extended functional reads

$$\begin{aligned} \mathcal{L} = \int_{\mathbb{R}^3 \times [0,\infty)} \Bigg\{ & - k f \, \log(f I^{-\delta/2+1}) \\ & - f \left(\lambda^{(0)} m + \sum_{i=1}^{3} \lambda_i^{(1)} m \, c_i + \mu^{(0)} \left(\frac{m}{2} |c|^2 + I \right) \right) \Bigg\} \mathrm{d}I \, \mathrm{d}c. \end{aligned}$$

The solution of the Euler-Lagrange equation $\delta\mathcal{L}/\delta f$ is given by

$$f = I^{\delta/2-1} \exp \left(-1 - \frac{m}{k}\lambda^{(0)} - \frac{m}{k} \sum_{i=1}^{3} \lambda_i^{(1)} c_i - \frac{1}{k} \mu^{(0)} \left(\frac{m}{2} |c|^2 + I \right) \right).$$

Substituting this form into the constraints (3.2.5) yields a system of algebraic equations, whose solution allows one to express the Lagrange multipliers in terms of the macroscopic densities, leading to the solution (3.2.6). □

Using the distribution function f_E, simple evaluations lead to $q^{(tot)} = 0$ and $p_{ij} = \delta_{ij} \rho \frac{kT}{m}$.

3.3 Method of Grad

In order to describe a higher-order moment system, in particular, higher than 5 moments presented in the previous section, it is necessary to prescribe a form of the distribution function. The method of Grad is based on the following expansion of the distribution function, around the local Maxwellian (3.2.6),

$$f_N = f_E \sum_{i=1}^{N} \alpha_{i_1 i_2 \dots i_n} \psi_{i_1 i_2 \dots i_n}(c, I), \tag{3.3.1}$$

where $\alpha_{i_1 i_2 \dots i_n}$ denotes the coefficient in front of the polynomial $\psi_{i_1 i_2 \dots i_n}(c, I)$, N is the total number of polynomials and f_E is the Maxwell distribution (3.2.6). In order to determine the coefficients $\alpha_{i_1 i_2 \dots i_n}$, the Grad method requires that the distribution function f_N satisfies the moment condition

$$u^{(a,b)}_{i_1 i_2 \dots i_n} = \int_{\mathbb{R}^3 \times [0,\infty)} m|v|^{2a} I^b v_{i_1} v_{i_2} \dots v_{i_n} f_N \, \mathrm{d}v \, \mathrm{d}I, \; \{i_1, i_2, \dots, i_n, \} \in \{1, 2, 3\}, \; \{a, b\} \in \mathbb{Z}^+. \tag{3.3.2}$$

Using this condition, the coefficients in the expansion of f_N can be expressed as functions of the first N moments $u^{(a,b)}_{i_1 i_2 \dots i_n}$.

Additionally, polynomials with special properties can be used in the expansion. For example, Laguerre or Hermite polynomials have orthogonality properties. Using orthogonal polynomials leads to a linear moment system in terms of $\alpha^{(a,b)}_{i_1 i_2 \dots i_n}$. However, the resulting moment equations conceal their nonlinear nature in the mapping between standard convective moments $u^{(a,b)}_{i_1 i_2 \dots i_n}$ and $\alpha^{(a,b)}_{i_1 i_2 \dots i_n}$ [10]. This approach can also be applied to polyatomic moment systems.

3.4 14-moment system

The system of 14 moments can be seen as an extension of the Navier-Stokes equations because it contains additional equations for the stress tensor p_{ij} and the total heat flux $q^{(tot)}$. It can be found in various references, for example, [31, 33, 18]. Here, we provide them in the convective form.

In order to derive the 14-moment system, one tests the Boltzmann equation with m, mv_i, mv_iv_j, $\frac{m}{2}|v|^2 + I$, and $\left(\frac{m}{2}|v|^2 + I\right) v_i$, which results in the evolution equations for

density, momentum, stress, total energy, and total heat flux

$$\begin{aligned}
\partial_t \rho + \partial_{x_i}(\rho U_i) &= 0,\\
\partial_t(\rho U_i) + \partial_{x_j}(\rho U_i U_j + p_{ij}) &= 0,\\
\partial_t(\rho U_i U_j + p_{ij}) + \partial_{x_k}\left(\rho U_i U_j U_k + 3U_{(i}p_{jk)} + p_{ijk}\right) &= P_{ij},\\
\partial_t\left(\frac{1}{2}\rho|U|^2 + \rho e\right) + \partial_{x_j}\left(\left(\frac{1}{2}\rho|U|^2 + \rho e\right)U_j + U_i p_{ij} + q_j^{(tot)}\right) &= 0,\\
\partial_t\left(\left(\frac{1}{2}\rho|U|^2 + \rho e\right)U_i + U_j p_{ij} + q_i^{(tot)}\right)&\\
+\partial_{x_k}\left(q_{ik} + s_{ik} + U_j p_{ijk} + \frac{1}{2}|U|^2 p_{ik} + q_k^{(tot)}U_i + p_{jk}U_i U_k + q_i^{(tot)}U_k\right.&\\
\left. + p_{ij}U_j U_k + \left(\frac{\rho}{2}|U|^2 + \rho e\right)U_i U_k\right) &= Q_i,
\end{aligned} \tag{3.4.1}$$

where the production terms are

$$\begin{pmatrix} P_{ij} \\ Q_i \end{pmatrix} = \int_{\mathbb{R}^3\times\mathbb{R}_+} \begin{pmatrix} m v_i v_j \\ \left(\frac{m}{2}|v|^2 + I\right) v_i \end{pmatrix} Q(f,f)\,\mathrm{d}I\,\mathrm{d}v. \tag{3.4.2}$$

These will be computed in one of the following sections. Note that due to collision invariants, we have conservation of mass, momentum, and energy.

From a hierarchical point of view, some authors distinguish between two hierarchies: one based on moments that involve only velocity in their definitions, and another that includes internal energy with their fluxes. From this point of view, the 14-moment system belongs to a mixed hierarchy.

3.4.1 Grad closure for 14-moment system

In order to compute the fluxes, we can use Grad's method. First, the distribution function is expanded as follows:

$$f_{14} = f_E\left(\lambda^{(0)}m + \lambda_i^{(1)}c_i + \lambda_{ij}^{(0)}c_i c_j + \mu^{(0)}\left(\frac{m}{2}|c|^2 + I\right) + \mu_i^{(0)}\left(\frac{m}{2}|c|^2 + I\right)c_i\right) \tag{3.4.3}$$

This method requires that the distribution function reproduces the following moments

$$\begin{pmatrix} \rho \\ 0_i \\ p_{ij} \\ \frac{3+\delta}{2}\rho\frac{k}{m}T \\ q_i^{(tot)} \end{pmatrix} = \int_{\mathbb{R}^3\times[0,\infty)} \begin{pmatrix} m \\ m c_i \\ m c_i c_j \\ \frac{m}{2}|c|^2 + I \\ \left(\frac{m}{2}|c|^2 + I\right)c_i \end{pmatrix} f_{14}(t,x,c,I)\,\mathrm{d}I\,\mathrm{d}c. \tag{3.4.4}$$

This leads to a system of algebraic equations

$$\begin{aligned}
\frac{1}{2}m\left(2\lambda^{(0)}+(3+\delta)\theta\mu^{(0)}+2\theta\lambda_{jj}^{(0)}\right)\rho&=\rho, \quad j=1,2,3\\
\frac{1}{2}\theta\left((5+\delta)\theta\mu_i^{(0)}+2\lambda_i^{(0)}\right)\rho&=0, \quad i=1,2,3\\
\frac{1}{2}m\theta\rho\left(2\lambda^{(0)}+(5+\delta)\theta\mu^{(0)}+2\theta\lambda_{kk}^{(0)}\right)\delta_{ij}+2m\theta^2\lambda_{ij}^{(0)}\rho&=p_{ij}, \quad i,j,k=1,2,3\\
\frac{1}{4}m\theta\left(2(3+\delta)\lambda^{(0)}+(5+\delta)\theta\left((3+\delta)\mu^{(0)}+2\lambda_{kk}^{(0)}\right)\right)\rho&=\frac{3+\delta}{2}\theta\rho,\\
\frac{1}{4}m(5+\delta)\theta^2\left((7+\delta)\theta\mu_i^{(0)}+2\lambda_i^{(0)}\right)\rho&=q_i^{(tot)}.
\end{aligned}$$

The solution is

$$\begin{aligned}
\lambda^{(0)}&=\frac{1}{m},\\
\lambda_i^{(0)}&=-\frac{q_i^{(tot)}}{m\theta^2\rho},\\
\lambda_{ij}^{(0)}&=-\frac{(\delta\theta\rho+3\theta\rho-3\mathscr{P})\delta_{ij}-\delta p_{ij}}{2\delta\theta^2 m\rho}=-\frac{-(3+\delta)\Pi\delta_{ij}-\delta\sigma_{ij}}{2\delta\theta^2 m\rho},\\
\mu^{(0)}&=-\frac{3\mathscr{P}-3\theta\rho}{m\delta\theta^2\rho},\\
\mu_i^{(0)}&=\frac{2q_i^{(tot)}}{m(5+\delta)\theta^3\rho}.
\end{aligned}$$

Plugging the solution back into the expansion (3.4.3) yields the distribution function

$$\begin{aligned}
f_{14}=f_E\Bigg\{1-\frac{\rho}{p^2}q^{(tot)}\cdot c-\frac{3}{\delta}\frac{\Pi\rho}{mp^2}\left(\frac{m}{2}|c|^2+I\right)\\
+\frac{\rho}{2p^2}\left(\sigma_{ij}+\frac{(\delta+3)}{\delta}\delta_{ij}\Pi\right)c_ic_j+\left(\frac{\delta+5}{2}\right)^{-1}\frac{\rho^2}{mp^3}q^{(tot)}\cdot c\left(\frac{m}{2}|c|^2+I\right)\Bigg\}. \quad (3.4.5)
\end{aligned}$$

This coincides with the distribution from extended thermodynamics [38].

With this we can evaluate non-convective fluxes by plugging the distribution function (3.4.5) into their definition

$$\begin{aligned}
p_{ijk}&=\left(\frac{\delta+5}{2}\right)^{-1}\left(q_i^{(tot)}\delta_{jk}+q_j^{(tot)}\delta_{ki}^{(tot)}+q_k^{(tot)}\delta_{ij}\right),\\
q_{ij}+s_{ij}&=\frac{\delta+7}{2}\frac{p}{\rho}p_{ij}-\frac{p^2}{\rho}\delta_{ij},
\end{aligned}$$

where we sum two fluxes for simplicity.

3.5 17-moment system

The system of 17 moments includes two equations for heat fluxes: one for translational q and one for internal heat flux s. This additional vector equation, compared to the 14-moment case, provides further information about the coupling between the two heat fluxes. In the case of a three-dimensional velocity space, there are in total 17 variables: two scalar variables—density ρ and temperature θ or pressure p; six variables for the symmetric tensor p_{ij}; and three vectors—translational heat flux q, internal heat flux s, and velocity U.

By taking m, mv_i, mv_iv_j, $\frac{1}{2}m|v|^2 + I$, $\frac{1}{2}m|v|^2v_i$, and Iv_i as test functions and integrating the Boltzmann equation (2.2.5), one obtains the 17-moment system

$$\begin{aligned}
\partial_t\rho + \partial_{x_i}(\rho U_i) &= 0,\\
\partial_t(\rho U_i) + \partial_{x_j}\left(\rho U_iU_j + p_{ij}\right) &= 0,\\
\partial_t\left(\rho U_iU_j + p_{ij}\right) + \partial_{x_k}\left(\rho U_iU_jU_k + 3U_{(i}p_{jk)} + p_{ijk}\right) &= P_{ij},\\
\partial_t\left(\frac{1}{2}\rho|U|^2 + \rho e\right) + \partial_{x_j}\left(\left(\frac{1}{2}\rho|U|^2 + \rho e\right)U_j + U_ip_{ij} + q_j^{(tot)}\right) &= 0,\\
\partial_t\left(\left(\frac{1}{2}\rho|U|^2 + \rho e_K\right)U_i + U_jp_{ij} + q_i\right) &\\
+\partial_{x_k}\Bigg(q_{ik} + U_jp_{ijk} + \frac{1}{2}|U|^2p_{ik} + q_kU_i + p_{jk}U_iU_k + q_iU_k &\\
+p_{ij}U_jU_k + \left(\frac{\rho}{2}|U|^2 + \rho e_K\right)U_iU_k\Bigg) &= Q_i,\\
\partial_t\left(s_i + U_i\rho e_I\right) + \partial_{x_k}\left(\rho e_IU_iU_k + U_is_k + U_ks_i + s_{ik}\right) &= S_i,
\end{aligned} \tag{3.5.1}$$

where the production terms are given by

$$\begin{pmatrix} P_{ij}\\ Q_i\\ S_i\end{pmatrix} = \int_{\mathbb{R}^3\times\mathbb{R}_+}\begin{pmatrix} mv_iv_j\\ \frac{m}{2}|v|^2v_i\\ Iv_i\end{pmatrix}Q(f,f)\,\mathrm{d}I\,\mathrm{d}v. \tag{3.5.2}$$

3.5.1 Grad closure for 17-moment system

In order to close the 17-moment system and compute closure and production terms, an approximate distribution function is used:

$$f_{17} = f_E\left(\lambda^{(0)}m + \lambda_i^{(1)}c_i + \lambda_{ij}^{(0)}c_ic_j + \mu^{(0)}\left(\frac{m}{2}|c|^2 + I\right) + \mu_i^{(0)}\frac{m}{2}|c|^2c_i + \mu_i^{(1)}Ic_i\right), \tag{3.5.3}$$

subject to the following moment conditions

$$\begin{pmatrix} \rho \\ 0_i \\ p_{ij} \\ \frac{3+\delta}{2}\rho\theta \\ q_i \\ s_i \end{pmatrix} = \int_{\mathbb{R}^3\times[0,\infty)} \begin{pmatrix} m \\ mc_i \\ mc_ic_j \\ \frac{m}{2}|c|^2 + I \\ \frac{m}{2}|c|^2 c_i \\ Ic_i \end{pmatrix} f_{17}(t,x,c,I)\,\mathrm{d}I\,\mathrm{d}c. \tag{3.5.4}$$

The use of expansion (3.5.3) leads to the following system of algebraic equations

$$\begin{aligned}
\frac{1}{2}m\left(2\lambda^{(0)} + (3+\delta)\theta\mu^{(0)} + 2\theta\lambda_{jj}^{(0)}\right)\rho &= \rho, \quad j = 1,2,3,\\
\frac{1}{2}\theta\left((5+\delta)\theta\mu_i^{(0)} + 2\lambda_i^{(0)}\right)\rho &= 0, \quad i = 1,2,3,\\
\frac{1}{2}m\theta\rho\left(2\lambda^{(0)} + (5+\delta)\theta\mu^{(0)} + 2\theta\lambda_{kk}^{(0)}\right)\delta_{ij} + 2m\theta^2\lambda_{ij}^{(0)}\rho &= p_{ij},\\
\frac{1}{4}m\theta\left(2(3+\delta)\lambda^{(0)} + (5+\delta)\theta\left((3+\delta)\mu^{(0)} + 2\lambda_{kk}^{(0)}\right)\right)\rho &= \frac{3+\delta}{2}\theta\rho,\\
\frac{5}{4}\theta^2 m\rho\left(\delta\theta\mu_i^{(1)} + 7\theta\mu_i^{(0)} + 2\lambda_i^{(0)}\right) &= q_i,\\
\frac{1}{4}\delta\theta^2 m\rho\left((\delta+2)\theta\mu_i^{(1)} + 5\theta\mu_i^{(0)} + 2\lambda_i^{(0)}\right) &= s_i.
\end{aligned}$$

The system above has the solution

$$\begin{aligned}
\lambda^{(0)} &= \frac{1}{m},\\
\lambda_i^{(0)} &= -\frac{q_i^{(tot)}}{m\theta^2\rho},\\
\lambda_{ij}^{(0)} &= -\frac{(\delta\theta\rho + 3\theta\rho - 3\mathscr{P})\delta_{ij} - \delta p_{ij}}{2\delta\theta^2 m\rho} = -\frac{-(3+\delta)\Pi\delta_{ij} - \delta\sigma_{ij}}{2\delta\theta^2 m\rho},\\
\mu^{(0)} &= -\frac{3\mathscr{P} - 3\theta\rho}{m\delta\theta^2\rho},\\
\mu_i^{(0)} &= \frac{2q_i}{5m\theta^3\rho},\\
\mu_i^{(1)} &= \frac{2s_i}{m\delta\theta^3\rho}.
\end{aligned}$$

This results in the following distribution function [19]

$$\begin{aligned}
f_{17} = f_E\Bigg\{1 - \frac{\rho}{p^2}(q+s)\cdot c - \frac{3}{\delta}\frac{\Pi\rho}{mp^2}\left(\frac{m}{2}|c|^2 + I\right)\\
+\frac{\rho}{2p^2}\left(\sigma_{ij} + \frac{(\delta+3)}{\delta}\delta_{ij}\Pi\right)c_ic_j + \frac{\rho^2}{mp^3}c\left(\frac{m}{5}|c|^2 q + \frac{2}{\delta}Is\right)\Bigg\}.
\end{aligned} \tag{3.5.5}$$

Therefore, the following expressions for the unknown fluxes are obtained

$$p_{ijk} = \frac{2}{5}\left(q_i\delta_{jk} + q_j\delta_{ki} + q_k\delta_{ij}\right),$$
$$q_{ij} = \frac{p}{2\rho}\left(7\sigma_{ij} + (5p + 10\Pi)\,\delta_{ij}\right), \qquad s_{ij} = \frac{p}{2\rho}\left(\delta\sigma_{ij} + (\delta\, p + (\delta - 3)\Pi)\,\delta_{ij}\right).$$

Now, it only remains to select the collision kernel and to compute the production terms. This will be discussed in following chapter.

Chapter 4

Moments of the collision operator

4.1 Initial model of the collision kernel

In order to compute production terms in the moment equations, one has to select a collision kernel. One of the first choices was the hard potentials used in the existence and uniqueness theory for the space homogeneous Boltzmann equation [23]

$$\begin{aligned}&\mathcal{B}(v, v_*, I, I_*, r, R, \sigma)\\&= b\left(\frac{v - v_*}{|v - v_*|} \cdot \sigma\right)\left(R^{\frac{\zeta}{2}}|v - v_*|^{\zeta} + \left(r(1-R)\frac{I}{m}\right)^{\frac{\zeta}{2}} + \left((1-r)(1-R)\frac{I_*}{m}\right)^{\frac{\zeta}{2}}\right),\end{aligned} \quad (4.1.1)$$

where b denotes the angular part function and $\zeta > 0$. After rewriting the collision kernel (4.1.1), it can be seen as the geometric mean of pre- and post-collision variables

$$\mathcal{B}(v, v_*, I, I_*, r, R, \sigma) = b\left(\frac{v - v_*}{|v - v_*|} \cdot \sigma\right)\left(\frac{|v' - v'_*|^{\zeta}\,|v - v_*|^{\zeta}}{\left(\frac{4}{m}E\right)^{\zeta/2}} + \frac{(I'I)^{\zeta/2} + (I'_*I_*)^{\zeta/2}}{(mE)^{\zeta/2}}\right). \quad (4.1.2)$$

This model is further improved in [19] by adding a new parameter $\eta \geq 0$ in order to control the influence of internal energies

$$\mathcal{B}(v, v_*, I, I_*, r, R, \sigma) = b\left(\frac{v - v_*}{|v - v_*|} \cdot \sigma\right) K_\delta \left(\frac{|v' - v'_*|^{\zeta}\,|v - v_*|^{\zeta}}{\left(\frac{4}{m}E\right)^{\zeta/2}} + \eta\frac{(I'I)^{\zeta/2} + (I'_*I_*)^{\zeta/2}}{(mE)^{\zeta/2}}\right), \quad (4.1.3)$$

with

$$K_\delta = \frac{2\,\Gamma\left(\delta + \frac{3}{2}\right)}{\sqrt{\pi}\,\Gamma\left(\delta/2\right)^2}$$

which ensures consistency with the monatomic case.

Using the collision kernel (4.1.1), explicit production terms of 14-moment system are calculated in [18], and for the model (4.1.3) and 17-moment in [19].

To include frozen collisions, we also use model (4.1.3) with a different parameter $\eta_{\mathrm{f}} \geq 0$

$$\overline{B}(v, v_*, I, I_*, \sigma) = b\left(\frac{v - v_*}{|v - v_*|} \cdot \sigma\right) \left(\frac{|v - v_*|^{2\zeta}}{\left(\frac{4}{m}E\right)^{\zeta/2}} + \eta_{\mathrm{f}} \frac{I^\zeta + I_*^\zeta}{(mE)^{\zeta/2}}\right) \tag{4.1.4}$$

4.2 Extended model of the collision kernel

The initial model of the collision kernel can be used in some cases where the Prandtl number is sufficiently large. However, in order to gain more flexibility, in [21] we extend the model in the following way.

Since the initial model has the dimension of $E^{\zeta/2}$, we factorize the term $R^{\zeta/2}|u|^\zeta$ in order to extract that same dimension, namely, we define

$$\begin{aligned}\mathcal{B} = b\left(\frac{u}{|u|} \cdot \sigma\right) |u|^\zeta \\ \times \left\{ \frac{2\,\Gamma\left(\delta + \frac{3}{2}\right)}{\sqrt{\pi}\,\Gamma\left(\delta/2\right)^2} \omega R^{\frac{\zeta}{2}} \left[1 + \hat{\eta}\left(\left(r(1-R)\frac{I}{E}\right)^{\frac{\hat{\zeta}}{2}} + \left((1-r)(1-R)\frac{I_*}{E}\right)^{\frac{\hat{\zeta}}{2}}\right)\right] \right. \\ \left. + (1-\omega)\,\delta_{r-r'}\delta_{R-R'} \left(\frac{m|u|^2}{4E}\right)^{\frac{\zeta}{2}} \left[1 + \hat{\eta}_{\mathrm{f}}\left(\left(\frac{I}{E}\right)^{\hat{\zeta}_{\mathrm{f}}} + \left(\frac{I_*}{E}\right)^{\hat{\zeta}_{\mathrm{f}}}\right)\right] \right\}, \end{aligned} \tag{4.2.1}$$

where $u = v - v_*$ is the relative velocity, and δ_z denotes the Dirac delta function. Here, $\omega \in [0, 1]$, $\zeta, \hat{\zeta}, \hat{\zeta}_{\mathrm{f}} \geq 0$, and $\hat{\eta}, \hat{\eta}_{\mathrm{f}}$ are new sets of parameters connected with the initial model via

$$\hat{\zeta} = \zeta, \quad \hat{\zeta}_{\mathrm{f}} = \zeta, \quad \hat{\eta} = \left(\frac{E}{Rm|u|^2}\right)^{\zeta/2} \eta, \quad \hat{\eta}_{\mathrm{f}} = \left(\frac{2E}{m|u|^2}\right)^{\zeta} \eta_{\mathrm{f}},$$

on the range $\hat{\eta}, \hat{\eta}_{\mathrm{f}} \geq 0$.

A crucial improvement in the extended model (4.2.1) is the possibility that $\hat{\eta}$ and $\hat{\eta}_{\mathrm{f}}$ can be negative. This follows from the requirement that the collision kernel $\mathcal{B}$ must be

non-negative which is satisfied if the following inequalities hold

$$1+\hat{\eta}\left(\left(r(1-R)\frac{I}{E}\right)^{\frac{\zeta}{2}}+\left((1-r)(1-R)\frac{I_*}{E}\right)^{\frac{\zeta}{2}}\right)\geq 0,$$
$$1+\hat{\eta}_{\mathrm{f}}\left(\left(\frac{I}{E}\right)^{\hat{\zeta}}+\left(\frac{I_*}{E}\right)^{\hat{\zeta}}\right)\geq 0.$$

Indeed, since $0\leq \frac{I}{E},\frac{I_*}{E}\leq 1$, $\zeta,\hat{\zeta}\geq 0$, and $r,R\in[0,1]$, we obtain

$$0\leq\left(r(1-R)\frac{I}{E}\right)^{\frac{\zeta}{2}}+\left((1-r)(1-R)\frac{I_*}{E}\right)^{\frac{\zeta}{2}}\leq 2,$$
$$0\leq\left(\frac{I}{E}\right)^{\hat{\zeta}}+\left(\frac{I_*}{E}\right)^{\hat{\zeta}}\leq 2,$$

which implies the range $-1/2\leq\hat{\eta},\hat{\eta}_{\mathrm{f}}\leq 0$ for non-negativity to hold.

4.3 General approach to compute production terms

In order to obtain a closed model based on the moment system, one must compute the production terms—in other words, the moments of the collision operator. The quadratic nature of the collision operator implies non-linear production terms that depend on the selected collision kernel.

The key steps of the collision operator evaluation procedure are as follows:

- Select the test function and the corresponding polynomial in the distribution function in the expansion (3.4.5) or (3.5.5).
- Use the weak form (2.2.17) of the collision operator to obtain the initial integral.
- Change to the relative velocity u and the center-of-mass peculiar velocity V_c using (A.1.3), and integrate over V_c and σ.
- Perform integration over R and r.
- Introduce spherical coordinates for u, and integrate over spherical ordinates, $|u|$, I, and I_*.

Based on the procedure above, Mathematica notebooks [16, 17] were created to enable the efficient computation of collision coefficients.

In the upcoming sections, we focus on the production terms of linear leading-order in non-equilibrium densities, as these provide a suitable framework for comparison with experimental data. As an example for computations, Appendix A presents calculations for the initial collision kernel and the 14-moment system.

4.4 First-order transport coefficients

Originally introduced in the Navier–Stokes–Fourier framework, the first-order transport coefficients provide a robust closure for the moment system, expressed as

$$p_{ij} = \left(p - \nu \sum_{k=1}^{3} \partial_{x_k} v_k\right) \delta_{ij} - 2\mu \frac{\partial v_{\langle i}}{\partial x_{j\rangle}}, \quad q_i^{(\text{tot})} = -\kappa \partial_{x_i} T, \qquad i,j \in \{1,2,3\}\,, \tag{4.4.1}$$

where μ is the shear viscosity, ν is the bulk viscosity, and κ is the heat conductivity. These transport coefficients can be measured experimentally and are typically used in the Navier–Stokes–Fourier equations for small Knudsen numbers.

In addition to experimental methods, kinetic theory provides theoretical estimates of transport coefficients at various orders. One such method involves applying the Maxwell iteration to the system of moment equations to obtain estimates for the first-order transport coefficients [41, 38]. This process inherently depends on the moments of the collision operator and the number of moments considered.

After computing the transport coefficients, one can easily evaluate dimensionless ratios such as the Prandtl number, which characterizes the relationship between shear viscosity and heat conductivity

$$\mathrm{Pr} = \frac{(5+\delta)}{2} \frac{k}{m} \frac{\mu}{\kappa}, \tag{4.4.2}$$

where a polytropic assumption is applied. An alternative estimate for the Prandtl number is given by the Eucken formula

$$\mathrm{Pr}^{(\text{Eucken})} = \frac{2(\delta+5)}{2\delta+15}, \tag{4.4.3}$$

which essentially assumes frozen collisions.

Our objective is to express and analyze the first-order transport coefficients for both the 14-moment and 17-moment systems, considering both the initial and extended collision kernels. To begin, we illustrate the case of the 14-moment system.

4.4.1 14-moment case

The production terms for the initial collision kernel (4.1.1), with $b\Big(\frac{u}{|u|}\cdot\sigma\Big) = K$, where K is a constant, are linearized around the global equilibrium state (3.2.6) and take the following form

$$\overline{P}^{14}_{ij} = -\tilde{\nu}\left(P_\sigma\,\sigma_{ij} + P_\Pi\,\Pi\,\delta_{ij}\right), \quad \overline{Q}^{14}_{i} = U_k\overline{P}^{14}_{ki} - \tilde{\nu}\,q_i^{(\text{tot})}P_{q^{(\text{tot})}}, \tag{4.4.4}$$

where

$$\tilde{\nu} = \frac{\rho}{m}\left(\frac{p}{\rho}\right)^{\frac{\zeta}{2}}. \tag{4.4.5}$$

Here, the collision coefficients $P_\sigma, P_\Pi, P_{q^{(\text{tot})}}$ are obtained by integrating the collision operator using the Mathematica notebook [17]. The detailed mathematical procedure is provided in Appendix A, using a simplified version of the initial collision kernel as presented in [18].

By applying Maxwell iteration to the 14-moment system, we obtain the following estimates for the first-order transport coefficients

$$\mu = p\,\tau_s, \quad \nu = \frac{2\delta}{3(\delta+3)}\,p\,\tau_\Pi, \quad \kappa = \left(\frac{\delta+5}{2}\right)\frac{p^2}{\rho T}\,\tau_q,$$

where τ_s, τ_Π, and τ_q are relaxation times derived from the general form of the production terms [37]

$$\overline{P}^{14}_{ij} = -\frac{1}{\tau_s}\,\sigma_{ij} - \frac{1}{\tau_\Pi}\,\Pi\,\delta_{ij}, \quad \overline{Q}^{14}_{i} = U_k\overline{P}^{14}_{ki} - \frac{1}{\tau_q}\,q_i. \tag{4.4.6}$$

A direct comparison of equations (4.4.4) and (4.4.6) leads to estimates for the first-order transport coefficients,

$$\mu = p\frac{1}{\tilde{\nu}P_\sigma}, \quad \nu = \frac{2\delta}{3(3+\delta)}p\frac{1}{\tilde{\nu}P_\Pi}, \quad \kappa = p\frac{k}{m}\frac{(\delta+5)}{2}\frac{1}{\tilde{\nu}P_{q^{(tot)}}}, \tag{4.4.7}$$

that giver the Prandtl number

$$\text{Pr}^{(14)} = \frac{P_{q^{(tot)}}}{P_\sigma}. \tag{4.4.8}$$

Initial model

Using the initial collision kernel, which depends on the parameters $\delta, \zeta, \omega, \eta, \eta_f$, and K, the coefficient in front of the stress is given by

$$P_\sigma = \frac{4K}{15c_1}\left[\omega c_2\left(15\eta k_1 + k_2\,2^{\zeta+2}(\zeta+5)\right) + (1-\omega)c_3\left(15\eta_f k_3 + k_4\,2^{\zeta+1}(2\zeta+5)\right)\right],$$

while for the bulk viscosity it reads

$$P_{\Pi} = \frac{K2(\delta+3)}{3c_1\delta(2\delta+\zeta+3)} \times \left[\omega c_2 \left(6\eta k_1(2\delta+\zeta) + k_2\, 2^{\zeta+4}\delta\right)\right],$$

and for the thermal conductivity is

$$\begin{aligned} P_{q^{(tot)}} =& \frac{4K}{9c_1(\delta+5)(2\delta+2\zeta+7)(2\delta+\zeta+3)} \\ & \times \left[\omega c_2(2\delta+2\zeta+7)\left(\eta k_1 9\left\{\delta^3+\delta^2+\delta(52-7\zeta)-3\zeta^2+30\zeta+40\right.\right.\right. \\ & \left. +(\delta+\zeta)\left[(\delta+\zeta+8)\zeta-\delta^2+7\delta-8\right]\right\} \\ & \left. +k_2\, 2^{\zeta+5}\left[3\delta^2+\frac{1}{2}\delta(7\zeta+33)+(\zeta+3)(\zeta+5)\right]\right) \\ & + (1-\omega)4c_3(2\delta+\zeta+3)\left\{3\eta_f k_3\left[6\delta^2+\delta(6\zeta^2+9\zeta+41)\right.\right. \\ & \left. +\zeta(3\zeta(\zeta+8)+41)+70\right] \\ & \left.\left. +k_4\, 2^{\zeta+2}\left[3\delta^2+\frac{1}{2}\delta(11\zeta+41)+(2\zeta+5)(2\zeta+7)\right]\right\}\right]. \end{aligned}$$

The constants used in the above expressions are

$$\begin{aligned} & c_1 = \Gamma\left(\frac{\delta}{2}\right)^2 \Gamma\left(\delta+\zeta+\frac{7}{2}\right)\Gamma\left(\frac{2\delta+\zeta+3}{2}\right), \quad c_2 = \Gamma\left(\delta+\frac{3}{2}\right)\Gamma\left(\delta+\zeta+\frac{7}{2}\right), \\ & c_3 = \sqrt{\pi}\Gamma\left(\frac{\delta}{2}\right)\Gamma\left(\frac{2\delta+\zeta+3}{2}\right)\Gamma\left(\frac{2\delta+\zeta+7}{2}\right), \\ & k_1 = \pi\Gamma\left(\frac{\delta+\zeta}{2}\right)^2, \quad k_2 = \Gamma\left(\frac{\delta}{2}\right)^2\Gamma\left(\frac{\zeta+3}{2}\right)\Gamma\left(\frac{\zeta+5}{2}\right), \\ & k_3 = \sqrt{\pi}\Gamma\left(\frac{\delta}{2}+\zeta\right), \quad k_4 = \Gamma\left(\frac{\delta}{2}\right)\Gamma\left(\zeta+\frac{5}{2}\right). \end{aligned} \tag{4.4.9}$$

We observe that all transport coefficients share the same temperature dependence. This is expected, as they are all derived from the integrals with same collision kernel.

Extended model

The extended collision kernel with 14-moments model produces the following collision coefficients for stress

$$P_\sigma = \frac{K\, 2^{\zeta+4}}{15\,\hat{c}_1}\left(2\hat{c}_2\omega(2\hat{\eta}\hat{k}_1+\hat{k}_2)+\hat{c}_3(1-\omega)(2\hat{\eta}_{\mathrm{f}}\hat{k}_3+\hat{k}_4)\right), \tag{4.4.10}$$

while the coefficient in front the dynamical pressure Π reads

$$P_{\Pi} = \frac{K\,\hat{c}_2(\delta+3)2^{\zeta+4}\omega}{3\hat{c}_1(\zeta+5)(2\delta+\zeta+\hat{\zeta}+3)}\left[\frac{4\hat{\eta}\hat{k}_1(2\delta+\hat{\zeta})}{\delta}+\frac{4\hat{k}_2(2\delta+\zeta+\hat{\zeta}+3)}{2\delta+\zeta+3}\right], \tag{4.4.11}$$

and in front of the total heat flux is

$$\begin{aligned}
P_{q^{(\mathrm{tot})}} = {} & \frac{K\,\hat{c}_2 2^{\zeta+4}\omega}{9\hat{c}_1(\delta+5)(\zeta+5)}\left\{\hat{k}_2\left(\delta\left(\frac{8}{2\delta+\zeta+3}+6\right)+4(\zeta+5)\right)\right. \\
& +\frac{\hat{\eta}\hat{k}_1}{(2\delta+\zeta+\hat{\zeta}+3)(2\delta+\zeta+\hat{\zeta}+7)}\left(\hat{\zeta}^2\left(12\delta^2+12\delta(\zeta+6)+(\zeta+9)(3\zeta+17)\right)\right. \\
& \qquad +2\hat{\zeta}\left(24\delta^2+2\delta(17\zeta+99)+\zeta(11\zeta+114)+291\right) \\
& \left.\left.+4(2\delta+\zeta+7)\left(6\delta^2+\delta(7\zeta+33)+2(\zeta+3)(\zeta+5)\right)+3\hat{\zeta}^3(2\delta+\zeta+7)\right)\right\} \\
& +\frac{K\,\hat{c}_3 2^{\zeta+4}(1-\omega)}{9\hat{c}_1(\delta+5)}\left(4\hat{\eta}_{\mathrm{f}}\hat{k}_3+\frac{1}{2\zeta+5}\left(\frac{\hat{\eta}_{\mathrm{f}}\,6\hat{k}_3(2\delta+\zeta+7)\left(\delta+\hat{\zeta}_{\mathrm{f}}^2+\hat{\zeta}_{\mathrm{f}}\right)}{2\delta+2\zeta+2\hat{\zeta}_{\mathrm{f}}+7}\right.\right. \\
& \qquad \left.\left.+\frac{\hat{k}_4\left(11\delta\zeta+\delta(6\delta+41)+8\zeta^2+48\zeta+70\right)}{2\delta+2\zeta+7}\right)\right),
\end{aligned} \tag{4.4.12}$$

where the constants are

$$\begin{aligned}
\hat{c}_1 = {} & \Gamma\left(\frac{\delta}{2}\right)^2\Gamma\left(\delta+\frac{\zeta}{2}+\frac{3}{2}\right)\Gamma\left(\delta+\zeta+\frac{7}{2}\right)\Gamma\left(\frac{1}{2}(2\delta+\zeta+\hat{\zeta}+3)\right) \\
& \times\Gamma\left(\frac{1}{2}(2\delta+\zeta+\hat{\zeta}+7)\right)\Gamma\left(\delta+\zeta+\hat{\zeta}_{\mathrm{f}}+\frac{7}{2}\right), \\
\hat{c}_2 = {} & \Gamma\left(\delta+\frac{3}{2}\right)\Gamma\left(\frac{\zeta+3}{2}\right)\Gamma\left(\frac{\zeta+7}{2}\right)\Gamma\left(\delta+\zeta+\frac{7}{2}\right)\Gamma\left(\delta+\zeta+\hat{\zeta}_{\mathrm{f}}+\frac{7}{2}\right), \\
\hat{c}_3 = {} & \sqrt{\pi}\Gamma\left(\frac{\delta}{2}\right)\Gamma\left(\zeta+\frac{7}{2}\right)\Gamma\left(\delta+\frac{\zeta}{2}+\frac{3}{2}\right)\Gamma\left(\delta+\frac{\zeta}{2}+\frac{7}{2}\right) \\
& \times\Gamma\left(\frac{1}{2}(2\delta+\zeta+\hat{\zeta}+3)\right)\Gamma\left(\frac{1}{2}(2\delta+\zeta+\hat{\zeta}+7)\right), \\
\hat{k}_1 = {} & \Gamma\left(\delta+\frac{\zeta}{2}+\frac{3}{2}\right)\Gamma\left(\delta+\frac{\zeta}{2}+\frac{7}{2}\right)\Gamma\left(\frac{\delta+\hat{\zeta}}{2}\right)^2, \\
\hat{k}_2 = {} & \Gamma\left(\frac{\delta}{2}\right)^2\Gamma\left(\frac{1}{2}(2\delta+\zeta+\hat{\zeta}+3)\right)\Gamma\left(\frac{1}{2}(2\delta+\zeta+\hat{\zeta}+7)\right), \\
\hat{k}_3 = {} & \Gamma\left(\delta+\zeta+\frac{7}{2}\right)\Gamma\left(\frac{\delta}{2}+\hat{\zeta}_{\mathrm{f}}\right), \quad \hat{k}_4 = \Gamma\left(\frac{\delta}{2}\right)\Gamma\left(\delta+\zeta+\hat{\zeta}_{\mathrm{f}}+\frac{7}{2}\right).
\end{aligned} \tag{4.4.13}$$

4.4.2 17-moment case

Because the 17-moment system provides two separate equations for the heat fluxes due to their coupling, the resulting expression for heat conductivity is fundamentally different. To obtain this result, we perform a Maxwell iteration on the 17-moment system (3.5.1). We consider only the linear, leading-order terms of the transport equations for the stress tensor,

$$2\rho\theta\partial_{\langle x_i} v_{j\rangle} = -\tilde{\nu} P_\sigma \sigma_{ij}, \tag{4.4.14}$$

and for translational and internal heat fluxes, with notation (4.4.5),

$$\begin{aligned} \tfrac{5}{2}\rho\theta\partial_{x_i}\theta &= -\tilde{\nu}\left(P_q^{(0)} q_i + P_q^{(1)} s_i\right) \\ \tfrac{\delta}{2}\rho\theta\partial_{x_i}\theta &= -\tilde{\nu}\left(P_s^{(0)} s_i + P_s^{(1)} q_i\right), \end{aligned} \tag{4.4.15}$$

and compute for stress tensor and total heat flux $q_i^{(\text{tot})} = q_i + s_i$

$$\sigma_{ij} = -2\frac{\rho\theta}{\tilde{\nu}}\frac{1}{P_\sigma}\partial_{\langle x_i} v_{j\rangle}, \tag{4.4.16}$$

$$q_i^{(\text{tot})} = -\frac{\rho\theta}{\tilde{\nu}}\frac{5(P_s^{(0)} - P_s^{(1)}) + \delta(P_q^{(0)} - P_q^{(1)})}{2(P_q^{(0)} P_s^{(0)} - P_q^{(1)} P_s^{(1)})}\partial_{x_i}\theta, \tag{4.4.17}$$

as the first order contribution. Then, we can compute transport coefficients

$$\mu = p\frac{1}{\tilde{\nu} P_\sigma}, \quad \nu = \frac{2\delta}{3(3+\delta)} p\frac{1}{\tilde{\nu} P_\Pi}, \quad \kappa = p\frac{k}{m}\frac{5\left(P_s^{(0)} - P_s^{(1)}\right) + \delta\left(P_q^{(0)} - P_q^{(1)}\right)}{2\tilde{\nu}\left(P_q^{(0)} P_s^{(0)} - P_q^{(1)} P_s^{(1)}\right)}. \tag{4.4.18}$$

in terms of production term coefficients.

Thus, evaluating the collision operator to explicitly compute the production terms allows us to formulate a model expression for the Prandtl number using its definition (4.4.2) and the models for the transport coefficients (4.4.18),

$$\mathrm{Pr}^{(17)} = \frac{(5+\delta)}{2}\frac{2\left(P_q^{(0)} P_s^{(0)} - P_q^{(1)} P_s^{(1)}\right)}{P_\sigma\left(5\left(P_s^{(0)} - P_s^{(1)}\right) + \delta\left(P_q^{(0)} - P_q^{(1)}\right)\right)}. \tag{4.4.19}$$

Note that this model depends on the choice of the collision kernel and all parameters included in it. Our approach is to select the values for the collision kernel parameters using a data-driven method.

Initial model

The collision coefficients for the stress σ_{ij} and dynamical pressure Π are same as those in 14-moment. For the heat flux subsystem the following result is obtained

$$P_q^{(0)} = \frac{2K}{45c_1}\left(\frac{c_2\omega\left(45\eta k_1(6\delta+3\zeta+4)+2^{\zeta+3}k_2(\delta(4\zeta+45)+2(\zeta+3)(\zeta+5))\right)}{2\delta+\zeta+3} \right.$$
$$\left. +4c_3(1-\omega)\left(15\eta_{\mathrm{f}}k_3+2^{\zeta+1}(2\zeta+5)k_4\right)\right),$$

$$P_q^{(1)} = \frac{10Kc_2\omega\left(3\eta k_1(2\delta+\zeta)+\delta 2^{\zeta+3}k_2\right)}{3c_1\delta(2\delta+\zeta+3)}, \quad P_s^{(1)} = \frac{2Kc_2\omega\left(3\eta k_1(2\delta+\zeta)+\delta 2^{\zeta+3}k_2\right)}{3c_1(2\delta+\zeta+3)},$$

$$P_s^{(0)} = \frac{K}{3c_1\delta^2}\left(\frac{8c_3\delta(1-\omega)\left(3\eta_{\mathrm{f}}k_3\left(\delta+\zeta^2+\zeta\right)+\delta 2^{\zeta+1}k_4\right)}{2\delta+2\zeta+7}\right.$$
$$\left. +\frac{c_2\delta\omega\left(\delta\, 2^{\zeta+4}k_2(2\delta+\zeta+6)+3\eta k_1\left((2\delta+5)\zeta^2+4(2\delta+3)\zeta+8\delta(\delta+3)+\zeta^3\right)\right)}{2\delta+\zeta+3}\right).$$

It is worth mentioning that the coefficients $P_q^{(1)}$ and $P_s^{(1)}$ are connected via

$$\frac{2}{5}P_q^{(1)} = \frac{2}{\delta}P_s^{(1)}, \tag{4.4.20}$$

that is also valid the extended model.

Extended model

For the extended model the collision coefficients are

$$P_q^{(0)} = \frac{K2^{\zeta+5}}{45\hat{c}_1}\left(\frac{\hat{c}_2\omega\left(\hat{k}_2\left(\frac{25\delta}{2\delta+\zeta+3}+2\zeta+10\right)+\frac{\eta\hat{k}_1(\delta(8\zeta+90)+4\zeta(\zeta+\hat{\zeta}+8)+45\hat{\zeta}+60)}{2\delta+\zeta+\hat{\zeta}+3}\right)}{\zeta+5}\right.$$
$$\left. +\hat{c}_3(1-\omega)(2\hat{\eta}_{\mathrm{f}}\hat{k}_3+\hat{k}_4)\right),$$

$$P_q^{(1)} = \frac{5\,K\,\hat{c}_2\,2^{\zeta+5}}{3\hat{c}_1(\zeta+5)}\omega\left(\frac{\eta\hat{k}_1(2\delta+\hat{\zeta})}{\delta(2\delta+\zeta+\hat{\zeta}+3)}+\frac{\hat{k}_2}{2\delta+\zeta+3}\right),$$

$$P_s^{(1)} = \frac{K\hat{c}_2 2^{\zeta+5}}{3\hat{c}_1(\zeta+5)}\omega\left(\frac{\eta\hat{k}_1(2\delta+\hat{\zeta})}{2\delta+\zeta+\hat{\zeta}+3}+\frac{\delta\hat{k}_2}{2\delta+\zeta+3}\right),$$

$$\begin{aligned}P_s^{(0)} = \frac{K2^{\zeta+4}}{3\hat{c}_1}\Bigg\{&(1-\omega)\frac{\hat{c}_3(2\delta+\zeta+7)}{\delta(2\zeta+5)(2\delta+2\zeta+7)(2\delta+2\zeta+2\hat{\zeta}_{\rm f}+7)}\\ &\times\left(2\hat{\eta}_{\rm f}\hat{k}_3(2\delta+2\zeta+7)\left(\delta+\hat{\zeta}_{\rm f}^2+\hat{\zeta}_{\rm f}\right)+\delta\hat{k}_4(2\delta+2\zeta+2\hat{\zeta}_{\rm f}+7)\right)\\ &+\frac{\omega\,\hat{c}_2}{\zeta+5}\Bigg[\hat{k}_2\left(\frac{6}{2\delta+\zeta+3}+2\right)+\frac{\hat{k}_1\eta}{\delta(2\delta+\zeta+\hat{\zeta}+3)(2\delta+\zeta+\hat{\zeta}+7)}\\ &\Big(\hat{\zeta}^2\left(4\delta^2+4\delta(\zeta+6)+\zeta(\zeta+12)+41\right)+2\hat{\zeta}\left(8\delta^2+\delta(6\zeta+46)+(\zeta+6)(\zeta+7)\right)\\ &+\hat{\zeta}^3(2\delta+\zeta+7)+4\delta(2\delta+\zeta+6)(2\delta+\zeta+7)\Big)\Bigg]\Bigg\}\end{aligned} \quad (4.4.21)$$

4.5 Fit to experimental data

The goal of this section is to fit the proposed collision kernel models (4.1.3) and (4.2.1) parameters to recover experimental data for shear viscosity, Prandtl number and ratio of shear and bulk viscosity [14]. Note that we restrict only to gases in polytropic regime listed in [32]. Experimental data are withdrawn from the database [1, 6, 9, 26] for gases that behave as calorically perfect on certain temperature range around room temperature.

4.5.1 Shear viscosity fit

It is known that the temperature dependence of shear viscosity μ can be modeled [13] as

$$\frac{\mu}{\mu_0} = \left(\frac{T}{T_0}\right)^{s_{\rm visc}}, \quad (4.5.1)$$

where μ_0 is the reference viscosity at temperature T_0. Here, we take $T_0 = 300$K, and μ_0 has units of μPa·s at a pressure of $p = 0.092$ bar. Using experimental data from [1], we can determine the viscosity exponent $s_{\rm visc}$.

On the other hand, integration of the both collision kernels also yields a power-law dependence, with exponent $1-\zeta/2$. Comparing these, we obtain

$$\zeta = 2\left(1 - s_{\rm visc}\right). \quad (4.5.2)$$

gas	N_2	O_2	NO	CO	H_2
temp. interval (in K)	$[300, 600]$	$[300, 430]$	$[300, 550]$	$[300, 550]$	$[300, 890]$
δ	2.01	2.07	2.18	2.01	1.94
ζ	0.533	0.441	0.42	0.53	0.607
s_{visc}	0.733	0.779	0.79	0.735	0.696
μ_0	17.878	20.633	19.27	17.84	8.938

Table 4.1: Gases that can be modeled as calorically perfect and temperature interval over which this assumption is valid. Value of δ connected with the experimentally measured $\hat{c}_v$ at 300K as given in (2.2.4). Value of ζ according to the fit with experimental data for the shear viscosity μ according to (4.5.2) and the reference value μ_0 of the shear viscosity in the units of μPa·s at temperature 300K and pressure $p = 0.092$bar.

gas	N_2	O_2	NO	CO	H_2
measured value of Pr	0.717	0.717	0.740	0.743	0.686
$\text{Pr}^{(\text{Eucken})}$	0.737	0.739	0.7417	0.737	0.735
$\text{Pr}^{(\text{Frozen})}$	0.697	0.705	0.708	0.698	0.691

Table 4.2: Values of the Prandtl number for calorically perfect gases listed in Table 4.1. The first one corresponds to the experimentally measured value using its definition (4.4.2), the second one corresponds to the value obtained according to the Eucken formula (4.4.3), while the third one is the value according to the frozen formula (4.5.4) which can be seen as a generalization of the Eucken formula.

Therefore, by performing the fit (4.5.1), we obtain a value for ζ, as summarized in Table 4.1.

Selecting values of ζ from Table 4.1 ensures the correct exponent. However, the initial value μ_0 is not guaranteed. To correct for this, we define

$$K = \frac{1}{\mu_0 \cdot 10^{-6}} m \left(\frac{kT_0}{m} \right)^{1-\zeta/2} \frac{1}{P_\sigma|_{K=1}}. \tag{4.5.3}$$

4.5.2 Prandtl number fit

The flexibility of the proposed models depends on the choice of the collision kernel used. To illustrate the possibilities of the initial and extended models in capturing the range of Prandtl numbers, we first extract relevant experimental values. By applying the formula for the Prandtl number (4.4.2), together with experimental data for shear viscosity and thermal conductivity, we obtain corresponding experimental values of the Prandtl number. For this purpose, we use the same database as in previous sections [1, 26]. The results are summarized in Table 4.2. After selecting a gas, the parameter δ is determined from the specific heat c_v, and ζ is obtained from the shear viscosity fit.

Depending on the chosen collision kernel, the Prandtl number becomes a function of the collision parameters: ω, η, and η_{f} in the case of the initial model, and ω, $\hat{\zeta}$, $\hat{\zeta}_{\mathrm{f}}$, $\hat{\eta}$, and $\hat{\eta}_{\mathrm{f}}$ in the case of the extended model. By varying these parameters for the fixed δ and ζ, one can explore the possible range of Prandtl numbers.

We begin with the initial model and the Prandtl number formulation based on the 17-moment approximation (4.4.19). Taking $\delta = 2$ as a representative value for the gases listed in Table 4.1, and varying $0 \leq \omega \leq 1$, $0 \leq \eta, \eta_f \leq 1$, we obtain the yellow region shown in Figure 4.1. Plotting against the viscosity parameter s_{visc} (or equivalently ζ by (4.5.2)), we show that the initial model can reproduce most of the experimental Prandtl numbers listed in Table 4.1 (indicated by blue dots). The Eucken formula is fully recovered when $\zeta = \omega = \eta_f = 0$. The lowest possible values are given by the so-called frozen formula

$$\mathrm{Pr}^{(\mathrm{Frozen})} = \frac{2(\delta+5)}{\delta\left(2+\frac{4}{5}\zeta\right)\frac{2\zeta+2\delta+7}{\zeta+2\delta+7}+15}, \tag{4.5.4}$$

which can be viewed as a generalization of the Eucken formula (4.4.3). The frozen formula above is identical for both the initial and the extended model.

However, the case of H_2 lies outside the range covered by the initial model. This discrepancy motivated the development of an extended model [21]. Using an analogous procedure with parameter variations $-\frac{1}{2} \leq \hat{\eta}, \hat{\eta}_{\mathrm{f}} \leq 2$, $0 \leq \hat{\zeta}, \hat{\zeta}_{\mathrm{f}} \leq 2$, we reproduce Figure 4.2. Thanks to the additional parameters in the collision kernel, the extended model (4.2.1) is capable of reproducing values below the frozen Prandtl formula (4.5.4). This extended range is due to the negative values that $\hat{\eta}$ and $\hat{\eta}_{\mathrm{f}}$ can take. Moreover, the exponents $\hat{\zeta}$ and $\hat{\zeta}_{\mathrm{f}}$ contribute significantly to the model's flexibility.

4.5.3 Shear-to-bulk viscosity ratio fit

The ratio of shear to bulk viscosity can be expressed, after evaluating the Boltzmann collision operator, as

$$\left(\frac{\nu}{\mu}\right)^{(\mathrm{Model})} = \frac{2\delta}{3(3+\delta)}\frac{P_\sigma^{(0)}}{P_\Pi^{(0)}}, \tag{4.5.5}$$

where $P_\sigma^{(0)}$ and $P_\Pi^{(0)}$ are functions of the collision kernel parameters. Our goal here is to identify values for the collision kernel parameters such that we simultaneously match the experimental data for both the Prandtl number and the shear-to-bulk viscosity ratio, using reference data from [14]. The experimental values of the viscosity ratio are summarized in Table 4.3.

Since the extended model demonstrates greater flexibility, we use it here. With the values of δ and ζ fixed from the heat capacity c_v and shear viscosity μ fit, we still need

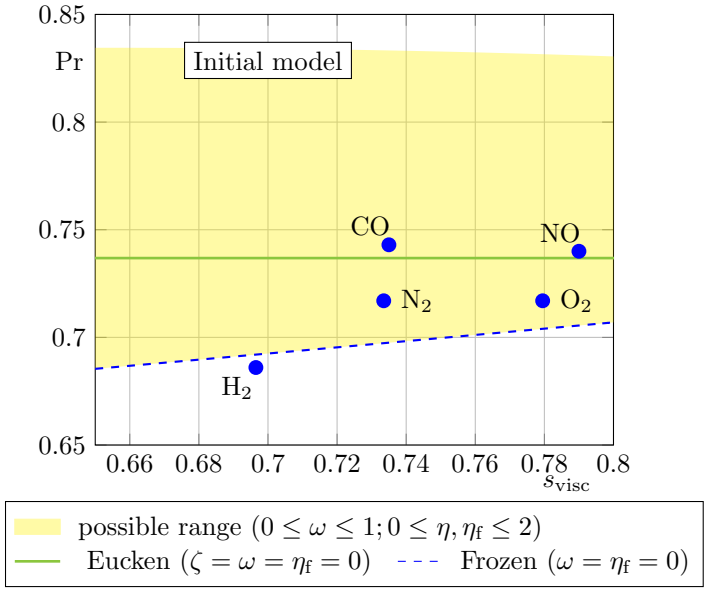

Figure 4.1: Possible range for the initial model (4.1.3) for fixed internal degrees of freedom $\delta = 2$, obtained by varying the parameters $0 \leq \omega \leq 1$, $0 \leq \eta, \eta_f \leq 2$. Blue points represent experimental data for the Prandtl number from Table 4.2 that correspond to the viscosity exponent s_{visc} from Table 4.1.

Gas	N_2	CO	H_2
Measured value of $\frac{\nu}{\mu}$	0.73	0.55	30

Table 4.3: Experimental values of the bulk-to-shear viscosity ratio at room temperature ($T = 300$ K), summarized in [14].

to determine appropriate values for the parameters ω, $\hat{\zeta}$, $\hat{\zeta}_f$, $\hat{\eta}$, and $\hat{\eta}_f$. This yields a system of two equations: the first fits the Prandtl number to its experimental value using (4.4.19) (cf. Table 4.4.2); the second fits the viscosity ratio using (4.5.5) to the corresponding value in Table 4.3. This system does not have a unique solution.

To proceed, we first arbitrarily select values for $\hat{\zeta}$, $\hat{\zeta}_f$, and $\hat{\eta}$, then solve the system numerically using a Mathematica notebook [17]. An example solution is presented in Table 4.4.

It is worth noting that the extended collision kernel allows for a wide range of values for the viscosity ratio, as illustrated in Figure 4.3. This flexibility arises from the fact that the collision term $P_{\Pi}^{(0)}$ is proportional to ω. By choosing sufficiently small values of ω, the ratio ν/μ can reach arbitrarily high values.

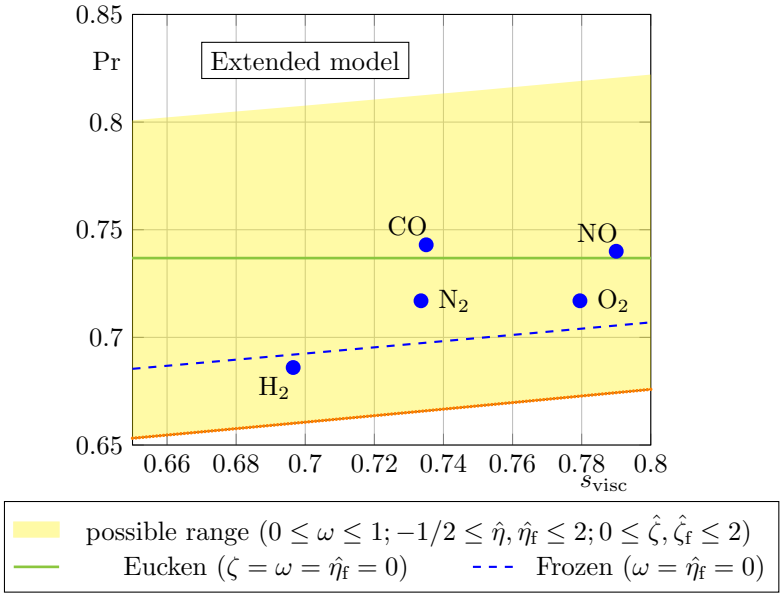

Figure 4.2: Possible range for the Prandtl number for fixed internal degrees of freedom $\delta = 2$, obtained by varying the parameters $-\frac{1}{2} \leq \hat{\eta}, \hat{\eta}_\mathrm{f} \leq 2$, $0 \leq \hat{\zeta}, \hat{\zeta}_\mathrm{f} \leq 2$ of the extended model (4.2.1). Blue points represent experimental data for the Prandtl number from Table 4.2 that correspond to the viscosity exponent s_visc from Table 4.1. Orange dots represent the lower limiting values of the extended model.

4.6 Comparison between 14 and 17 moment approximation

In this section, we examine the differences between the 14- and 17-moment theories regarding their estimates of first-order transport coefficients for a fixed collision kernel (4.1.3). Both theories, for a given choice of collision kernel, yield identical values for the shear and bulk viscosities. The only difference arises in the estimation of heat conductivity, which leads to two distinct predictions, given by (4.4.2) and (4.4.19), respectively. Consequently, comparing the two Prandtl numbers is equivalent to comparing the corresponding heat conductivities [22].

To gain an initial insight into the behavior of the two Prandtl numbers, we plot them as functions of the parameter ω in Figure 4.4, for $\delta = 2$ and $\zeta = 0.5$, considering different values of η and η_f. The figure shows that the 17-moment theory tends to yield lower values of the Prandtl number compared to the 14-moment theory, particularly for values of ω close to zero. In the context of moment approximations, this suggests that one must increase the number of moments in order to achieve convergence or stability in the Prandtl number prediction—especially for those parameter values that exhibit significant discrepancies in Figure 4.4. On the other hand, parameter combinations for which both the 14- and 17-moment theories yield matching Prandtl numbers indicate

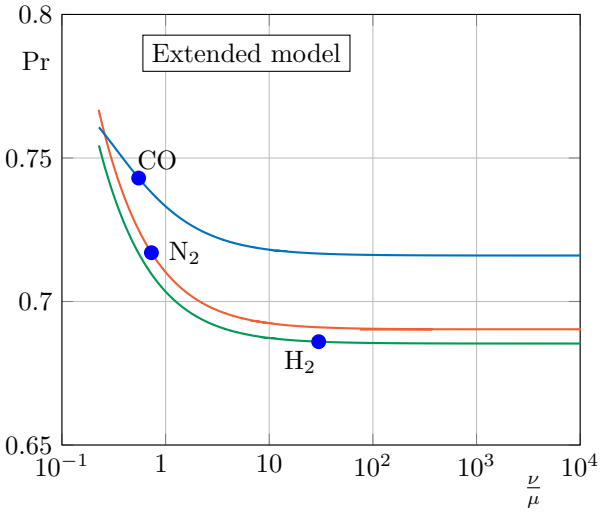

Figure 4.3: Parametric plot of the Prandtl number and ratio of bulk and shear viscosities as a function of $\omega \in [0, 1]$, for other extended model parameters set as in Table 4.4. Blue points represent experimental values for the pair (ratio of bulk and shear viscosities $\frac{\nu}{\mu}$, Prandtl number Pr).

convergence of the moment approximation cascade.

Figure 4.4 also highlights the significance of the frozen part of the collision operator in achieving lower Prandtl number values. The case of $\omega = 1$, $\eta = 1$ is analyzed in [18], showing deviation even from the Eucken formula (4.4.3), which is often regarded as a benchmark.

To obtain a more refined understanding, we examine the relative difference between the Prandtl number estimates:

$$\frac{|\mathrm{Pr}^{(14)} - \mathrm{Pr}^{(17)}|}{\mathrm{Pr}^{(14)}} \tag{4.6.1}$$

as a function of the two primary parameters ω and η. The results are presented as contour plots with logarithmic scaling in Figure 4.6, for fixed $\delta = 2$, $\zeta = 0.5$, and different values of $\eta_{\mathrm{f}} \in \{0, 0.2, 1, 2\}$. In all cases, a blue region emerges where the relative error is minimal for specific combinations of η and ω. Note that cases with zero relative error are not visible in Figure 4.6 due to the logarithmic scale. In order to close the model—meaning that all parameters in the collision kernel (4.1.3) are fully specified after initially fixing δ and ζ—the parameters ω, η, and η_{f} can be chosen such that both moment systems yield the same estimates for the transport coefficients. However, this choice influences the range of Prandtl numbers that can be approximated. Figure 4.5 illustrates the possible values of the Prandtl number for selected values of ζ within the interval $[0.4, 0.7]$, assuming a fixed $\delta = 2$, under the constraint that the relative error (4.6.1) is less than 10^{-4}. The yellow region in the figure is generated by varying

gas	N_2	CO	H_2
ω	0.312052	0.540506	0.0101187
$\hat{\eta}$	-0.3	-0.453	-0.453
$\hat{\eta}_f$	-0.207793	0.570111	-0.133879
$\hat{\zeta}$	0.965	0.965	0.965
$\hat{\zeta}_f$	0.3	0.965	0.965

Table 4.4: One possible combination of free collision kernel (4.2.1) parameters that provides matching with experimental data for the Prandtl number and for the ratio of bulk and shear viscosities. Viscosity exponent s_{visc} and number of internal degrees of freedom δ are given in Table 4.1.

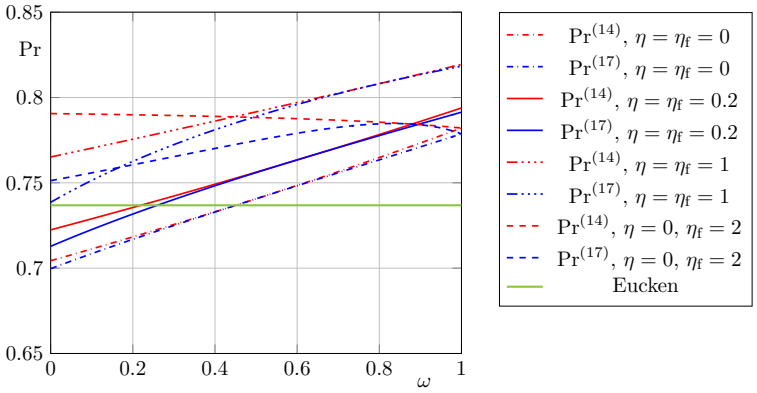

Figure 4.4: Possible values of the two estimates for the Prandtl number for specific choices of parameters plotted over ω. We use $\delta = 2$ and $\zeta = 0.5$. All red curves correspond to Prandtl numbers from 14-moment equations and blue ones from 17-moment equations. For some specific choices of parameters both estimates give the same value.

gas	CO
δ	2.01
ζ	0.53
ω	0.295533
η	0.762079
η_f	0.00104185
relative error (4.6.1)	0.000398379

Table 4.5: Fit for the parameters in the initial collision kernel that minimizes the relative error between two Prandtl numbers and simultaneously produces the experimental values of the Prandtl number and ratio of the shear and bulk viscosities $\frac{\nu}{\mu}$.

$0 \leq \omega \leq 1$ and $0 \leq \eta, \eta_f \leq 2$, and then retaining only those parameter combinations where the relative absolute error between the two Prandtl number estimates is below

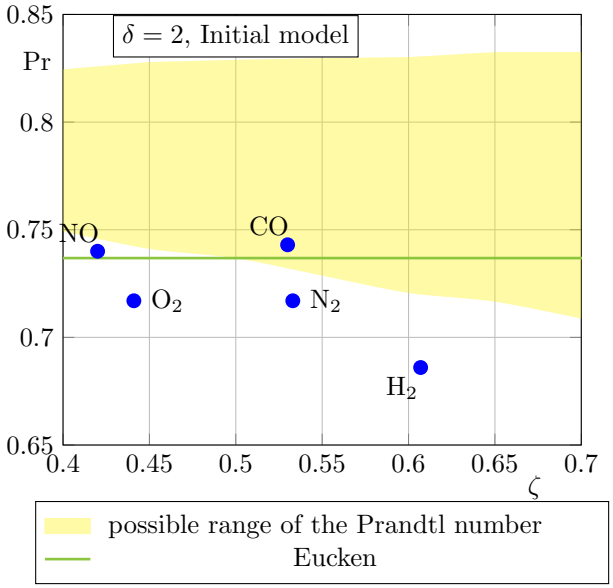

Figure 4.5: Possible values of the Prandtl number that can be estimated with 14-moment and 17-moment equations simultaneously with relative error lower than 10^{-4}. The yellow area is produced by fixing the value $\delta = 2$ on the abcissa while varying $0 \leq \omega \leq 1$, $0 \leq \eta, \eta_f \leq 2$ and then selecting the values of the Prandtl number for which relative error between the two estimates is smaller than 10^{-4}. The parameters of the collision kernel allow to find cases that provide matching estimates from 14-moment and 17-moment equations, and at the same time provide the flexibility to choose the value of the Prandtl number in the yellow area. The blue dots represent experimental values from Table 4.2.

10^{-4} for each selected ζ.

These collision kernel parameters allow for the identification of cases in which the 14- and 17-moment systems produce matching estimates of transport coefficients while still allowing flexibility in the value of the Prandtl number. However, as shown in Figure 4.5, such matching is not always possible for the initial model. For instance, in the case of CO gas, we identify parameters such that the relative error (4.6.1) is negligible, and both moment systems reproduce the experimental Prandtl number to within rounding error. This is achieved through a minimization procedure subject to constraints that require both moment systems to produce the same Prandtl number and match the experimental value of the viscosity ratio. The results are presented in Table 4.5. Note that the values of ζ and δ are selected based on the shear viscosity fit and heat capacity, respectively.

A similar procedure can be performed for the extended collision kernel, which includes additional free parameters $\hat{\eta}$, $\hat{\eta}_f$, $\hat{\zeta}$, and $\hat{\zeta}_f$, in addition to the ζ obtained from the shear

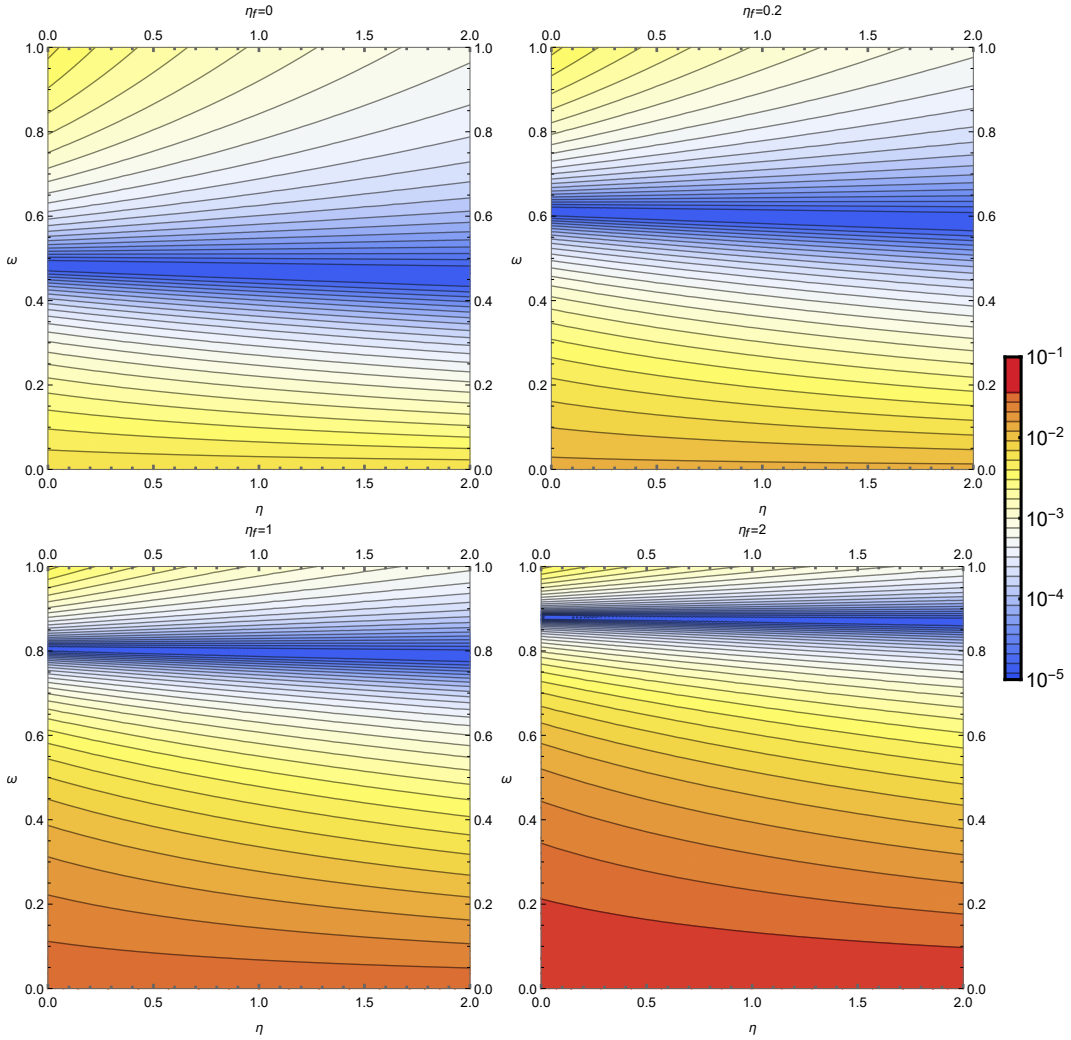

Figure 4.6: Absolute relative error between the two estimates for the Prandtl number obtained by the 14- and 17-moment system for different choices of the parameter $\eta_\mathrm{f} = \{0, 0.2, 1, 2\}$ plotted by color contours on a logarithmic scale. Here we use $\zeta = 0.5$ and $\delta = 2$. In all cases vanishing errors are achieved for specific pairs (η, ω), however showing little dependency on the value for η. Note that the contour where the error is zero is not visible due to cut-off of the logarithmic scale.

viscosity fit. By varying these free parameters and collecting those configurations for which the relative error in the Prandtl number is below 10^{-4}, we obtain the region shown in Figure 4.7. It is evident that the extended model enables to recover experimental Prandtl numbers as well. Using a minimization routine implemented in *Mathematica*, we enforce constraints to match the experimental values of both the Prandtl number and the viscosity ratio ν/μ. The results are provided in Table 4.6.

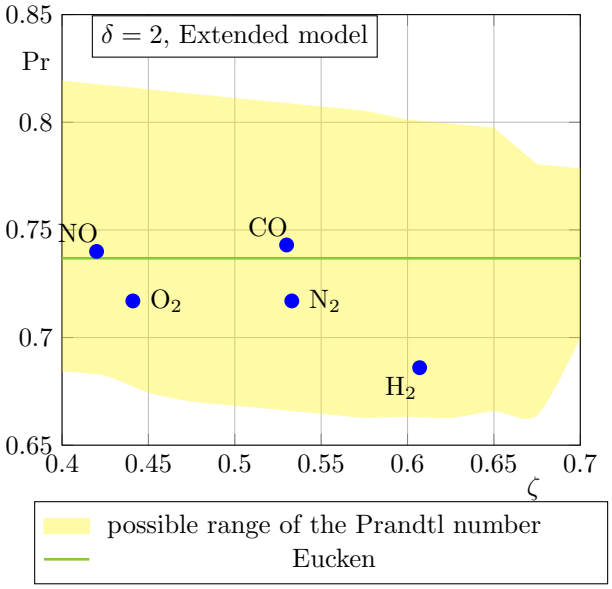

Figure 4.7: Possible val ues of the Prandtl number that can be estimated with 14-moment and 17-moment equations simultaneously with relative error lower than 10^{-4}. The yellow area is produced by fixing the value $\delta = 2$ on the abscissa while varying $0 \leq \omega \leq 1$, $-1/2 \leq \hat{\eta}, \hat{\eta}_f \leq 2$, $0 \leq \hat{\zeta}, \hat{\zeta}_f \leq 2$ and then selecting the values of the Prandtl number for which relative error between the two estimates is smaller than 10^{-4}. The parameters of the collision kernel allow to find cases that provide matching estimates from 14-moment and 17-moment equations, and, at the same time, provide the flexibility to choose the value of the Prandtl number in the yellow area. The blue dots represent experimental values from Table 4.2.

gas	N_2	CO	H_2
δ	2.01	2.01	1.94
ζ	0.533	0.53	0.607
ω	0.295824	0.42322	0.00363119
$\hat{\eta}$	0.273253	0.358118	0.460997
$\hat{\eta}_f$	-0.271329	0.217425	-0.310027
$\hat{\zeta}$	0.834	1.11093	1.01831
$\hat{\zeta}_f$	1.36301	1.19048	0.0838794
relative error (4.6.1)	$6.35256*10^{-6}$	0.000811569	0.00197874

Table 4.6: The combination of free collision kernel (4.2.1) parameters that provides matching with experimental data for the Prandtl number and for the ratio of bulk and shear viscosities. The fit minimizes the relative error between 17 and 14 moment approximation of the Prandtl number with constrains on reconstructing experimental values.

Chapter 5

Regularized moment equations

The ratio of the mean free path of the gas molecules to the characteristic length scale is called the Knudsen number, and it characterizes the extent to which non-equilibrium effects dominate in a gas. For small Knudsen numbers (Kn < 0.01), the flow is in the continuum regime, and the classical Navier–Stokes–Fourier (NSF) equations are valid [35]. To model flows in the transition regime ($0.01 <$ Kn < 1), higher-order models derived from the Boltzmann equation are employed. Two well-known approaches for this derivation are the Chapman–Enskog expansion and the Grad moment method.

The Chapman–Enskog method expands the distribution function in powers of the Knudsen number, yielding the Euler equations at zeroth order, the NSF equations at first order, the Burnett equations at second order, and the super-Burnett equations at third order [47, 2]. Unfortunately, higher-order equations such as the Burnett equations are linearly unstable for processes involving short wavelengths or high frequencies, and thus cannot be used reliably in numerical simulations [36, 42]. To address this, some authors have proposed modifications to the Burnett equations to improve their stability [40].

On the other hand, the Grad method yields a system of moment equations, which typically suffers from issues of hyperbolicity. For example, in the monatomic Grad 13-moment system, the equilibrium state does not lie within the hyperbolicity region [11]. To improve hyperbolicity, regularization techniques—consisting of additional terms added to the moment equations—have been developed [42].

Regarding polyatomic gases, Rahimi and Struchtrup derived the regularized 18-moment equations based on the Bhatnagar–Gross–Krook (BGK) collision operator

$$Q(f,f)_{BGK} = -\frac{1}{\tau}(f - f_E). \tag{5.0.1}$$

However, this operator is known to give incorrect Prandtl numbers and inaccurate relaxation times for higher moments [34]. This work was extended using the two term BGK-type collision operator, resulting in a regularized 19-moment system derived via the order-of-magnitude method [42].

In this thesis, we derive the regularized 17-moment equations (3.5.1) using the regularization method proposed in [42]. To begin, we introduce new variables that describe the deviation of higher-order fluxes from their Grad-17 values:

$$\begin{pmatrix} m_{ijk} \\ R_{ij} \\ \mathcal{R} \\ S_{ik} \\ \mathcal{S} \end{pmatrix} = \int_{\mathbb{R}^3\times[0,\infty)} \begin{pmatrix} mc_{\langle i}c_jc_{k\rangle} \\ m(|c|^2-7\theta)c_{\langle i}c_{j\rangle} \\ m(|c|^4-10\theta|c|^2+15\theta^2) \\ \left(I-m\frac{\delta}{2}\theta\right)c_{\langle i}c_{j\rangle} \\ |c|^2I-3\theta I-m\frac{\delta}{2}\left(\theta|c|^2-3\theta^2\right) \end{pmatrix} f\,\mathrm{d}c\,\mathrm{d}I, \qquad i,j\in\{1,2,3\}. \tag{5.0.2}$$

After adding the fluxes in (5.0.2) into the 17-moment system (3.5.1) and rewriting it, we obtain the following nonlinear system

$$\begin{aligned}
&\partial_t\rho+\partial_{x_j}(\rho U_j)=0,\\
&\rho\partial_tU_i+\partial_{x_i}(\rho\theta_{tr})+\rho U_k\partial_{x_k}U_i+\partial_{x_k}\sigma_{ik}=0,\\
&\partial_t\sigma_{ij}+2\rho\theta_{tr}\frac{\partial U_{\langle j}}{\partial x_{i\rangle}}+\frac{4}{5}\frac{\partial q_{\langle i}}{\partial x_{j\rangle}}+\partial_{x_k}\left(U_k\sigma_{ij}+m_{ijk}\right)+2\sigma_{k\langle i}\frac{\partial U_{j\rangle}}{\partial x_k}=P_{\langle ij\rangle},\\
&\rho\frac{3}{2}\partial_t\theta_{tr}+\rho\theta_{tr}\partial_{x_k}U_k+\frac{3}{2}\rho U_k\partial_{x_k}\theta_{tr}+\partial_{x_k}q_k+\frac{3}{2}\sigma_{kj}\partial_{x_k}U_j=P,\\
&\rho\frac{\delta}{2}\partial_t\theta_{int}+\frac{\delta}{2}\rho U_k\partial_{x_k}\theta_{int}+\partial_{x_k}s_k=-P,\\
&\partial_tq_i-\frac{5}{2}\theta_{tr}\left(\partial_{x_k}\sigma_{ik}+\partial_{x_i}(\rho\theta_{tr})\right)-\frac{1}{\rho}\sigma_{ik}\partial_{x_k}(\rho\theta_{tr})+q_k\partial_{x_k}U_i\\
&\quad+\partial_{x_k}\left(q_iU_k+\frac{1}{2}R_{ik}+\frac{7}{2}\theta\sigma_{ik}+\delta_{ik}\left\{\frac{5\rho\theta}{2}(2\theta_{tr}-\theta)+\frac{1}{6}\mathcal{R}\right\}\right)\\
&\quad-\frac{1}{\rho}\sigma_{ij}\partial_{x_k}\sigma_{kj}+\left(m_{ijk}+\frac{6}{5}q_{(i}\delta_{j)k}\right)\partial_{x_k}U_j=Q_i-U_iP,\\
&\partial_ts_i+\frac{\delta}{2}\theta_{int}\left(-\partial_{x_k}\sigma_{ki}-\partial_{x_i}(\rho\theta_{tr})\right)+s_k\partial_{x_k}U_i\\
&\quad+\partial_{x_k}\left(S_{ik}+\frac{\delta}{2}\sigma_{ik}\theta+\delta_{ik}\left\{\frac{\delta\rho\theta(\theta_{tr}+\theta_{int}-\theta)}{2}+\frac{1}{3}\mathcal{S}\right\}+U_ks_i\right)=S_i+U_iP,
\end{aligned} \tag{5.0.3}$$

where the production are

$$\begin{pmatrix} P_{\langle ij\rangle} \\ P \\ Q_i \\ S_i \end{pmatrix} = \int_{\mathbb{R}^3\times[0,\infty)} \begin{pmatrix} mc_{\langle i}c_{j\rangle} \\ \frac{m}{2}|c|^2 \\ \frac{m}{2}|c|^2c_i \\ Ic_i \end{pmatrix} Q(f,f)\,\mathrm{d}I\,\mathrm{d}c. \tag{5.0.4}$$

Using the Grad-17 distribution function from [19, 21],

$$f_{17} = \frac{\rho}{m}\frac{I^{\frac{\delta}{2}-1}e^{-\frac{|c|^2}{2\theta}-\frac{I}{\theta m}}}{(2\pi\theta)^{3/2}\,\Gamma\left(\frac{\delta}{2}\right)(m\theta)^{\frac{\delta}{2}}}\left(1-\frac{c\cdot(q+s)}{\theta^2\rho}+\frac{\sigma_{ij}}{2\theta^2\rho}c_{\langle i}c_{j\rangle}\right.$$
$$\left.-\frac{\delta(\theta_{int}-\theta_{tr})}{m\theta^2(\delta+3)}\left\{\frac{m}{2}|c|^2-\frac{3}{\delta}I\right\}+\frac{|c|^2c\cdot q}{5\theta^3\rho}+\frac{2Ic\cdot s}{\delta\theta^3m\rho}\right), \quad (5.0.5)$$

regularization fluxes defined in (5.0.2) vanish.

To obtain a linearized version of the regularized 17-moment system, we expand the variables around a reference equilibrium state:

$$\rho=\rho_0+\epsilon\tilde{\rho},\quad U=\epsilon\tilde{U},\quad \theta_{tr}=\theta_0+\epsilon\tilde{\theta}_{tr},\quad \theta_{int}=\theta_0+\epsilon\tilde{\theta}_{int}, \quad (5.0.6)$$
$$\sigma=\epsilon\tilde{\sigma},\quad q=\epsilon\tilde{q},\quad s=\epsilon\tilde{s},\quad m_{ijk}=\epsilon\tilde{m}_{ijk},\quad R_{ij}=\epsilon\tilde{R}_{ij}, \quad (5.0.7)$$
$$\mathcal{R}=\epsilon\tilde{\mathcal{R}},\quad S_{ij}=\epsilon\tilde{S}_{ij},\quad \mathcal{S}=\epsilon\tilde{\mathcal{S}}. \quad (5.0.8)$$

After removing the tildes and assuming linearization, the system becomes

$$\begin{aligned}
&\partial_t\rho+\rho_0\partial_{x_k}U_k=0,\\
&\rho_0\partial_tU_i+\partial_{x_i}(\rho_0\theta_{tr}+\theta_0\rho)+\partial_{x_k}\sigma_{ik}=0,\\
&\partial_t\sigma_{ij}+2\rho_0\theta_0\partial_{\langle i}U_{j\rangle}+\frac{4}{5}\partial_{\langle j}q_{i\rangle}+\partial_{x_k}m_{ijk}=-\frac{\rho_0}{m}(\theta_0)^{\zeta/2}P_\sigma\sigma_{ij},\\
&\frac{3}{2}\rho_0\partial_t\theta_{tr}+\rho_0\theta_0\partial_{x_k}U_k+\partial_{x_k}q_k=-\frac{\rho_0}{m}(\theta_0)^{\zeta/2}(P_\theta\theta_{tr}-P_\theta\theta_{int}),\\
&\frac{\delta}{2}\rho_0\partial_t\theta_{int}+\partial_{x_k}s_k=-\frac{\rho_0}{m}(\theta_0)^{\zeta/2}(P_\theta\theta_{int}-P_\theta\theta_{tr}),\\
&\partial_tq_i+\frac{5}{2}\theta_0\rho_0\partial_{x_i}\theta_{tr}+\theta_0\partial_{x_k}\sigma_{ik}+\frac{1}{2}\partial_{x_k}R_{ik}+\frac{1}{6}\partial_{x_i}\mathcal{R}=-\frac{\rho_0}{m}(\theta_0)^{\zeta/2}\left(P_q^{(0)}q-P_q^{(1)}s\right),\\
&\partial_ts_i+\frac{\delta}{2}\theta_0\rho_0\partial_{x_i}\theta_{int}+\partial_{x_k}S_{ik}+\frac{1}{3}\partial_{x_i}\mathcal{S}=-\frac{\rho_0}{m}(\theta_0)^{\zeta/2}\left(P_s^{(0)}s-P_s^{(1)}q\right),
\end{aligned}$$

where P_σ, $P_s^{(1)}$, $P_s^{(0)}$, $P_q^{(1)}$ and $P_q^{(0)}$ are the collision coefficients from (4.4.15) with

$$P_\theta=\frac{3}{2}\frac{\delta}{\delta+3}P_\Pi.$$

Next, we introduce dimensionless variables

$$\hat{x}_i:=\frac{x_i}{L},\quad \hat{t}:=\frac{t}{t_0},\quad \hat{\rho}:=\frac{\rho}{\rho_0},\quad \hat{\theta}_{tr}:=\frac{\theta_{tr}}{\theta_0},\quad \hat{\theta}_{int}:=\frac{\theta_{int}}{\theta_0},\quad \hat{U}_i:=\frac{U_i}{\sqrt{\theta_0}}, \quad (5.0.9)$$

which yields the reference scalings

$$\begin{aligned}
&\hat{\sigma}_{ij}=\frac{\sigma_{ij}}{\rho_0\theta_0},\quad \hat{q}_i=\frac{q_i}{\rho_0\theta_0\sqrt{\theta_0}},\quad \hat{s}_i=\frac{s_i}{\rho_0\theta_0\sqrt{\theta_0}},\quad \hat{m}_{ijk}=\frac{m_{ijk}}{\rho_0\theta_0\sqrt{\theta_0}},\\
&\hat{R}_{ij}=\frac{R_{ij}}{\rho_0\theta_0^2},\quad \hat{\mathcal{R}}=\frac{\mathcal{R}}{\rho_0\theta_0^2},\quad \hat{S}_{ij}=\frac{S_{ij}}{\rho_0\theta_0^2},\quad \hat{\mathcal{S}}=\frac{\mathcal{S}}{\rho_0\theta_0^2}.
\end{aligned} \quad (5.0.10)$$

Assuming $\frac{t_0\sqrt{\theta_0}}{L} = 1$, we define the Knudsen number as

$$\mathrm{Kn} = \frac{\sqrt{\theta_0}}{L\frac{\rho_0}{m}(\theta_0)^{\zeta/2}P_\sigma} = \frac{\sqrt{\theta_0}}{L}\frac{\mu(T_0)}{p_0}. \tag{5.0.11}$$

Finally, under steady-state conditions and omitting hats, the linearized regularized 17-moment system becomes

$$\begin{aligned}
\nabla\cdot U &= 0,\\
\nabla\mathscr{P} + \nabla\cdot\sigma &= 0,\\
2(\nabla U)_{\mathrm{stf}} + \frac{4}{5}(\nabla q)_{\mathrm{stf}} + \nabla\cdot m &= -\frac{1}{\mathrm{Kn}}\sigma,\\
\nabla\cdot q &= -\frac{K_\theta}{\mathrm{Kn}}(\theta_{tr}-\theta_{int}),\\
\frac{5}{2}\nabla\theta_{tr} + \nabla\cdot\sigma + \frac{1}{2}\nabla\cdot R + \frac{1}{6}\nabla\mathcal{R} &= -\frac{1}{\mathrm{Kn}}(P_q q - \tfrac{5}{2}P_{qs}s),\\
\nabla\cdot s &= -\frac{K_\theta}{\mathrm{Kn}}(\theta_{int}-\theta_{tr}),\\
\frac{\delta}{2}\nabla\theta_{int} + \nabla\cdot S + \frac{1}{3}\nabla\mathcal{S} &= -\frac{1}{\mathrm{Kn}}(P_s s - \tfrac{\delta}{2}P_{qs}q).
\end{aligned} \tag{5.0.12}$$

Here we used $\nabla\mathscr{P} = \nabla(p+\Pi) = \nabla(\rho\theta_{tr})$ that is after linearization and scaling with $\rho_0\theta_0$ equivalent to $\nabla\theta_{tr} + \nabla\rho$. The scaled coefficients in system (5.0.12) are

$$K_\theta = \frac{3}{2}\frac{\delta}{\delta+3}\frac{P_\Pi}{P_\sigma} = \left(\frac{\delta}{\delta+3}\right)^2\frac{\mu}{\nu}, \quad P_q = \frac{P_q^{(0)}}{P_\sigma}, \quad P_s = \frac{P_s^{(0)}}{P_\sigma}, \quad P_{qs} = \frac{2P_q^{(1)}}{5P_\sigma}.$$

However, the system (5.0.12) is not closed. To compute closures in the equations for the higher-order fluxes in (5.0.2), we employ the BGK collision operator. This provides a starting model that can later be refined by using the full Boltzmann collision operator (2.2.11), although it will introduces additional coupling.

In order to compute the closure, the moment equations for the fluxes (5.0.2) will be employed. Since we are aiming for the linear version of the regularized 17-moment

equations, after performing linearization, the resulting moment equations take the form

$$\begin{aligned}
&\partial_t m_{ijk} + 3\theta_0 \frac{\partial \sigma_{\langle ij}}{\partial x_{k\rangle}} + \frac{3}{7}\frac{\partial R_{\langle ij}}{\partial x_{k\rangle}} = -\frac{1}{\tau} m_{ijk},\\
&\partial_t R_{ij} + 2\theta_0 \partial_{x_k} m_{ijk} + \theta_0 \frac{28}{5}\frac{\partial q_{\langle i}}{\partial x_{j\rangle}} = -\frac{1}{\tau} R_{ij},\\
&\partial_t \mathcal{R} + 8\theta_0 \partial_{x_k} q_k = -\frac{1}{\tau}\mathcal{R},\\
&\partial_t S_{ij} + 2\theta_0 \frac{\partial s_{\langle i}}{\partial x_{j\rangle}} = -\frac{1}{\tau} S_{ij},\\
&\partial_t \mathcal{S} + 2\theta_0 \partial_{x_k} s_k = -\frac{1}{\tau}\mathcal{S},
\end{aligned} \tag{5.0.13}$$

where the BGK operator (5.0.1) is used as the collision model. Assuming that the regularization fluxes (5.0.2) relax more faster than the standard 17 moments, i.e., σ_{ij} and q_i, a small parameter $\epsilon \ll 1$ is introduced on the right-hand side of system (5.0.13), yielding

$$\begin{aligned}
&\partial_t m_{ijk} + 3\theta_0 \frac{\partial \sigma_{\langle ij}}{\partial x_{k\rangle}} + \frac{3}{7}\frac{\partial R_{\langle ij}}{\partial x_{k\rangle}} = -\frac{1}{\tau\epsilon} m_{ijk},\\
&\partial_t R_{ij} + 2\theta_0 \partial_{x_k} m_{ijk} + \theta_0 \frac{28}{5}\frac{\partial q_{\langle i}}{\partial x_{j\rangle}} = -\frac{1}{\tau\epsilon} R_{ij},\\
&\partial_t \mathcal{R} + 8\theta_0 \partial_{x_k} q_k = -\frac{1}{\tau\epsilon}\mathcal{R},\\
&\partial_t S_{ij} + 2\theta_0 \frac{\partial s_{\langle i}}{\partial x_{j\rangle}} = -\frac{1}{\tau\epsilon} S_{ij},\\
&\partial_t \mathcal{S} + 2\theta_0 \partial_{x_k} s_k = -\frac{1}{\tau\epsilon}\mathcal{S}.
\end{aligned} \tag{5.0.14}$$

Now, the equations (5.0.14) are expanded in terms of the small parameter ϵ

$$\begin{aligned}
m_{ijk} = m_{ijk}^{(0)} + \epsilon m_{ijk}^{(1)} + \cdots, \quad R_{ij} = R_{ij}^{(0)} + \epsilon R_{ij}^{(1)} + \cdots, \quad \mathcal{R} = \mathcal{R}^{(0)} + \epsilon \mathcal{R}^{(1)} + \cdots,\\
S_{ij} = S_{ij}^{(0)} + \epsilon S_{ij}^{(1)} + \cdots, \quad \mathcal{S} = \mathcal{S}^{(0)} + \epsilon \mathcal{S}^{(1)} + \cdots.
\end{aligned}$$

Balancing the terms of order $\mathcal{O}(\frac{1}{\epsilon})$ yields the zeroth-order approximation:

$$m_{ijk}^{(0)} = R_{ij}^{(0)} = \mathcal{R}^{(0)} = S_{ij}^{(0)} = \mathcal{S}^{(0)} = 0, \tag{5.0.15}$$

while balancing the terms of order $\mathcal{O}(1)$ (i.e., ϵ^0) leads to

$$\begin{aligned}
&\left[\partial_t m_{ijk} + 3\theta_0 \frac{\partial \sigma_{\langle ij}}{\partial x_{k\rangle}} + \frac{3}{7}\frac{\partial R_{\langle ij}}{\partial x_{k\rangle}}\right]_{|f_{17}} = -\frac{1}{\tau} m^{(1)}_{ijk},\\
&\left[\partial_t R_{ij} + 2\theta_0 \partial_{x_k} m_{ijk} + \theta_0 \frac{28}{5}\frac{\partial q_{\langle i}}{\partial x_{j\rangle}}\right]_{|f_{17}} = -\frac{1}{\tau} R^{(1)}_{ij},\\
&\left[\partial_t \mathcal{R} + 8\theta_0 \partial_{x_k} q_k\right]_{|f_{17}} = -\frac{1}{\tau}\mathcal{R}^{(1)},\\
&\left[\partial_t S_{ij} + 2\theta_0 \frac{\partial s_{\langle i}}{\partial x_{j\rangle}}\right]_{|f_{17}} = -\frac{1}{\tau} S^{(1)}_{ij},\\
&\left[\partial_t \mathcal{S} + 2\theta_0 \partial_{x_k} s_k\right]_{|f_{17}} = -\frac{1}{\tau}\mathcal{S}^{(1)}.
\end{aligned} \tag{5.0.16}$$

Evaluating the left-hand sides using the distribution function (5.0.5), setting the $\epsilon = 1$ and using definitions (5.0.9)- (5.0.10) yields the following closure relations

$$\begin{aligned}
m = m^{(1)} &= -3\,\mathrm{Kn}\,(\nabla\sigma)_{\mathrm{stf}}\,,\\
R = R^{(1)} &= -\mathrm{Kn}\frac{28}{5}\,(\nabla q)_{\mathrm{stf}}\,,\\
\mathcal{R} = \mathcal{R}^{(1)} &= -8\,\mathrm{Kn}\,\nabla\cdot q,\\
S = S^{(1)} &= -2\,\mathrm{Kn}\,(\nabla s)_{\mathrm{stf}}\,,\\
\mathcal{S} = \mathcal{S}^{(1)} &= -2\,\mathrm{Kn}\,\nabla\cdot s.
\end{aligned} \tag{5.0.17}$$

Here, the subscript "stf" denotes the symmetric trace-free part of a tensor. In the following, we shall refer to equations (5.0.12) and (5.0.17) as the R17 equations, where "R" stands for "regularized," and 17 denotes the number of variables.

It is worth noting that the subsystem $(\mathscr{P}, U, \theta_{tr}, \sigma, q)$ follows a structure similar to that presented in [42, 43], but with different closure relations. Setting the regularization terms in (5.0.2) to zero recovers the standard 17-moment polyatomic equations (3.5.1). Thus, regularization can be interpreted as a specific type of closure for the Grad 17 system, analogous to how the Navier–Stokes–Fourier equations act as a regularization of the Euler equations, as discussed in [42].

In order to perform numerical simulations, one must equip the system with appropriate boundary conditions. Here, we consider that the distribution function on the boundary, with normal vector n and tangential vector t, satisfies the Maxwell accommodation model, which is given by

$$f(v_n, v_t) = \begin{cases} \chi f_w(v_n, v_t) + (1-\chi) f(-v_n, v_t), & \text{if } v\cdot n > 0,\\ f(v_n, v_t), & \text{if } v\cdot n < 0, \end{cases}$$

where the parameter χ controls the ratio of particles accommodated on the wall with distribution function f_W and those reflected. From this, we can extract the odd part of the distribution function with respect to the normal direction, which is

$$f^{(\text{odd})}(v_n, v_t) = \begin{cases} \chi\left(f_v(v_n, v_t) - f^{(\text{even})}(v_n, v_t)\right) - (1-\chi) f^{(\text{odd})}(v_n, v_t), & \text{if } v \cdot n > 0, \\ f^{(\text{odd})}(v_n, v_t), & \text{if } v \cdot n < 0. \end{cases}$$

Using the same argument of decomposition into odd and even parts of the distribution function, we define a polynomial to be odd with respect to the normal direction as

$$\psi^{(\text{odd})}(c, I) = \Big(mc_n, mc_n c_t, \frac{m}{2}|c|^2 c_n, mc_{\langle n} c_n c_{n\rangle}, mc_{\langle n} c_t c_{t\rangle}, \\ m(|c|^2 - 7\theta) c_{\langle n} c_{t\rangle}, Ic_n, \left(I - m\frac{\delta}{2}\theta\right) c_{\langle n} c_{t\rangle}\Big)^T \quad (5.0.18)$$

and similarly define the even part as

$$\psi^{(\text{even})}(c, I) = \Big(m, mc_t, \frac{m}{2}|c|^2, mc_{\langle n} c_{n\rangle}, mc_{\langle t} c_{t\rangle}, \frac{m}{2}|c|^2 c_t, \\ mc_{\langle n} c_n c_{t\rangle}, mc_{\langle t} c_t c_{t\rangle}, m(|c|^4 - 10\theta|c|^2 + 15\theta^2), m(|c|^2 - 7\theta) c_{\langle n} c_{n\rangle}, \\ m(|c|^2 - 7\theta) c_{\langle t} c_{t\rangle}, I, Ic_t, \left(I - m\frac{\delta}{2}\theta\right) c_{\langle n} c_{n\rangle}, \\ \left(I - m\frac{\delta}{2}\theta\right) c_{\langle t} c_{t\rangle}, |c|^2 I - 3\theta I - m\tfrac{\delta}{2}\left(\theta|c|^2 - 3\theta^2\right)\Big)^T. \quad (5.0.19)$$

With this, we define a moment variable as odd with respect to the velocity component in the normal direction if it is generated using the odd polynomial $\psi^{(\text{odd})}(c, I)$. Conversely, a moment is even if it is the projection of the distribution function f using $\psi^{(\text{even})}(c, I)$

$$\mathcal{U}^{(\text{odd})} := \int_{\mathbb{R}^3 \times [0,\infty)} \psi^{(\text{odd})}(c, I) f \,\mathrm{d}c \,\mathrm{d}I, \quad \mathcal{U}^{(\text{even})} := \int_{\mathbb{R}^3 \times [0,\infty)} \psi^{(\text{even})}(c, I) f \,\mathrm{d}c \,\mathrm{d}I. \quad (5.0.20)$$

Therefore, on the boundary, odd moment variables are related to even ones through the relation

$$\int_{\mathbb{R}^3 \times [0,\infty)} \psi^{(\text{odd})}(c, I) f \,\mathrm{d}c \,\mathrm{d}I = \\ \frac{2\chi}{2-\chi} \int_{\mathbb{R}^2 \times [0,\infty)^2} \psi^{(\text{odd})}(c, I) \left(f_w - f^{(\text{even})}(c, I)\right) \mathrm{d}c_t \,\mathrm{d}c_n \,\mathrm{d}I. \quad (5.0.21)$$

For the particles accommodated on the boundary, we use the Maxwell distribution

$$f_w(v, I) = \frac{\rho_w}{m(m\theta^w)^{\delta/2}\Gamma(\delta/2)} \left(\frac{1}{2\pi\theta^w}\right)^{3/2} I^{\delta/2-1} \exp\left(-\frac{1}{\theta^w}\left(\frac{1}{2}|v - U^w|^2 + \frac{I}{m}\right)\right), \quad (5.0.22)$$

where ρ_w is the mass density, θ^w is the temperature, and U^w is the velocity on the boundary. Note that the values in f_w do not necessarily correspond to the physical temperature or velocity at the boundary. In particular, ρ_w can be considered as a fictitious parameter, which may be determined from other moments to ensure that, for instance, $U_n = 0$.

The procedure described above yields nonlinear boundary conditions. However, since we are aiming for a linear boundary condition compatible with the weak formulation of the R17 system, a linearized approach is necessary.

As noted in the work of Bünger et al., the boundary conditions given in (5.0.21), after linearization, are not always entropy stable [10]. Therefore, boundary conditions of the Onsager type are proposed, which take the following form

$$\mathcal{U}^{(\text{odd})} = \frac{2\chi}{2-\chi}\left(L\mathbb{A}\mathcal{U}^{(\text{even})} + G\right), \tag{5.0.23}$$

where the matrix L is symmetric and positive definite.

In the case of polyatomic gases, the matrices $\mathbb{A}$, L, and G take the following specific forms

$$L = \frac{1}{\sqrt{2\pi}}\begin{pmatrix} 1 & 0 & -\frac{1}{2} & -\frac{2}{5} & \frac{1}{5} & 0 & 0 & 0 \\ 0 & 1 & 0 & 0 & 0 & -1 & 0 & 0 \\ -\frac{1}{2} & 0 & \frac{9}{4} & -\frac{1}{5} & \frac{1}{10} & 0 & 0 & 0 \\ -\frac{2}{5} & 0 & -\frac{1}{5} & \frac{56}{25} & -\frac{28}{25} & 0 & 0 & 0 \\ \frac{1}{5} & 0 & \frac{1}{10} & -\frac{28}{25} & \frac{39}{25} & 0 & 0 & 0 \\ 0 & -1 & 0 & 0 & 0 & 13 & 0 & 0 \\ 0 & 0 & 0 & 0 & 0 & 0 & 1 & 0 \\ 0 & 0 & 0 & 0 & 0 & 0 & 0 & 1 \end{pmatrix}, \quad G = \begin{pmatrix} \rho_w \\ U_t^w \\ -2\theta^w \\ \frac{2}{5}\theta^w \\ -\frac{1}{5}\theta^w \\ U_t^w \\ \frac{\delta}{2}\theta^w \end{pmatrix}. \tag{5.0.24}$$

$$\mathbb{A} = \begin{pmatrix} 2 & 0 & 1 & 1 & 0 & 0 & 0 & 0 & 0 & 0 & 0 & 0 & 0 & 0 & 0 & 0 \\ 0 & 1 & 0 & 0 & 0 & \frac{2}{5} & 1 & 0 & 0 & 0 & 0 & 0 & 0 & 0 & 0 & 0 \\ 0 & 0 & 1 & \frac{2}{5} & 0 & 0 & 0 & 0 & \frac{1}{15} & \frac{1}{5} & 0 & 0 & 0 & 0 & 0 & 0 \\ 0 & 0 & 0 & 1 & \frac{1}{2} & 0 & 0 & 0 & 0 & 0 & 0 & 0 & 0 & 0 & 0 & 0 \\ 0 & 0 & 0 & \frac{1}{2} & 1 & 0 & 0 & 0 & 0 & 0 & 0 & 0 & 0 & 0 & 0 & 0 \\ 0 & 0 & 0 & 0 & 0 & \frac{1}{5} & 0 & 0 & 0 & 0 & 0 & 0 & 0 & 0 & 0 & 0 \\ 0 & 0 & 0 & 0 & 0 & 0 & 0 & 0 & 0 & 0 & 0 & \frac{\delta}{2} & 0 & 1 & 0 & \frac{1}{3} \\ 0 & 0 & 0 & 0 & 0 & 0 & 0 & 0 & 0 & 0 & 0 & 0 & 1 & 0 & 0 & 0 \end{pmatrix}. \tag{5.0.25}$$

To eliminate the density ρ_w, we relate it to other moments such that $U_n = 0$ holds at the boundary. This step is equivalent to a single Gauss elimination step applied to the

matrix L. Accordingly, the stable boundary conditions for the R17 system take the form

$$U_n = 0, \tag{5.0.26}$$

$$\sigma_{nt} = \tilde{\chi}\left(U_t - U_t^w + m_{nnt} + \frac{1}{5}q_t\right), \tag{5.0.27}$$

$$q_n = \tilde{\chi}\left(2(\theta_{tr} - \theta^w) + \frac{2}{5}R_{nn} + \frac{2}{15}R + \frac{1}{2}\sigma_{nn}\right), \tag{5.0.28}$$

$$m_{nnn} = \tilde{\chi}\left(-\frac{2}{5}(\theta_{tr} - \theta^w) - \frac{2}{25}R_{nn} - \frac{2}{75}R + \frac{7}{5}\sigma_{nn}\right), \tag{5.0.29}$$

$$m_{ntt} = \tilde{\chi}\left(\frac{1}{5}(\theta_{tr} - \theta^w) + \frac{1}{25}R_{nn} + \frac{1}{75}R - \frac{1}{5}\sigma_{nn} + \sigma_{tt}\right), \tag{5.0.30}$$

$$R_{nt} = \tilde{\chi}\left(-(U_t - U_t^w) - m_{nnt} + \frac{22}{10}q_t\right), \tag{5.0.31}$$

$$s_n = \tilde{\chi}\left(\frac{\delta}{2}(\theta_{int} - \theta^w) + \frac{1}{3}S + S_{nn}\right), \tag{5.0.32}$$

$$S_{nt} = \tilde{\chi}s_t, \tag{5.0.33}$$

where $\tilde{\chi} = \frac{\sqrt{\frac{2}{\pi}}\chi}{\chi - 2}$, and n and t denote the normal and tangential directions, respectively.

However, in cases where one wishes to control inflow or outflow, the trivial boundary condition $U_n = 0$ in (5.0.26) should be replaced with

$$U_n - U_n^w = \tilde{\chi}\tilde{\eta}\left(\mathscr{P} - p^w + \sigma_{nn}\right), \tag{5.0.34}$$

which also ensures the unique solution for the pressure $\mathscr{P}$, since its gradient only contributes to the momentum conservation equation in (5.0.3).

5.1 Derivation of R17 weak formulation

In this section, we derive the variational (weak) formulation of the R17 system of equations. Analyzing the structure of the R17 equations reveals that the system can be divided into two subsystems.

The first five equations in (5.0.12) describe the evolution of variables corresponding to projections onto velocity polynomials—namely, density, velocity, stress, translational temperature, and translational heat flux. We collectively refer to this group as the translational heat flux–stress subsystem.

The remaining two equations in (5.0.12) govern the evolution of internal temperature and internal heat flux, which result from projections involving the internal energy variable I. We refer to these as the internal heat flux subsystem. These two subsystems

are further coupled through production terms appearing on the right-hand side of the equations.

For the translational heat flux–stress subsystem, we adopt the procedure outlined by Theisen et al., as the equations share a similar structure with the regularized 13-moment equations for monatomic gases [43]. The weak formulation is obtained via partial integration, applied to every second equation, starting from the equation involving the highest-order flux, in order to incorporate all relevant boundary conditions. A similar integration strategy is employed for the internal heat flux subsystem.

In this thesis, we focus on the two-dimensional version of the R17 equations, defined over the domain $\Omega \subset \mathbb{R}^2$, and we present the weak formulation for this setting.

We begin by defining the trial function vector as

$$\mathcal{U} = (\theta_{tr}, q, \mathscr{P}, U, \sigma, \theta_{int}, s), \tag{5.1.1}$$

where each variable in $\mathcal{U}$ belongs to a suitable Sobolev space $\mathbb{V}_\star$, such that

$$\mathcal{U} \in \mathbb{H} := \mathbb{V}_{\theta_{tr}} \times \mathbb{V}_q \times \mathbb{V}_{\mathscr{P}} \times \mathbb{V}_U \times \mathbb{V}_\sigma \times \mathbb{V}_{\theta_{int}} \times \mathbb{V}_s.$$

Correspondingly, we define the test function vector as

$$\mathcal{V} := (\phi, r, \tilde{q}, v, \psi, \vartheta, \xi) \in \mathbb{H}.$$

With these definitions established, the derivation of the weak formulation is presented in the subsequent sections.

5.1.1 Weak formulation of the translational heat flux-stress subsystem

Weak formulation of the translational heat flux balance

For the translational heat flux equation, we take a test function $r : \Omega \to \mathbb{R}^2$. Using partial integration, we obtain

$$\begin{aligned}
&\frac{2}{5\mathrm{Kn}} \int_\Omega \left(P_q\, q - \frac{5}{2} P_{qs} s \right) \cdot r \,\mathrm{d}x \\
&\quad - \int_\Omega \theta_{tr} \nabla \cdot r \,\mathrm{d}x + \int_\Gamma (r \cdot n) \theta_{tr} \,\mathrm{d}l - \frac{2}{5} \int_\Omega \nabla r : \sigma \,\mathrm{d}x + \frac{2}{5} \int_\Gamma (\sigma \cdot n) \cdot r \,\mathrm{d}l \\
&\quad - \frac{1}{5} \int_\Omega \nabla r : R \,\mathrm{d}x + \frac{1}{5} \int_\Gamma (R \cdot n) \cdot r \,\mathrm{d}l - \frac{1}{15} \int_\Omega \mathcal{R} \cdot \nabla r \,\mathrm{d}x + \frac{1}{15} \int_\Gamma \mathcal{R} r \cdot n \,\mathrm{d}l = 0.
\end{aligned}$$

Here, the operation ":" denotes second-order tensor contraction, and $\Gamma = \partial\Omega$. The expressions in the boundary integrals can be rewritten as

$$(r \cdot n)\theta_{tr} = \theta_{tr} \begin{pmatrix} r_n \\ r_t \end{pmatrix} \cdot \begin{pmatrix} 1 \\ 0 \end{pmatrix} = \theta_{tr} r_n,$$
$$(r \cdot n)\mathcal{R} = \mathcal{R} \begin{pmatrix} r_n \\ r_t \end{pmatrix} \cdot \begin{pmatrix} 1 \\ 0 \end{pmatrix} = \mathcal{R} r_n,$$

$$(\sigma \cdot n) \cdot r = \begin{pmatrix} \sigma_{nn} & \sigma_{nt} & 0 \\ \sigma_{tn} & \sigma_{tt} & 0 \\ 0 & 0 & -\sigma_{nn} - \sigma_{tt} \end{pmatrix} \begin{pmatrix} 1 \\ 0 \\ 0 \end{pmatrix} \cdot \begin{pmatrix} r_n \\ r_t \\ 0 \end{pmatrix} = \sigma_{nn} r_n + \sigma_{nt} r_t,$$

$$(R \cdot n) \cdot r = \begin{pmatrix} R_{nn} & R_{nt} & 0 \\ R_{tn} & R_{tt} & 0 \\ 0 & 0 & -R_{nn} - R_{tt} \end{pmatrix} \begin{pmatrix} 1 \\ 0 \\ 0 \end{pmatrix} \cdot \begin{pmatrix} r_n \\ r_t \\ 0 \end{pmatrix} = R_{nn} r_n + R_{nt} r_t.$$

After regrouping according to the normal and tangential components of the vector r, we obtain

$$\begin{aligned} &\frac{2}{5\mathrm{Kn}} \int_\Omega \left(P_q\, q - \frac{5}{2} P_{qs} s \right) \cdot r \,\mathrm{d}x \\ &- \int_\Omega \theta_{tr} \nabla \cdot r \,\mathrm{d}x - \frac{2}{5} \int_\Omega \nabla r : \sigma \mathrm{d}x - \frac{1}{5} \int_\Omega \nabla r : R \,\mathrm{d}x - \frac{1}{15} \int_\Omega \mathcal{R} \cdot \nabla r \,\mathrm{d}x \\ &+ \int_\Gamma \left(\left(\theta_{tr} + \frac{1}{5} R_{nn} + \frac{1}{15} \mathcal{R} + \frac{2}{5} \sigma_{nn} \right) r_n + \left(\frac{2}{5} \sigma_{nt} + \frac{1}{5} R_{nt} \right) r_t \right) \mathrm{d}l = 0. \end{aligned}$$

Substituting the boundary condition (5.0.28) and combining (5.0.27) with (5.0.31), we obtain

$$\theta_{tr} + \frac{1}{5} R_{nn} + \frac{1}{15} \mathcal{R} = \theta^w - \frac{1}{4} \sigma_{nn} + \frac{1}{2\tilde{\chi}} q_n, \quad \frac{1}{5} R_{nt} = \tilde{\chi} \frac{12}{5} q_t - \frac{1}{5} \sigma_{nt}.$$

Together with the closure relation, this leads to the weak formulation for the translational heat flux balance

$$\begin{aligned} &\frac{2}{5\mathrm{Kn}} \int_\Omega \left(P_q\, q - \frac{5}{2} P_{qs} s \right) \cdot r \,\mathrm{d}x \\ &- \int_\Omega \theta_{tr} \nabla \cdot r \,\mathrm{d}x - \frac{2}{5} \int_\Omega \nabla r : \sigma \mathrm{d}x + \mathrm{Kn} \frac{28}{25} \int_\Omega \nabla r : (\nabla q)_{\mathrm{stf}} \,\mathrm{d}x + \frac{8}{15} \mathrm{Kn} \int_\Omega (\nabla \cdot q) \cdot (\nabla r) \,\mathrm{d}x \\ &+ \int_\Gamma \left(\left(\frac{3}{20} \sigma_{nn} + \theta^w + \frac{1}{2\tilde{\chi}} q_n \right) r_n + \left(\frac{1}{5} \sigma_{nt} + \tilde{\chi} \frac{12}{5} q_t \right) r_t \right) \mathrm{d}l = 0. \end{aligned}$$

As the terms in the heat flux balance suggest, the weak formulation also reflects coupling with the stress σ_{ij}, translational temperature θ_{tr}, and internal heat flux s_i. For easier identification of this coupling, we define the following functionals

$$\begin{aligned}
a(q,r) &= \frac{2}{5\mathrm{Kn}}\int_\Omega P_q\, q\cdot r\,\mathrm{d}x + \frac{28}{25}\mathrm{Kn}\int_\Omega (\nabla q)_{\mathrm{stf}} : \nabla r\,\mathrm{d}x + \frac{8}{15}\mathrm{Kn}\int_\Omega (\nabla\cdot q)(\nabla\cdot r)\,\mathrm{d}x \\
&\quad + \int_\Gamma \left(\frac{1}{2\tilde{\chi}} q_n r_n + \tilde{\chi}\frac{12}{25} q_t r_t\right)\mathrm{d}l, \\
b(\theta_{tr},r) &= \int_\Omega \theta_{tr}(\nabla\cdot r)\,\mathrm{d}x, \\
a_{12}(r,s) &= \frac{1}{\mathrm{Kn}} P_{qs}\int_\Omega s\cdot r\,\mathrm{d}x, \\
c(\sigma,r) &= \frac{2}{5}\int_\Omega \sigma : \nabla r\,\mathrm{d}x - \int_\Gamma \left(\frac{3}{20}\sigma_{nn} r_n + \frac{1}{5}\sigma_{nt} r_t\right)\mathrm{d}l, \\
l_1(r) &= -\int_\Gamma \theta^w r_n\,\mathrm{d}l,
\end{aligned}$$

This leads to the final weak formulation of the translational heat flux balance in functional form

$$a(q,r) - b(\theta_{tr},r) - c(\sigma,r) - a_{12}(r,s) = l_1(r). \tag{5.1.2}$$

Weak formulation of the translational temperature balance

Using the test function $\phi : \Omega \to \mathbb{R}$, one obtains the bilinear form for the translational temperature equation

$$\int_\Omega (\nabla\cdot q)\,\phi\,\mathrm{d}x + \frac{1}{\mathrm{Kn}}\int_\Gamma K_\theta \theta_{tr}\phi\,\mathrm{d}x - \frac{1}{\mathrm{Kn}}\int_\Gamma K_\theta \theta_{int}\phi\,\mathrm{d}x = 0$$

Defining the functional

$$a_3(\theta_{tr},\phi) = K_\theta \frac{1}{\mathrm{Kn}}\int_\Gamma \theta_{tr}\phi\,\mathrm{d}x$$

and using the functional b, the weak formulation of the translational temperature balance reads

$$b(\phi,q) + a_3(\theta_{tr},\phi) - a_3(\theta_{int},\phi) = 0. \tag{5.1.3}$$

Weak formulation of the stress balance

For the stress balance, we first rescale the equation by a factor of $1/2$. Using the test function $\psi : \Omega \to \mathbb{R}^{3\times 3}_{\text{stf}}$ and applying partial integration leads to

$$\begin{aligned}
&\frac{1}{2\text{Kn}} \int_\Omega \sigma : \psi \,\mathrm{d}x \\
&-\frac{2}{5}\int_\Omega q \cdot (\nabla \cdot \psi)\, \mathrm{d}x - \int_\Omega U \cdot (\nabla \cdot \psi)\,\mathrm{d}x - \frac{1}{2}\int_\Omega m \therefore \nabla\psi \,\mathrm{d}x \\
&+\frac{2}{5}\int_\Gamma (\psi \cdot n)\cdot q \,\mathrm{d}l + \int_\Gamma (\psi \cdot n)\cdot U \,\mathrm{d}l \\
&+\frac{1}{2}\int_\Gamma (m \cdot n) : \psi \,\mathrm{d}l = 0.
\end{aligned} \tag{5.1.4}$$

Here, $\therefore$ denotes the contraction of a third-order tensor with the gradient. The expressions in the boundary integrals can be rewritten as

$$\begin{aligned}
\psi \cdot n &= \begin{pmatrix} \psi_{nn} & \psi_{nt} & 0 \\ \psi_{nt} & \psi_{tt} & 0 \\ 0 & 0 & -(\psi_{nn}-\psi_{tt}) \end{pmatrix} \begin{pmatrix} 1 \\ 0 \\ 0 \end{pmatrix} = \begin{pmatrix} \psi_{nn} \\ \psi_{nt} \\ 0 \end{pmatrix}, \\
(\psi \cdot n)\cdot q &= \begin{pmatrix} \psi_{nn} \\ \psi_{nt} \\ 0 \end{pmatrix} \cdot \begin{pmatrix} q_n \\ q_t \\ 0 \end{pmatrix} = \psi_{nn}q_n + \psi_{nt}q_t, \\
(\psi \cdot n)\cdot U &= \begin{pmatrix} \psi_{nn} \\ \psi_{nt} \\ 0 \end{pmatrix} \cdot \begin{pmatrix} U_n \\ U_t \\ 0 \end{pmatrix} = \psi_{nn}U_n + \psi_{nt}U_t, \\
m \cdot n &= \begin{pmatrix} m_{nnn} & m_{nnt} & 0 \\ m_{nnt} & m_{ntt} & 0 \\ 0 & 0 & -(m_{nnn}+m_{ntt}) \end{pmatrix}, \\
(m \cdot n) : \psi &= \begin{pmatrix} m_{nnn} & m_{nnt} & 0 \\ m_{nnt} & m_{ntt} & 0 \\ 0 & 0 & -(m_{nnn}+m_{ntt}) \end{pmatrix} \begin{pmatrix} \psi_{nn} & \psi_{nt} & 0 \\ \psi_{nt} & \psi_{tt} & 0 \\ 0 & 0 & -(\psi_{nn}+\psi_{tt}) \end{pmatrix} \\
&= m_{nnn}\psi_{nn} + 2m_{nnt}\psi_{nt} + m_{ntt}\psi_{tt} + (-m_{ntt}-m_{nnn})(-\psi_{tt}-\psi_{nn}) \\
&= \frac{3}{2}m_{nnn}\psi_{nn} + 2m_{nnt}\psi_{nt} + 2\left(m_{ntt}+\frac{1}{2}m_{nnn}\right)\left(\psi_{tt}+\frac{1}{2}\psi_{nn}\right).
\end{aligned}$$

After substituting the rewritten boundary integrals, the weak formulation (5.1.4) becomes

$$\begin{aligned}
&\frac{1}{2\mathrm{Kn}}\int_\Omega \sigma : \psi \,\mathrm{d}x - \frac{2}{5}\int_\Omega q\cdot(\nabla\cdot\psi)\,\mathrm{d}x - \int_\Omega U\cdot(\nabla\cdot\psi)\,\mathrm{d}x - \frac{1}{2}\int_\Omega m \mathbin{\therefore} \nabla\psi\,\mathrm{d}x\\
&+\int_\Gamma\left(\left(\frac{3}{4}m_{nnn}+U_n+\frac{2}{5}q_n\right)\psi_{nn}+\left(U_t+m_{nnt}+\frac{2}{5}q_t\right)\psi_{nt}\right)\mathrm{d}l\\
&+\int_\Gamma\left(m_{ntt}+\frac{1}{2}m_{nnn}\right)\left(\psi_{tt}+\frac{1}{2}\psi_{nn}\right)\mathrm{d}l = 0.
\end{aligned}$$

Next, we apply the boundary conditions. We combine conditions (5.0.29) and (5.0.30), and transform the boundary value for σ_{nt} using (5.0.27)

$$\begin{aligned}
U_t + m_{nnt} &= \frac{\sigma_{nt}}{\tilde{\chi}} - \frac{1}{5}q_t + U_t^w, \quad m_{nnt}+\frac{1}{2}m_{nnn} = \tilde{\chi}\left(\frac{1}{2}\sigma_{nn}+\sigma_{tt}\right),\\
\frac{3}{4}m_{nnn}+U_n &= \tilde{\chi}\frac{9}{8}\sigma_{nn} - \frac{3}{20}q_n + U_n^w + \tilde{\eta}\left(\mathscr{P} - p^w + \sigma_{nn}\right).
\end{aligned}$$

After applying these boundary conditions and the closure relations (5.0.17), the final bilinear form of the stress balance becomes

$$\begin{aligned}
&\frac{1}{2\mathrm{Kn}}\int_\Omega \sigma:\psi\,\mathrm{d}x + \mathrm{Kn}\frac{3}{2}\int_\Omega (\nabla\sigma)_{\mathrm{stf}} \mathbin{\therefore} \nabla\psi\,\mathrm{d}x\\
&+\int_\Gamma\left(\tilde{\chi}\left(\frac{1}{2}\sigma_{nn}+\sigma_{tt}\right)\left(\psi_{tt}+\frac{1}{2}\psi_{nn}\right)+\frac{1}{\tilde{\chi}}\sigma_{nt}\psi_{nt}+\left(\tilde{\chi}\frac{9}{8}\sigma_{nn}+\tilde{\chi}\tilde{\eta}\sigma_{nn}\right)\psi_{nn}\right)\mathrm{d}l\\
&-\int_\Omega U\cdot(\nabla\cdot\psi)\,\mathrm{d}x + \int_\Gamma \tilde{\chi}\tilde{\eta}\mathscr{P}\psi_{nn}\,\mathrm{d}l\\
&-\frac{2}{5}\int_\Omega q\cdot(\nabla\cdot\psi)\,\mathrm{d}x + \int_\Gamma\left(\frac{1}{4}q_n\psi_{nn}+\frac{1}{5}q_t\psi_{nt}\right)\mathrm{d}l\\
&= -\int_\Gamma\left(U_t^w\psi_{nt}+\left(U_n^w-\tilde{\chi}\tilde{\eta}p^w\right)\psi_{nn}\right)\mathrm{d}l.
\end{aligned}$$

To express this in functional form, we define the following functionals

$$\begin{aligned}
d(\sigma,\psi) &= \frac{1}{2\mathrm{Kn}}\int_\Omega \sigma:\psi\,\mathrm{d}x + \mathrm{Kn}\frac{3}{2}\int_\Omega(\nabla\sigma)_{\mathrm{stf}}\mathbin{\therefore}\nabla\psi\,\mathrm{d}x + \int_\Gamma\left(\tilde{\chi}\frac{9}{8}\sigma_{nn}+\tilde{\chi}\tilde{\eta}\sigma_{nn}\right)\psi_{nn}\,\mathrm{d}l\\
&\quad+\int_\Gamma\left(\tilde{\chi}\left(\frac{1}{2}\sigma_{nn}+\sigma_{tt}\right)\left(\psi_{tt}+\frac{1}{2}\psi_{nn}\right)+\frac{1}{\tilde{\chi}}\sigma_{nt}\psi_{nt}\right)\mathrm{d}l,\\
e(U,\psi) &= \int_\Omega U\cdot(\nabla\cdot\psi)\,\mathrm{d}x,\\
f(\psi,\mathscr{P}) &= \int_\Gamma \tilde{\chi}\tilde{\eta}\mathscr{P}\psi_{nn}\,\mathrm{d}l,\\
\tilde{c}(q,\psi) &= \frac{2}{5}\int_\Omega q\cdot(\nabla\cdot\psi)\,\mathrm{d}x - \int_\Gamma\left(\frac{1}{4}q_n\psi_{nn}+\frac{1}{5}q_t\psi_{nt}\right)\mathrm{d}l = -c(\psi,q),\\
l_2(\psi) &= -\int_\Gamma\left(U_t^w\psi_{nt}+\left(U_n^w-\tilde{\chi}\tilde{\eta}p^w\right)\psi_{nn}\right)\mathrm{d}l.
\end{aligned}$$

This yields the final functional form of the stress balance

$$d(\sigma,\psi) - e(U,\psi) + f(\psi,\mathscr{P}) + c(\psi,q) = l_2(\psi). \tag{5.1.5}$$

Weak formulation of the momentum balance

For the weak form of momentum conservation, we use the test function $v : \Omega \to \mathbb{R}^2$, which leads to the bilinear form

$$\int_\Omega (\nabla\cdot\sigma)\cdot v\,\mathrm{d}x + \int_\Omega \nabla\mathscr{P}\cdot v\,\mathrm{d}x = 0.$$

In functional form, this reads

$$e(\sigma,v) + g(\mathscr{P},v) = 0, \tag{5.1.6}$$

where

$$e(\sigma,v) = \int_\Omega (\nabla\cdot\sigma)\cdot v\,\mathrm{d}x, \quad g(\mathscr{P},v) = \int_\Omega \nabla\mathscr{P}\cdot v\,\mathrm{d}x.$$

Weak formulation od the mass balance

For the lowest-order equation in the translational heat flux–stress subsystem, namely mass conservation, we perform partial integration using the test function $\tilde{q} : \Omega \to \mathbb{R}$

$$\int_\Omega (\nabla\cdot U)\tilde{q}\,\mathrm{d}x = -\int_\Omega U\cdot\nabla\tilde{q}\,\mathrm{d}x + \int_\Gamma (U\cdot n)\,\tilde{q}\,\mathrm{d}l = 0.$$

Here, the boundary condition (5.0.34) is employed, resulting in

$$-\int_\Omega U\cdot\nabla\tilde{q}\,\mathrm{d}x + \int_\Gamma (U_n^w + \tilde{\chi}\tilde{\eta}\,(\mathscr{P} - p^w + \sigma_{nn}))\,\tilde{q}\,\mathrm{d}l = 0, \tag{5.1.7}$$

or equivalently, in functional form,

$$f(\sigma,\tilde{q}) - g(U,\tilde{q}) + h(\mathscr{P},\tilde{q}) = l_3(\tilde{q}), \tag{5.1.8}$$

where

$$f(\sigma,\tilde{q}) = \int_\Gamma \tilde{\chi}\tilde{\eta}\,\tilde{q}\,\sigma_{nn}\,\mathrm{d}l, \quad g(U,\tilde{q}) = \int_\Omega U\cdot\nabla\tilde{q}\,\mathrm{d}x,$$
$$h(\mathscr{P},\tilde{q}) = \int_\Gamma \tilde{\chi}\tilde{\eta}\mathscr{P}\tilde{q}\,\mathrm{d}l, \quad l_3(\tilde{q}) = -\int_\Gamma (U_n^w - \tilde{\chi}\tilde{\eta}p^w)\,\tilde{q}\,\mathrm{d}l.$$

5.1.2 Weak formulation of the internal heat flux subsystem

In a similar manner, we apply partial integration to every second equation. Since in the internal heat flux subsystem the highest-order term is the internal heat flux, we apply partial integration with the test function $\xi : \Omega \to \mathbb{R}^2$, resulting in

$$\begin{aligned}
&\frac{1}{\mathrm{Kn}}\frac{2}{\delta}\int_\Omega \left(P_s s - \frac{\delta}{2}P_{qs}q\right)\cdot\xi \,\mathrm{d}x \\
&\quad - \int_\Omega (\nabla\cdot\xi)\,\theta_{int}\,\mathrm{d}x - \frac{1}{3}\frac{2}{\delta}\int_\Omega (\nabla\cdot\xi)\cdot\mathcal{S}\,\mathrm{d}x - \frac{2}{\delta}\int_\Omega \nabla\xi : S\,\mathrm{d}x \\
&\quad + \int_\Gamma \theta_{int}\xi_n\,\mathrm{d}l + \frac{1}{3}\frac{2}{\delta}\int_\Gamma \mathcal{S}\xi_n\,\mathrm{d}l + \frac{2}{\delta}\int_\Gamma (S_{nn}\xi_n + S_{nt}\xi_t)\,\mathrm{d}l = 0.
\end{aligned}$$

Grouping terms with respect to the components of the vector ξ yields

$$\begin{aligned}
&\frac{1}{\mathrm{Kn}}\frac{2}{\delta}\int_\Omega \left(P_s s - \frac{\delta}{2}P_{qs}q\right)\cdot\xi \,\mathrm{d}x \\
&\quad - \int_\Omega (\nabla\cdot\xi)\,\theta_{int}\,\mathrm{d}x - \frac{1}{3}\frac{2}{\delta}\int_\Omega (\nabla\cdot\xi)\cdot\mathcal{S}\,\mathrm{d}x - \frac{2}{\delta}\int_\Omega \nabla\xi : S\,\mathrm{d}x \\
&\quad + \frac{2}{\delta}\int_\Gamma \left(\frac{\delta}{2}\theta_{int} + \frac{1}{3}\mathcal{S} + S_{nn}\right)\xi_n\,\mathrm{d}l + \frac{2}{\delta}\int_\Gamma S_{nt}\xi_t\,\mathrm{d}l = 0,
\end{aligned}$$

which reveals that the boundary conditions (5.0.32) and (5.0.33) naturally fit:

$$\frac{\delta}{2}\theta_{int} + \frac{1}{3}\mathcal{S} + S_{nn} = \frac{s_n}{\tilde{\chi}} + \frac{\delta}{2}\theta^w, \qquad S_{nt} = \tilde{\chi}s_t.$$

Using the closure relations (5.0.17), we obtain the variational formulation of the internal heat flux balance:

$$\begin{aligned}
&\frac{1}{\mathrm{Kn}}\frac{2}{\delta}\int_\Omega \left(P_s s - \frac{\delta}{2}P_{qs}q\right)\cdot\xi \,\mathrm{d}x \\
&\quad - \int_\Omega (\nabla\cdot\xi)\,\theta_{int}\,\mathrm{d}x + \frac{4}{3\delta}\mathrm{Kn}\int_\Omega (\nabla\cdot\xi)\cdot(\nabla\cdot s)\,\mathrm{d}x + \frac{4}{\delta}\mathrm{Kn}\int_\Omega \nabla\xi : (\nabla s)_{\mathrm{stf}}\,\mathrm{d}x \\
&\quad + \frac{2}{\delta}\int_\Gamma \left(\frac{s_n}{\tilde{\chi}} + \frac{\delta}{2}\theta^w\right)\xi_n\,\mathrm{d}l + \frac{2}{\delta}\int_\Gamma \tilde{\chi}s_t\xi_t\,\mathrm{d}l = 0,
\end{aligned}$$

which is equivalent to

$$a_2(s,\xi) - a_{12}(q,\xi) - b(\theta_{int},\xi) = l_4(\xi), \tag{5.1.9}$$

where

$$
\begin{aligned}
a_2(s,\xi) &= \frac{1}{\mathrm{Kn}}\frac{2}{\delta}\int_\Omega P_s s\cdot\xi\,\mathrm{d}x + \frac{4}{3\delta}\mathrm{Kn}\int_\Omega (\nabla\cdot\xi)\cdot(\nabla\cdot s)\,\mathrm{d}x \\
&\quad + \frac{4}{\delta}\mathrm{Kn}\int_\Omega \nabla\xi : (\nabla s)_{\mathrm{stf}}\,\mathrm{d}x + \frac{2}{\delta}\int_\Gamma \frac{s_n}{\tilde{\chi}}\xi_n\,\mathrm{d}l + \frac{2}{\delta}\int_\Gamma \tilde{\chi}s_t\xi_t\,\mathrm{d}l, \\
a_{12}(q,\xi) &= \frac{1}{\mathrm{Kn}}\int_\Omega P_{qs}q\cdot\xi\,\mathrm{d}x, \\
b(\theta_{int},\xi) &= \int_\Omega (\nabla\cdot\xi)\,\theta_{int}\,\mathrm{d}x, \\
l_4(\xi) &= -\int_\Gamma \theta^w\xi_n\,\mathrm{d}l.
\end{aligned}
\tag{5.1.10}
$$

Weak formulation of the internal temperature balance

For internal temperature balance and test function $\vartheta : \Omega \to \mathbb{R}$, one obtains the following weak formulation

$$
\int_\Omega (\nabla\cdot s)\,\vartheta\,\mathrm{d}x + \frac{1}{\mathrm{Kn}}\int_\Omega K_\theta\,\theta_{int}\,\vartheta\,\mathrm{d}x - \frac{1}{\mathrm{Kn}}\int_\Omega K_\theta\,\theta_{tr}\,\vartheta\,\mathrm{d}x = 0,
$$

which is equivalent to the variational formulation

$$
b(\vartheta,s) + a_3(\theta_{int},\vartheta) - a_3(\theta_{tr},\vartheta) = 0, \tag{5.1.11}
$$

where the bilinear and linear forms are given by

$$
\begin{aligned}
b(\vartheta,s) &= \int_\Omega (\nabla\cdot s)\,\vartheta\,\mathrm{d}x, \\
a_3(\theta_{int},\vartheta) &= \frac{1}{\mathrm{Kn}}\int_\Omega K_\theta\,\theta_{int}\,\vartheta\,\mathrm{d}x.
\end{aligned}
$$

5.1.3 General structure of R17 weak formulation

Using the Galerkin method, the variational formulation of the steady-state linearized R17 system reads: Find $\mathcal{U}$ such that

$$
\mathcal{A}(\mathcal{U},\mathcal{V}) = \mathcal{L}(\mathcal{V}), \quad \forall\mathcal{V}\in\mathbb{H} \tag{5.1.12}
$$

where the bilinear form $\mathcal{A}$ is given by

$$\begin{aligned}\mathcal{A}(\mathcal{U},\mathcal{V}) := {} & a(q,r) - b(\theta_{tr},r) - c(\sigma,r) - a_{12}(r,s) \\ & + b(\phi,q) + a_3(\theta_{tr},\phi) - a_3(\theta_{int},\phi) \\ & + d(\sigma,\psi) - e(U,\psi) + f(\psi,\mathscr{P}) + c(\psi,q) \\ & + e(\sigma,v) + g(\mathscr{P},v) \\ & + f(\sigma,\tilde{q}) - g(U,\tilde{q}) + h(\mathscr{P},\tilde{q}) \\ & + a_2(s,\xi) - a_{12}(q,\xi) - b(\theta_{int},\xi) \\ & + b(\vartheta,s) + a_3(\theta_{int},\vartheta) - a_3(\theta_{tr},\vartheta)\end{aligned} \tag{5.1.13}$$

and

$$\mathcal{L}(\mathcal{V}) := l_1(r) + l_2(\psi) + l_3(\tilde{q}) + l_4(\xi). \tag{5.1.14}$$

5.1.4 Finite element discretization

Let us consider a conforming and shape-regular partition T_h of the computational domain $\Omega \subset \mathbb{R}^2$ into triangular elements τ, that is, $T_h = \{\tau\}_{\tau\in T_h}$. Next, we define the discrete version of the space $\mathbb{V}_\star$ as

$$\mathbb{V}_{\star,h} := \{u \in \mathbb{V}_\star : u|_\tau \in \mathbb{P}_m(\tau)\ \forall \tau \in T_h\},$$

where $\mathbb{P}_m(\tau)$ denotes the space of polynomials of maximum degree m, for a given $m \in \mathbb{N}$.

After restricting the function spaces to the finite-dimensional subspace $\mathbb{H}_h \subset \mathbb{H}$ by choosing polynomial ansatz functions for all fields, the standard conforming finite element approach leads to the following discrete algebraic system

$$\left(\begin{array}{cc|ccc|cc} A_{3,h} & B_h & & & & -A_{3,h} & 0 \\ -B_h^T & A_h & & & -C_h^T & 0 & -A_{12,h} \\ \hline & & H_h & -G_h^T & F_h^T & & \\ & & G_h & 0 & E_h & & \\ & C_h & F_h & -E_h^T & D_h & & \\ \hline -A_{3,h} & 0 & & & & A_{3,h} & B_h \\ 0 & -A_{12,h} & & & & -B_h^T & A_{2,h} \end{array}\right) \left(\begin{array}{c} \theta_{tr,h} \\ q_h \\ \hline \mathscr{P}_h \\ U_h \\ \sigma_h \\ \hline \theta_{int,h} \\ s_h \end{array}\right) = \left(\begin{array}{c} 0 \\ L_{1,h} \\ \hline L_{3,h} \\ 0 \\ L_{2,h} \\ \hline 0 \\ L_{4,h} \end{array}\right). \tag{5.1.15}$$

It is worthwhile to mention that the zero diagonal entry corresponding to the unknown U_h indicates that the algebraic system is of saddle-point type [5]. Additionally, the diagonal block associated with $\mathscr{P}$ may also require stabilization. This becomes particularly relevant when using $\tilde{\eta} = 0$ or imposing the boundary condition $U_n = 0$, both of which

result in a zero diagonal contribution. Therefore, stabilization techniques such as Continuous Interior Penalty (CIP) methods are proposed, as applied in similar gas dynamic problems modeled by the Stokes or R13 equations [43, 46].

5.1.5 Stabilization

In this thesis, we employ the Galerkin Least Squares (GLS) stabilization method. The stabilization term $\mathscr{S}$ is defined as

$$\mathscr{S}(\mathcal{U},\mathcal{V}) := \mathscr{S}_{\theta_{tr}}(\mathcal{U},\mathcal{V}) + \mathscr{S}_{\theta_{int}}(\mathcal{U},\mathcal{V}) + \mathscr{S}_q(\mathcal{U},\mathcal{V}) + \mathscr{S}_s(\mathcal{U},\mathcal{V}) \tag{5.1.16}$$

$$+ \mathscr{S}_{\mathscr{P}}(\mathcal{U},\mathcal{V}) + \mathscr{S}_U(\mathcal{U},\mathcal{V}) + \mathscr{S}_\sigma(\mathcal{U},\mathcal{V}) \tag{5.1.17}$$

where

$$\begin{aligned}
\mathscr{S}_{\theta_{tr}}(\mathcal{U},\mathcal{V}) :=& \tau_\theta h_\theta \int_\Omega (\nabla\cdot q + \nabla\cdot U + \frac{K_\theta}{\mathrm{Kn}}(\theta_{tr}-\theta_{int}))\cdot(\nabla\cdot r + \nabla\cdot v + \frac{K_\theta}{\mathrm{Kn}}(\phi-\vartheta))\mathrm{d}x,\\
\mathscr{S}_{\theta_{int}}(\mathcal{U},\mathcal{V}) :=& \tau_\theta h_\theta \int_\Omega (\nabla\cdot s + \frac{K_\theta}{\mathrm{Kn}}(\theta_{int}-\theta_{tr}))\cdot(\nabla\cdot \xi + \frac{K_\theta}{\mathrm{Kn}}(\vartheta-\phi))\mathrm{d}x,\\
\mathscr{S}_q(\mathcal{U},\mathcal{V}) :=& \tau_q h_q \int_\Omega \left(\frac{5}{2}\nabla\theta_{tr} + \nabla\cdot\sigma - \frac{14}{5}\mathrm{Kn}\,(\nabla\cdot(\nabla q)_{\mathrm{stf}})\right.\\
&\left. -\frac{4}{3}\mathrm{Kn}\nabla(\nabla\cdot q) + \frac{1}{\mathrm{Kn}}\left(P_q q - \frac{5}{2}P_{qs}s\right)\right)\\
&\cdot\left(\frac{5}{2}\nabla\phi + \nabla\cdot\psi - \frac{14}{5}\mathrm{Kn}\,(\nabla\cdot(\nabla r)_{\mathrm{stf}})\right.\\
&\left. -\frac{4}{3}\mathrm{Kn}\nabla(\nabla\cdot r) + \frac{1}{\mathrm{Kn}}\left(P_q r - \frac{5}{2}P_{qs}\xi\right)\right)\mathrm{d}x,\\
\mathscr{S}_s(\mathcal{U},\mathcal{V}) :=& \tau_q h_q \int_\Omega \left(\frac{\delta}{2}\nabla\theta_{int} - 2\,\mathrm{Kn}\nabla\cdot(\nabla s)_{\mathrm{stf}} - \frac{2}{3}\mathrm{Kn}\nabla(\nabla\cdot s) + \frac{1}{\mathrm{Kn}}(P_s s - \tfrac{\delta}{2}P_{qs}q)\right)\\
&\cdot\left(\frac{\delta}{2}\nabla\vartheta - 2\,\mathrm{Kn}\nabla\cdot(\nabla\xi)_{\mathrm{stf}} - \frac{2}{3}\mathrm{Kn}\nabla(\nabla\cdot\xi) + \frac{1}{\mathrm{Kn}}(P_s\xi - \tfrac{\delta}{2}P_{qs}r)\right)\mathrm{d}x,\\
\mathscr{S}_{\mathscr{P}}(\mathcal{U},\mathcal{V}) :=& \tau_{\mathscr{P}} h_{\mathscr{P}} \int_\Omega (\nabla\cdot v)\cdot(\nabla\cdot U)\mathrm{d}x,\\
\mathscr{S}_U(\mathcal{U},\mathcal{V}) :=& \tau_U h_U \int_\Omega (\nabla\tilde{q} + (\nabla\cdot\psi))\cdot(\nabla\mathscr{P} + (\nabla\cdot\sigma))\mathrm{d}x,\\
\mathscr{S}_\sigma(\mathcal{U},\mathcal{V}) :=& \tau_\sigma h_\sigma \int_\Omega \left(\frac{4}{5}(\nabla r)_{\mathrm{stf}} + 2(\nabla v)_{\mathrm{stf}} - 3\mathrm{Kn}\nabla\cdot(\nabla\psi)_{\mathrm{stf}} + \frac{1}{\mathrm{Kn}}\psi\right)\\
&: \left(\frac{4}{5}(\nabla q)_{\mathrm{stf}} + 2(\nabla U)_{\mathrm{stf}} - 3\mathrm{Kn}\nabla\cdot(\nabla\sigma)_{\mathrm{stf}} + \frac{1}{\mathrm{Kn}}\sigma\right)\mathrm{d}x.
\end{aligned} \tag{5.1.18}$$

The parameters $\tau_\theta, \tau_q, \tau_{\mathscr{P}}, \tau_U, \tau_\sigma$ in (5.1.18) are stabilization coefficients, while the terms $h_\theta, h_q, h_{\mathscr{P}}, h_U, h_\sigma$ are mesh-dependent scaling factors. Due to the lack of established guidelines in the literature, these values are chosen empirically to achieve optimal convergence behavior.

The final stabilized weak formulation is then given by

$$\tilde{\mathcal{A}}(\mathcal{U},\mathcal{V}) := \mathcal{A}(\mathcal{U},\mathcal{V}) + \mathscr{S}(\mathcal{U},\mathcal{V}) = \mathcal{L}(\mathcal{V}) \tag{5.1.19}$$

Chapter 6

Numerical results

6.1 Implementation and convergence result

The FEniCS framework [28, 3] enables finite element implementations based on weak formulations for a wide range of partial differential equations. It provides both a modern Python interface and the computational efficiency of a C++ backend. At the core of the FEniCS framework is the DOLFIN library, which manages communication between various modules and external software packages. DOLFIN also offers essential tools for constructing key data structures such as meshes, function spaces, and symbolic function representations.

In this thesis, we employ the FEniCS framework to implement the vibrational form of the R17 equations, as described in (5.1.19). Since the R17 system shares a similar structure with the monatomic R13 equations, we extend the existing FEniCSR13 software [43]. This extension involves defining new functionals and adapting existing ones. As an example, we present the Python implementation of the fictional functional $a_2(s, \xi)$ from (5.1.10)

```
def a2(s, xi):
return sum([(
# => stf(grad s): grad xi = sym (grad s): sym(grad xi)-(1/3)*(dev s dev xi)
+ 2 *(2/delta)*( regs[reg]["kn"]) *df.inner( df.sym(df.grad(s)), df.sym(df.
    grad(xi)))
-(1/3)*2 *(2/delta)*( regs[reg]["kn"]) * df.div(s) * df.div(xi)
+ (4 / 3)  *(2/delta) * ( regs[reg]["kn"]) * df.div(s) * df.div(xi)
+(2/delta)*( 1 / ( regs[reg]["kn"])) *Pss*df.inner(s,xi)
) * df.\de \bm x(reg) for reg in regs.keys()]) + sum([(
+ (2/delta)*(1 / ( bcs[bc]["chi_tilde"])) * n(s) * n(xi)
+ (2/delta)* bcs[bc]["chi_tilde"] * t1(s) * t1(xi)
+ (2/delta)* bcs[bc]["chi_tilde"] * t2(s) * t2(xi)
```

```
12 ) * df.ds(bc) for bc in bcs.keys()])
```

Listing 6.1: Implementation of the functional a_2 in the weak formulation

6.1.1 Analytical solution

In general, finding an analytical solution for a general domain $\Omega \subset \mathbb{R}^2$ is challenging. However, for special geometries such as the two-cylinder scenario

$$\Omega = \{x : R_1 \leq \|x\|_2 \leq R_2\}, \tag{6.1.1}$$

an analytical solution is available [43]. Following the traditional values from [43], we take $R_1 = 0.5$ and $R_2 = 2$. For convenience, we denote the inner cylinder boundary by Γ_1 and the outer boundary by Γ_2. On the inner wall, we impose the boundary conditions $U_n^w|_{\Gamma_1} = 0$ and $U_t^w|_{\Gamma_1} = 0$. The velocity on the outer wall is set as $U_n^w|_{\Gamma_2} = n_x = \cos\phi$ and $U_t^w|_{\Gamma_2} = -n_y = -\sin\phi$.

To ensure a non-trivial temperature profile, we set the wall temperatures as $\theta^w|_{\Gamma_1} = 1$ and $\theta^w|_{\Gamma_2} = 2$. The pressure on the outer wall is prescribed as $p^w|_{\Gamma_2} = -0.27\cos\phi$, while on the inner wall we set $p^w|_{\Gamma_1} = 0$. The accommodation coefficient on both Γ_1 and Γ_2 is taken as $\tilde{\chi} = 1$. The remaining parameters are chosen as $\tilde{\eta}|_{\Gamma_1} = 10^{-3}$ and $\tilde{\eta}|_{\Gamma_2} = 10^3$, which induces a pressure-dominated process on the outer wall. The Knudsen number is fixed at $\mathrm{Kn} = 1$.

Due to the complexity of the solution, we provide the analytical expressions in Mathematica notebook, which is publicly available at [20].

Figure 6.1 shows, on the left, the analytical solution for the stress component σ_{xy} overlaid with velocity streamlines. One can observe that the flow is tangential to the inner cylinder, consistent with [43]. On the right, the total temperature θ is depicted along with the total heat flux $q + s$, illustrating non-trivial heat flux streamlines. The temperature jump observed is a consequence of the large Knudsen number and the presence of a cooler zone on the right side of the inner wall.

6.1.2 Empirical convergence study

For the two-cylinder domain, an analytical solution can be computed using Mathematica notebook [20], and the relative L^2 error between the numerical solution $\mathcal{U}_h$ and the analytical solutions $\mathcal{U}_{\text{ex}}$ is defined as

$$e_{L^2} = \frac{||\mathcal{U}_{\text{ex}} - \mathcal{U}_h||_{L^2(\Omega)}}{\max\{|\mathcal{U}_{\text{ex}}|_{n\in\eta}\}}, \tag{6.1.2}$$

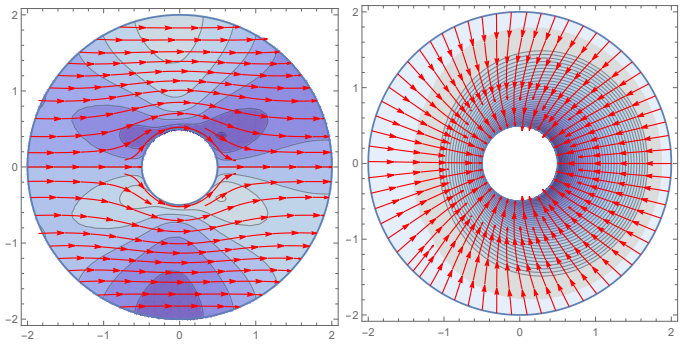

(a) Analytical solution for σ_{xy} with velocity streamlines U_i.

(b) Analytical solution for total temperature θ with streamlines of total heat flux $q + s$.

Figure 6.1: Analytical solution in the two-cylinder domain for Kn $= 1$.

where η denotes the set of all nodes in the domain Ω. Based on the boundary conditions described in Section 6.1.1, we compute numerical results for different meshes. For this purpose, we use unstructured triangular meshes generated with Gmsh [24], varying the number of nodes—or, equivalently, the maximum triangle size $h_{\max}$. Figure 6.2 shows a series of these meshes. As the mesh is refined, the inner boundary is better approximated, resulting in a more regular domain representation.

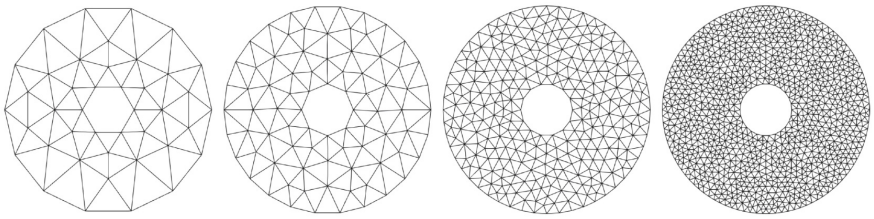

(a) $h_{\max} = 0.99$. (b) $h_{\max} = 0.63$. (c) $h_{\max} = 0.33$. (d) $h_{\max} = 0.17$.

Figure 6.2: Series of unstructured meshes used for the convergence study. With a small number of nodes, the inner cylinder boundary is poorly approximated.

All simulations are performed using $\mathbb{P}1$ (linear) elements, both with and without GLS stabilization. The following stabilization parameters are used: $\tau_\theta = \tau_q = 0.001$ and $\tau_{\mathscr{P}} = \tau_U = \tau_\sigma = 0.01$. Figure 6.3 presents the relative L^2 error e_{L^2} for various values of $h_{\max}$.

For coarse meshes, the error exhibits oscillations due to geometric irregularities near the inner boundary Γ_1, where sharp corners protrude into the domain Ω. As the mesh is refined, the relative error decreases. With the application of GLS stabilization, all variables demonstrate empirical second-order convergence.

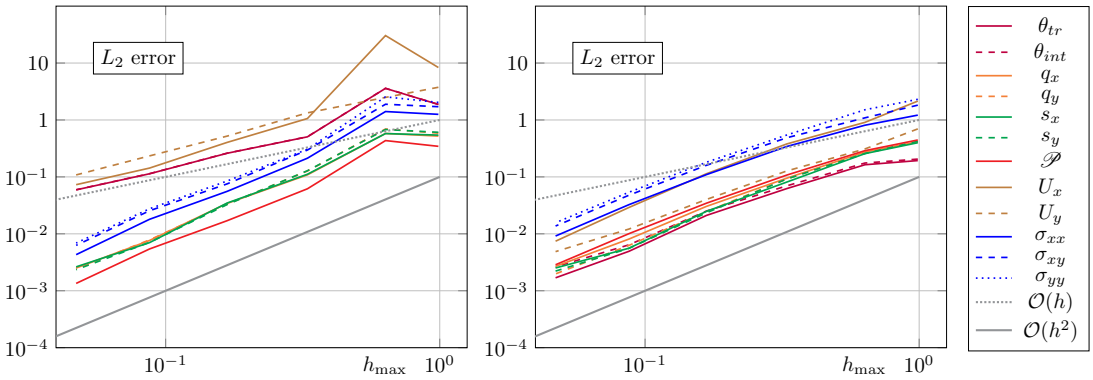

Figure 6.3: Relative L^2 error for different mesh sizes $h_{\max}$. Simulations are performed using $\mathbb{P}1$ (linear) elements. The left figure shows results without stabilization, while GLS stabilization is applied in the right figure. Empirical convergence is observed for all relevant variables, with a maximum order of two. The convergence order of θ_{tr}, θ_{int}, and U, initially first-order, improves to second-order with GLS stabilization.

6.2 Polyatomic heat conduction process

Given that convergence has been confirmed, we proceed with a simulation of heat conduction in a 2D domain containing two circular inclusions with different wall temperatures and accommodation coefficients, as illustrated in Figure 6.4.

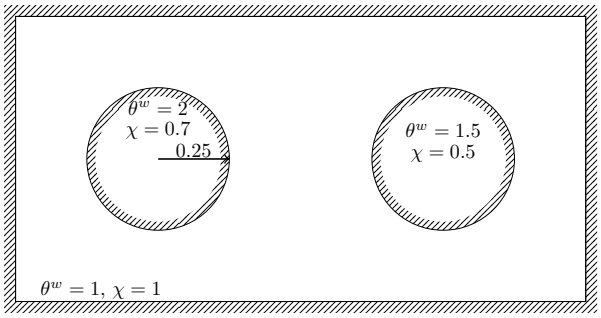

Figure 6.4: Geometry for the simulation of polyatomic heat conduction. The domain includes two circles of radius 0.5 inside a rectangular box of dimensions 2×1. The left circle has a wall temperature of $\theta^w = 2$ with accommodation coefficient $\chi = 0.7$, while the right circle has $\theta^w = 1.5$ and $\chi = 0.9$. The outer walls are maintained at $\theta^w = 1$ with $\chi = 1$. For all boundaries, the velocity is set to $U^w = 0$, pressure $p^w = 0$, and $\tilde{\eta} = 10^{-3}$.

In this setup, we simulate heat flow for nitrogen gas (N_2), using polyatomic parameters from Table 4.4. We take $\delta = 2.01$ and $\zeta = 0.533$, yielding the following coefficients (calculated via a Mathematica notebook [17]): $K_\theta = 0.220492$, $P_q = 0.789162$, $P_{qs} = 0.731318$, and $P_s = 0.903166$. Using these coefficients in the R17 system, we

investigate heat transfer behavior for various Knudsen numbers. The results are presented in Figure 6.6 and demonstrate that the difference between internal and translational temperatures diminishes as the Knudsen number decreases.

This observation is consistent with the findings of van der Woude et al. for the lid-driven cavity problem with polyatomic gases [44] . The physical explanation lies in the fact that, as the flow approaches equilibrium (i.e., small Kn), the dynamical pressure

$$\Pi = \frac{\delta}{\delta + 3}(\theta_{tr} - \theta_{int})$$

tends to vanish, indicating minimal deviation between non-equilibrium temperatures.

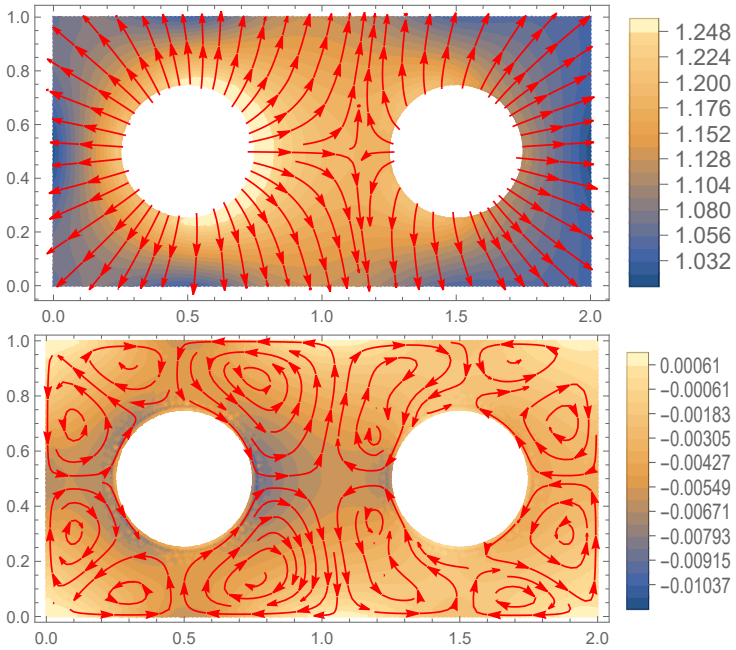

Figure 6.5: Top: Total temperature distribution with total heat flux streamlines for polyatomic heat conduction. Bottom: Dynamical pressure Π with velocity streamlines. The simulation is performed for N_2 gas with Kn $= 0.2$ and the following R17 coefficients: $\delta = 2.01$, $K_\theta = 0.220492$, $P_q = 0.789162$, $P_{qs} = 0.731318$, and $P_s = 0.903166$. All variables are discretized using $\mathbb{P}_1$ elements with GLS stabilization.

6.2.1 Effect of bulk viscosity

Compared to monatomic gases, which exhibit negligible bulk viscosity, polyatomic gases demonstrate significantly higher values of bulk viscosity [14]. The aim of this section is to explore the influence of bulk viscosity in polyatomic gas dynamics.

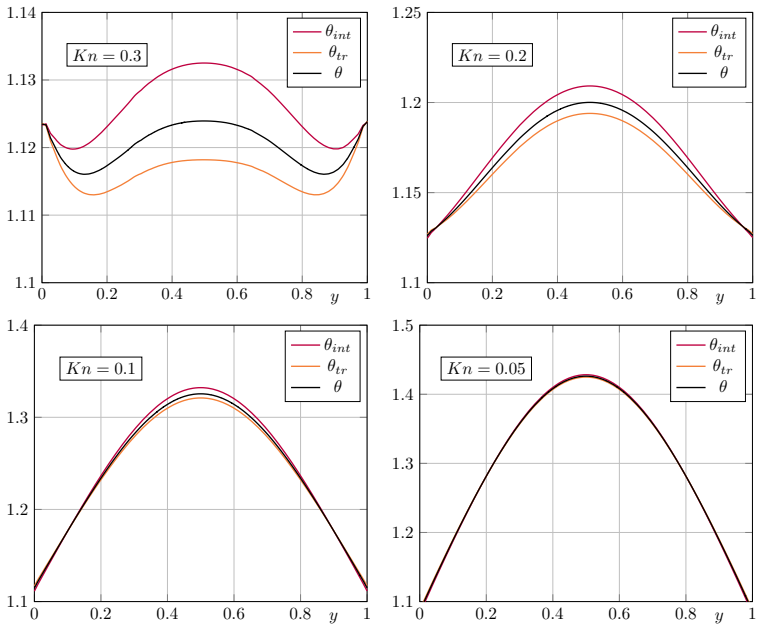

Figure 6.6: Temperature profiles along the y-axis at $x = 1$ for varying Knudsen numbers. Plots show internal, translational, and total temperatures. As the Knudsen number decreases, the internal and translational temperatures converge, indicating the transition toward equilibrium. Simulation is performed for N_2 gas using $\mathbb{P}_1$ elements with GLS stabilization. R17 parameters are as follows: $\delta = 2.01$, $K_\theta = 0.220492$, $P_q = 0.789162$, $P_{qs} = 0.731318$, and $P_s = 0.903166$.

To gain initial insight, we simulate a heat conduction process using hydrogen (H_2), employing the same geometry and boundary conditions shown in Figure 6.4, in order to directly compare with the nitrogen case. Hydrogen has a notably higher bulk-to-shear viscosity ratio than nitrogen, making it a suitable test case for comparison.

The polyatomic parameters for hydrogen are listed in Table 4.6, leading to the following coefficients: $K_\theta = 0.00514077$, $P_q = 0.669523$, $P_{qs} = 0.00176659$, and $P_s = 0.742166$. It is important to note the significant difference in these coefficients compared to the nitrogen case. This discrepancy is primarily due to the high bulk-to-shear viscosity ratio ν/μ, which necessitates a small value of K_θ. Since both K_θ and P_{qs} are both proportional to ω, setting ω near zero causes these coefficients to approach zero as well.

For the hydrogen case, the Knudsen number is set to $\mathrm{Kn} = 0.372737$. This is due to the difference in molecular masses and viscosities μ_0 between hydrogen and nitrogen. After fixing the reference temperature $T_0 = 300\,\mathrm{K}$, reference pressure $p_0 = 0.092\,\mathrm{bar}$, and the characteristic length L, this leads to the value $\mathrm{Kn} = 0.372737$ according to the definition (5.0.11).

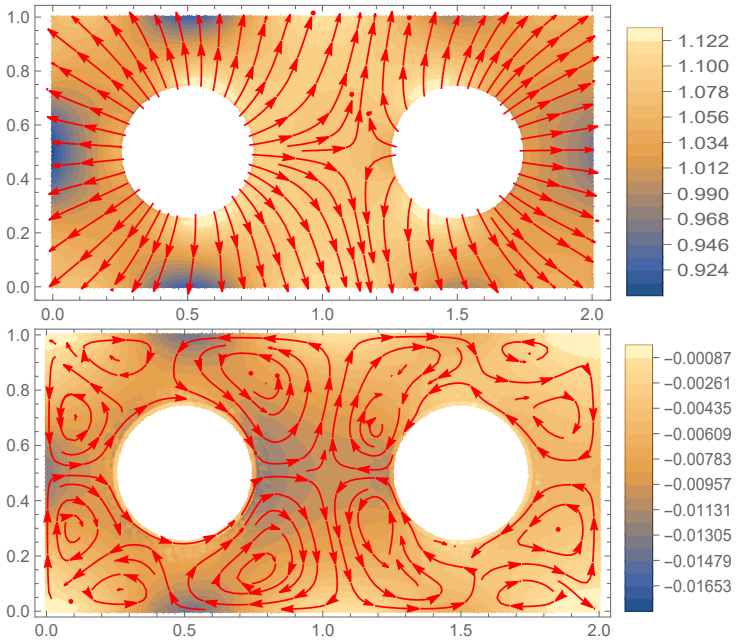

Figure 6.7: Top: Total temperature with heat flux streamlines for polyatomic heat conduction using H_2 gas. Bottom: Dynamical pressure Π with velocity streamlines. The simulation uses Kn $= 0.372737$ and polyatomic R17 coefficients: $\delta = 1.94$, $K_\theta = 0.00514077$, $P_q = 0.669523$, $P_{qs} = 0.00176659$, $P_s = 0.742166$. All variables are discretized using $\mathbb{P}_1$ elements with GLS stabilization.

By comparing Figure 6.7 with Figure 6.5 for nitrogen, we observe that hydrogen produces a slightly different dynamical pressure near the outer wall. The total temperature field is also affected, which can be explained as a consequence of the change in the Knudsen number. To obtain the same Knudsen number Kn $= 0.2$ for hydrogen, the value of p_0 in the hydrogen simulation can be adjusted while keeping the other reference values $T_0 = 300\,\mathrm{K}$ and L the same as for nitrogen. This results in nearly identical outcomes to those shown for nitrogen in Figure 6.5. Therefore, the Knudsen number appears to be the most influential parameter in this context.

However, the influence of other parameters on the results is not entirely clear. To investigate this, we consider a hypothetical gas characterized by the parameters: $\delta = 2$, $\zeta = 0.5$, and Pr $= 0.7$. We fix the value of $P_\sigma = 8K$, where K is a constant, and determine the remaining parameters from the collision kernel to ensure that P_σ, the Prandtl number Pr $= 0.7$, and a prescribed bulk-to-shear viscosity ratio are all satisfied. The resulting sets of parameters are presented in Table 6.1, and used to generate the numerical results shown in Figure 6.8.

Figure 6.8 demonstrates that increasing the bulk-to-shear viscosity ratio leads to a

ν/μ	K_θ	P_q	P_s	P_{qs}
1	0.160000	0.755556	0.827827	0.0533333
5	0.032000	0.684444	0.801542	0.0106667
10	0.016000	0.675556	0.796449	0.0053333
30	0.005333	0.669630	0.800047	0.0017778

Table 6.1: Polyatomic parameters used to reproduce a constant Prandtl number $\mathrm{Pr} = 0.7$ and shear viscosity $P_\sigma = 8K$ for various bulk-to-shear viscosity ratios. Parameters are fixed at $\delta = 2$, $\zeta = 0.5$.

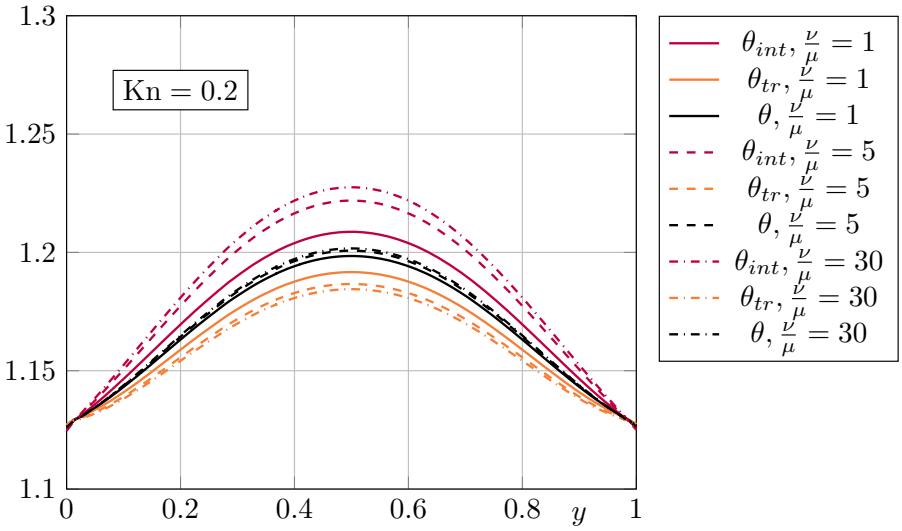

Figure 6.8: Temperature profiles for different bulk-to-shear viscosity ratios. All simulations are performed with the same shear viscosity ($P_\sigma = 8K$) and Prandtl number ($\mathrm{Pr} = 0.7$). The results indicate that increasing the bulk-to-shear viscosity ratio amplifies the difference between the non-equilibrium temperatures, thus increasing the dynamical pressure Π. The total temperature, however, remains largely unaffected.

greater deviation between the two non-equilibrium temperatures, indicating an increase in the dynamical pressure Π. On the other hand, the total temperature remains largely unaffected.

Chapter 7

Summary and future work

In this thesis, we presented models for polyatomic gases at two different levels.

At the mesoscopic level, we used the Boltzmann equation for polyatomic gases with the collision operator introduced in [8]. Based on this form, we proposed new models for the collision kernel by adapting a kernel that ensures existence and uniqueness for the space homogeneous Boltzmann equation, as shown in [4]. Both the initial and extended models include a set of parameters that can be tuned to match the behavior of specific gases.

At the macroscopic level, we modeled flows in the transition regime using moment equations. By applying Grad's method, various hierarchies of moment systems can be derived. In this work, we focused on the 14- and 17-moment systems. These two systems provide a foundational framework for estimating first-order transport coefficients via Maxwellian iteration. To enable this, the collision operator must first be integrated with respect to a set of test functions. This integration—facilitated by a Mathematica notebook [17]—yields collision coefficients for the chosen moment system and collision kernel. These coefficients allow for the estimation of transport properties such as bulk viscosity, shear viscosity, and thermal conductivity.

Using a data-driven approach, we then fit the collision kernel parameters (and equivalently, the collision coefficients in the production terms) to reproduce experimentally observed values for viscosity, the bulk-to-shear viscosity ratio, and the Prandtl number. With this, the model is fully closed and ready for numerical simulation. We also examined the flexibility of the proposed collision kernels and found that the extended kernel offers greater adaptability, although the initial model remains applicable for certain gases. Regarding the moment hierarchy, we observed that both the 14- and 17-moment systems can be used effectively. The collision parameters can be chosen so that both

hierarchies closely match experimental data, with minimal differences.

A second major goal of this thesis was the development and implementation of numerical simulations. To this end, we derived the steady-state, linearized, and regularized 17-moment equations and equipped them with entropy-stable boundary conditions. A variational formulation was then constructed by adapting techniques developed for the monatomic R13 system [43]. This enabled finite element simulations within the FEniCS framework. Our simulations demonstrated mesh-dependent convergence to the analytical solution in a double-cylinder domain, achieving up to second-order accuracy.

With this validated setup, we explored heat conduction in polyatomic gases, examining the effects of both the Knudsen number and bulk viscosity. We found that for small Knudsen numbers, the two non-equilibrium temperatures coincide—consistent with the findings of van der Woude et al. [44]. We also observed that bulk viscosity mainly affects the profile of the dynamical pressure, while the total temperature profile remains relatively stable.

In this thesis, we used the BGK-type collision operator as basis to close the R17 equations. A natural extension of this work would be to explore closures derived directly from the polyatomic Boltzmann collision operator. Further research could also focus on analyzing the properties of the R17 system itself. Additionally, the full nonlinear form of the R17 equations could be applied to one-dimensional shock wave problems, following the approach taken by Song et al. with the 14- and 17-moment systems [39].

Appendix A

Computation of the production terms for the 14-moment model

For the sake of simplicity, the equilibrium distribution function (3.2.6) will be written as

$$f_E = I^{\delta/2-1} L_0 e^{-\frac{1}{kT}(\frac{m}{2}|c|^2+I)} \quad \text{where} \quad L_0 = \frac{\rho}{m}\left(\frac{m}{2\pi kT}\right)^{\frac{3}{2}} \frac{1}{\Gamma(\delta/2)} \frac{1}{(kT)^{\delta/2}}.$$

Our aim is to compute the production terms in the fourteen moments approximation, which amounts to plug the approximative distribution function f_{14} (3.4.5) into the definition of the product terms (3.4.2),

$$P_{ij}^{14} = \int_{\mathbb{R}^3\times\mathbb{R}_+} m v_i v_j Q(f_{14}, f_{14})(v, I) \mathrm{d}I \, \mathrm{d}v,$$

$$Q_i^{14} = \int_{\mathbb{R}^3\times\mathbb{R}_+} \left(\frac{m}{2}|v|^2 + I\right) v_i \, Q(f_{14}, f_{14})(v, I) \, \mathrm{d}I \, \mathrm{d}v.$$

Introducing the peculiar velocity $c = v - U$ and using annihilations of the collision operator weak form due collisional invariant, and after the change of variables $v \mapsto c$ the expressions (3.4.2) simplify to

$$P_{ij}^{14} = \int_{\mathbb{R}^3\times\mathbb{R}_+} m c_i c_j Q(f_{14}, f_{14})(c + U, I) \mathrm{d}I \, \mathrm{d}c, \tag{A.0.1}$$

$$Q_i^{14} = \sum_{k=1}^{3} U_k P_{ki} + \int_{\mathbb{R}^3\times\mathbb{R}_+} c_i \left(\frac{m}{2}|c|^2 + I\right) Q(f_{14}, f_{14})(c + U, I) \mathrm{d}I \, \mathrm{d}c. \tag{A.0.2}$$

As non-equilibrium effects are supposed to be small, products of the distribution functions appearing in the collision integral can be linearized with respect to the non-equilibrium quantities, σ_{ij}, Π, q_i. Using the microscopic conservation laws (2.2.6), it follows

$$\begin{aligned} f_{14}^{'} f_{14*}^{'} - f_{14} f_{14*} \;\approx\; & f_E f_{E*} \Bigg\{ \frac{\rho}{2p^2} \left(\sigma_{kl} + \frac{(\delta+3)}{\delta} \delta_{kl} \Pi \right) \\ & \times (c_k' c_l' + c_{*k}' c_{*l}' - c_k c_l - c_{*k} c_{*l}) + \left(\frac{\delta+5}{2} \right)^{-1} \frac{\rho^2}{mp^3} q_n^{(tot)} \\ & \times \left(\left(\frac{m}{2} |c'|^2 + I' \right) c_n' + \left(\frac{m}{2} |c_*'|^2 + I_*' \right) c_{*n}' \right. \\ & \left. - \left(\frac{m}{2} |c|^2 + I \right) c_n - \left(\frac{m}{2} |c_*|^2 + I_* \right) c_{*n} \right) \Bigg\}. \end{aligned} \tag{A.0.3}$$

Placing (A.0.3) into (A.0.1) and (A.0.2) yields a suitable approximation for the source terms P_{ij}^{14} and Q_i^{14}, denoted by $\overline{P}_{ij}^{14}$ and $\overline{Q}_i^{14}$, respectively.

We now introduce the following notation,

$$\begin{aligned} \mathcal{P}_{ijkl} = \int m\, c_i\, c_j \left(c_k' c_l' + c_{*k}' c_{*l}' - c_k c_l - c_{*k} c_{*l} \right) f_E f_{E*} \\ \times \mathcal{B} H_\delta \, \mathrm{d}\sigma \, \mathrm{d}r \, \mathrm{d}R \, \mathrm{d}I_* \, \mathrm{d}c_* \, \mathrm{d}I \, \mathrm{d}c, \end{aligned}$$

$$\begin{aligned} \mathcal{Q}_{in} = \int \left(\frac{m}{2} |c|^2 + I \right) c_i \left(\left(\frac{m}{2} |c'|^2 + I' \right) c_n' + \left(\frac{m}{2} |c_*'|^2 + I_*' \right) c_{*n}' \right. \\ \left. - \left(\frac{m}{2} |c|^2 + I \right) c_n - \left(\frac{m}{2} |c_*|^2 + I_* \right) c_{*n} \right) f_E f_{E*} \\ \times \mathcal{B} H_\delta \, \mathrm{d}\sigma \, \mathrm{d}r \, \mathrm{d}R \, \mathrm{d}I_* \, \mathrm{d}c_* \, \mathrm{d}I \, \mathrm{d}c. \end{aligned}$$

Now the parity arguments imply

$$\overline{P}_{ij}^{14} = \frac{\rho}{2p^2} \left(\sigma_{kl} + \frac{(\delta+3)}{\delta} \delta_{kl} \Pi \right) \mathcal{P}_{ijkl}, \tag{A.0.4}$$

$$\overline{Q}_i^{14} = U_k \overline{P}_{ki}^{14} + \left(\frac{\delta+5}{2} \right)^{-1} \frac{\rho^2}{mp^3} q_n^{(tot)} \mathcal{Q}_{in}. \tag{A.0.5}$$

For sake of demonstration we calculate the production terms $\overline{P}_{ij}^{14}$ and $\overline{Q}_i^{14}$ in following sections for the simplified version of initial collision kernel (4.1.3) with $\omega = 1$ and $\eta = 1$

$$\begin{aligned} & \mathcal{B}(v, v_*, I, I_*, r, R, \sigma) \\ & \qquad = K \left(R^{\frac{\zeta}{2}} |u|^\zeta + \left(r(1-R) \frac{I}{m} \right)^{\frac{\zeta}{2}} + \left((1-r)(1-R) \frac{I_*}{m} \right)^{\frac{\zeta}{2}} \right), \end{aligned} \tag{A.0.6}$$

where K is a constant, $u := v - v_*$, $\zeta > 0$. This can be done on easier way with use of Mathematica notebook [16]

A.1 Computation of $\overline{P}_{ij}^{14}$

Firstly, we exploit the parity arguments for the term $\mathcal{P}_{ijkl}$. Note that it vanishes unless indices are equal by pairs - the integral is non zero when $i = j$ and $k = l$ or $i = k$ and $j = l$ or $i = l$ and $j = k$. By symmetry, the last two terms lead to the same result and thus $\mathcal{P}_{ijkl}$ can be represented in the following form:

$$\mathcal{P}_{ijkl} = \mathcal{P}_1\delta_{ij}\delta_{kl} + \mathcal{P}_2(\delta_{ik}\delta_{jl} + \delta_{il}\delta_{jk}). \tag{A.1.1}$$

Combining (A.0.4) and (A.1.1) with the fact that pressure tensor is symmetric, we get

$$\overline{P}_{ij}^{14} = \frac{\rho}{2p^2}\left(2\sigma_{ij}\mathcal{P}_2 + \frac{1}{3}\delta_{ij}\frac{(\delta+3)}{\delta}\Pi\mathcal{P}_{rrtt}\right).$$

The term $\mathcal{P}_2$ can be determined from the system of equations obtained from the representation (A.1.1)

$$\mathcal{P}_{rrtt} = 9\mathcal{P}_1 + 6\mathcal{P}_2, \qquad \mathcal{P}_{rtrt} = 3\mathcal{P}_1 + 12\mathcal{P}_2,$$

whose solution is

$$\mathcal{P}_1 = \frac{1}{15}(2\mathcal{P}_{rrtt} - \mathcal{P}_{rtrt}), \qquad \mathcal{P}_2 = \frac{1}{30}(3\mathcal{P}_{rtrt} - \mathcal{P}_{rrtt}).$$

A.1.1 Computation of $\mathcal{P}_{rrtt}$

We first concentrate on the term

$$\begin{aligned}\mathcal{P}_{rrtt} = mL_0^2 \int_{\mathbb{R}^6\times[0,\infty)^2\times[0,1]^2\times S^2} & e^{-\frac{1}{kT}\left(\frac{m}{2}(|c|^2+|c_*|^2)+I+I_*\right)} \\ & \times |c|^2\left(|c'|^2 + |c'_*|^2 - |c|^2 - |c_*|^2\right) \\ & \times \mathcal{B}H_\delta I^{\delta/2-1} I_*^{\delta/2-1}\,\mathrm{d}\sigma\,\mathrm{d}r\,\mathrm{d}R\,\mathrm{d}I_*\,\mathrm{d}c_*\,\mathrm{d}I\,\mathrm{d}c.\end{aligned} \tag{A.1.2}$$

Now we pass to the relative velocity u and center of mass peculiar velocity V_c by means of the following change of variables

$$(c, c_*) \mapsto \left(u := c - c_*, V_c = \frac{c + c_*}{2}\right) \quad \Rightarrow \quad c = V_c + \frac{u}{2},\ c_* = V_c - \frac{u}{2}, \tag{A.1.3}$$

with unit Jacobian. Therefore, the terms under integral in new variables become

$$|c'|^2 + |c'_*|^2 - |c|^2 - |c_*|^2 = \frac{1}{2}(R-1)|u|^2 + \frac{2R}{m}(I+I_*)$$

and

$$|c|^2 + |c_*|^2 = 2|V_c|^2 + \frac{1}{2}|u|^2. \tag{A.1.4}$$

Therefore, we can express the primed quantities from (A.1.2) in center-of-mass framework,

$$\begin{aligned}\mathcal{P}_{rrtt} = mL_0^2 \int_{\mathbb{R}^6\times[0,\infty)^2\times[0,1]^2\times S^2} & e^{-\frac{1}{kT}\left(m|V_c|^2+\frac{m}{4}|u|^2+I+I_*\right)} \\ & \times \left(|V_c|^2 + V_c\cdot u + \frac{1}{4}|u|^2\right)\left(\frac{1}{2}(R-1)|u|^2 + \frac{2R}{m}(I+I_*)\right) \\ & \times \mathcal{B}H_\delta I^{\delta/2-1} I_*^{\delta/2-1}\,\mathrm{d}\sigma\,\mathrm{d}r\,\mathrm{d}R\,\mathrm{d}I_*\,\mathrm{d}I\,\mathrm{d}u\,\mathrm{d}V_c.\end{aligned}$$

The form of the cross-section (A.0.6)

$$\mathcal{B}(v, v_*, I, I_*, r, R, \sigma) = K\tilde{B}(|u|, I, I_*, r, R), \tag{A.1.5}$$

allows to immediately integrate with respect to V_c and σ,

$$\begin{aligned}\mathcal{P}_{rrtt} = mKL_0^2\left(\frac{\pi kT}{m}\right)^{\frac{3}{2}} 2\pi \int_{\mathbb{R}^3\times[0,\infty)^2\times[0,1]^2} & e^{-\frac{1}{kT}\left(\frac{m}{4}|u|^2+I+I_*\right)} \\ & \times \left(3\frac{kT}{m} + \frac{1}{2}|u|^2\right)\left(\frac{1}{2}(R-1)|u|^2 + \frac{2R}{m}(I+I_*)\right) \\ & \times \tilde{B}H_\delta I^{\delta/2-1} I_*^{\delta/2-1}\,\mathrm{d}r\,\mathrm{d}R\,\mathrm{d}I_*\,\mathrm{d}I\,\mathrm{d}u.\end{aligned}$$

Next, we pass to the spherical coordinates for the relative velocity u. Denoting $y = |u|$, and performing integration with respect to the angular part, we obtain

$$\begin{aligned}\mathcal{P}_{rrtt} &= mKL_0^2\left(\frac{\pi kT}{m}\right)^{\frac{3}{2}} 8\pi^2 \int_{[0,\infty)^3\times[0,1]^2} e^{-\frac{1}{kT}\left(\frac{m}{4}y^2+I+I_*\right)} \\ &\times \left(3\frac{kT}{m} + \frac{1}{2}y^2\right)\left(\frac{1}{2}(R-1)y + \frac{2R}{m}(I+I_*)\right) \\ &\times \left(R^{\frac{\zeta}{2}}|u|^\zeta + \left(r(1-R)\frac{I}{m}\right)^{\frac{\zeta}{2}} + \left((1-r)(1-R)\frac{I_*}{m}\right)^{\frac{\zeta}{2}}\right) \\ &\times y^2 H_\delta I^{\delta/2-1} I_*^{\delta/2-1}\,\mathrm{d}r\,\mathrm{d}R\,\mathrm{d}I_*\,\mathrm{d}I\,\mathrm{d}y.\end{aligned}$$

Now we expand all the involved expressions and perform integration with respect to r and R. For the constant issuing from the integration respect to r and R, we introduce

the following notation

$$\begin{aligned} C_{(a,b,c)} &= \int_{[0,1]^2} (r(1-r))^{\delta/2-1} (1-R)^{\delta-1} R^{\frac{1}{2}} (1-R)^a R^b r^c \mathrm{d}r \, \mathrm{d}R \\ &= \frac{\Gamma(\delta+a)\,\Gamma\big(b+\frac{3}{2}\big)\,\Gamma\big(\frac{\delta}{2}+c\big)\,\Gamma\big(\frac{\delta}{2}\big)}{\Gamma\big(\delta+a+b+\frac{3}{2}\big)\,\Gamma(\delta+c)}, \end{aligned} \tag{A.1.6}$$

where Γ stands for the Gamma function. Using the notation (A.1.6), we obtain

$$\begin{aligned} \mathcal{P}_{rrtt} &= mKL_0^2 \left(\frac{\pi kT}{m}\right)^{\frac{3}{2}} 8\pi^2 \int_{[0,\infty)^3} e^{-\frac{1}{kT}\left(\frac{m}{4}y^2+I+I_*\right)} y^2 I^{\delta/2-1} I_*^{\delta/2-1} \\ &\times \left(3\frac{kT}{m}+\frac{1}{2}y^2\right)\Bigg\{ -\frac{1}{2}C_{\left(1,\frac{\zeta}{2},0\right)} y^{\zeta+2} + 2C_{\left(0,\frac{\zeta}{2}+1,0\right)} y^{\zeta}\left(\frac{I}{m}+\frac{I_*}{m}\right) \\ &- \frac{1}{2}C_{\left(\frac{\zeta}{2}+1,0,\frac{\zeta}{2}\right)} y^2 \left(\left(\frac{I}{m}\right)^{\frac{\zeta}{2}} + \left(\frac{I_*}{m}\right)^{\frac{\zeta}{2}}\right) \\ &+ C_{\left(\frac{\zeta}{2},0,\frac{\zeta}{2}\right)}\Bigg(\left(\frac{I}{m}\right)^{\frac{\zeta}{2}+1} + \left(\frac{I}{m}\right)^{\frac{\zeta}{2}} \frac{I_*}{m} \\ &+ \left(\frac{I_*}{m}\right)^{\frac{\zeta}{2}} \frac{I}{m} + \left(\frac{I_*}{m}\right)^{\frac{\zeta}{2}+1}\Bigg)\Bigg\} \mathrm{d}I_* \, \mathrm{d}I \, \mathrm{d}y. \end{aligned}$$

Finally, after performing integration with respect to I, I_* and y, we get

$$\begin{aligned} \mathcal{P}_{rrtt} = -K\frac{\rho^2}{m}\left(\frac{p}{\rho}\right)^{\frac{\zeta}{2}+2} &\frac{2\sqrt{\pi}}{\Gamma(\frac{2\delta+\zeta+5}{2})} \\ &\times \left\{ 3(2\delta+\zeta)\pi\Gamma\left(\frac{\delta+\zeta}{2}\right)^2 + 2^{\zeta+4}\frac{\delta}{2}\Gamma\left(\frac{\delta}{2}\right)^2 \Gamma\left(\frac{\zeta+3}{2}\right)\Gamma\left(\frac{\zeta+5}{2}\right)\right\}, \end{aligned}$$

where the relation $p = \frac{\rho}{m}kT$ was used.

A.1.2 Computation of $\mathcal{P}_{rtrt}$

For the term

$$\begin{aligned} \mathcal{P}_{rtrt} = mL_0^2 \int_{\mathbb{R}^6\times[0,\infty)^2\times[0,1]^2\times S^2} &e^{-\frac{1}{kT}\left(\frac{m}{2}(|c|^2+|c_*|^2)+I+I_*\right)} \\ &\times \left((c\cdot c')^2 + (c\cdot c'_*)^2 - (c\cdot c)^2 - (c\cdot c_*)^2\right) \\ &\times \mathcal{B}H_\delta I^{\delta/2-1} I_*^{\delta/2-1} \, \mathrm{d}\sigma \, \mathrm{d}r \, \mathrm{d}R \, \mathrm{d}I_* \, \mathrm{d}c_* \, \mathrm{d}I \, \mathrm{d}c, \end{aligned}$$

after change of variable (A.1.3) term under integral yields

$$(c\cdot c')^2+(c\cdot c'_*)^2-(c\cdot c)^2-(c\cdot c_*)^2=\\ \frac{1}{2}(V_c\cdot u')^2+\frac{1}{2}(V_c\cdot u')(V_c\cdot u)+\frac{1}{8}(u\cdot u')^2-\frac{1}{2}(V_c\cdot u)^2-\frac{1}{2}(V_c\cdot u)|u|^2-\frac{1}{8}|u|^4.$$

Next, the form of cross section (A.1.5) allow to perform an integration with respect to V_c,

$$\mathcal{P}_{rtrt}=mKL_0^2\left(\frac{\pi kT}{m}\right)^{\frac{3}{2}}\frac{1}{4}\int_{\mathbb{R}^3\times[0,\infty)^2\times[0,1]^2\times S^2}e^{-\frac{1}{kT}\left(\frac{m}{4}|u|^2+I+I_*\right)}\\ \times\left(\frac{kT}{m}(|u'|^2-|u|)+\frac{1}{2}((u'u)^2-|u|^4)\right)\\ \times\tilde{B}H_\delta I^{\delta/2-1}I_*^{\delta/2-1}\,\mathrm{d}\sigma\,\mathrm{d}r\,\mathrm{d}R\,\mathrm{d}I_*\,\mathrm{d}I\,\mathrm{d}u.$$

Using relations (2.2.8) we can express

$$|u'|^2=\frac{4RE}{m}=R|u|^2+\frac{4R}{m}(I+I_*),$$

$$(u\cdot u')^2=\frac{4RE}{m}(u\cdot\sigma)^2=\left(R|u|^2+\frac{4R}{m}(I+I_*)\right)(u\cdot\sigma)^2,$$

after which we perform integration respect to σ, that yields

$$\mathcal{P}_{rtrt}=mKL_0^2\left(\frac{\pi kT}{m}\right)^{\frac{3}{2}}\pi\int_{\mathbb{R}^3\times[0,\infty)^2\times[0,1]^2}e^{-\frac{1}{kT}\left(\frac{m}{4}|u|^2+I+I_*\right)}\\ \times\left(\frac{kT}{m}(R-1)|u|^2+\frac{1}{2}\left(\frac{R}{3}-1\right)|u|^4+\frac{4R}{m}(I+I_*)\left(\frac{kT}{m}+\frac{1}{6}|u|^2\right)\right)\\ \times\tilde{B}\,H_\delta I^{\delta/2-1}I_*^{\delta/2-1}\,\mathrm{d}r\,\mathrm{d}R\,\mathrm{d}I_*\,\mathrm{d}I\,\mathrm{d}u.$$

Now we switch to spherical coordinates for the relative velocity u, and integrate with respect to r and R using the notation (A.1.6) for the constants coming up from this

integration,

$$\begin{aligned}
\mathcal{P}_{rtrt} &= mKL_0^2\left(\frac{\pi kT}{m}\right)^{\frac{3}{2}} 4\pi^2 \int_{[0,\infty)^3} e^{-\frac{1}{kT}\left(\frac{m}{4}y^2+I+I_*\right)} y^2 I^{\delta/2-1} I_*^{\delta/2-1} \\
&\times \left\{ -\frac{kT}{m} C_{\left(1,\frac{\zeta}{2},0\right)} y^{\zeta+2} + \frac{1}{2}\left(\frac{1}{3}C_{\left(0,\frac{\zeta}{2}+1,0\right)} - C_{\left(0,\frac{\zeta}{2},0\right)}\right) y^{\zeta+4} \right. \\
&+ \frac{4}{m} C_{\left(0,1+\frac{\zeta}{2},0\right)} \left(\frac{kT}{m}+\frac{1}{6}y^2\right)(I+I_*) y^{\zeta} \\
&+ \left(-\frac{kT}{m} C_{\left(\frac{\zeta}{2}+1,0,\frac{\zeta}{2}\right)} y^2 + \frac{1}{2}\left(\frac{1}{3}C_{\left(\frac{\zeta}{2},1,\frac{\zeta}{2}\right)} - C_{\left(\frac{\zeta}{2},0,\frac{\zeta}{2}\right)}\right) y^4\right) \\
&\times \left(\left(\frac{I}{m}\right)^{\frac{\zeta}{2}} + \left(\frac{I_*}{m}\right)^{\frac{\zeta}{2}}\right) \\
&+ \left. \frac{4}{m}\left(\frac{kT}{m}+\frac{1}{6}y^2\right) C_{\left(\frac{\zeta}{2},1,\frac{\zeta}{2}\right)} \left(\left(\frac{I}{m}\right)^{\frac{\zeta}{2}} + \left(\frac{I_*}{m}\right)^{\frac{\zeta}{2}}\right)(I+I_*) \right\} \mathrm{d}I_* \, \mathrm{d}I \, \mathrm{d}y.
\end{aligned}$$

Finally, performing the integration with respect to I, I_*, and y yields

$$\begin{aligned}
\mathcal{P}_{rtrt} = -K\frac{\rho^2}{m}\left(\frac{p}{\rho}\right)^{\frac{\zeta}{2}+2} \frac{2\sqrt{\pi}}{\Gamma\left(\frac{2\delta+\zeta+5}{2}\right)} \left\{ 9(4\delta+2\zeta+5)\pi\Gamma\left(\frac{\delta+\zeta}{2}\right)^2 \right. \\
\left. +2^{\zeta+2}\left(4\left(\frac{\delta}{2}-1\right)(\zeta+6)+\zeta(\zeta+12)+39\right)\Gamma\left(\frac{\delta}{2}\right)^2\Gamma\left(\frac{\zeta+3}{2}\right)\Gamma\left(\frac{\zeta+5}{2}\right)\right\}.
\end{aligned}$$

A.2 Computation of $\overline{Q}_i^{14}$

The parity arguments imply that $\mathcal{Q}_{in}$ vanishes unless $i = n$, which for the production term (A.0.5) implies

$$\overline{Q}_i^{14} = U_k \overline{P}_{ki}^{14} + \left(\frac{\delta+5}{2}\right)^{-1} \frac{\rho^2}{mp^3} q_i^{(tot)} \frac{1}{3}\mathcal{Q}_{rr}.$$

A.2.1 Computation of $\mathcal{Q}_{rr}$

We now compute the term

$$\begin{aligned}\mathcal{Q}_{rr} &= L_0^2 \int_{\mathbb{R}^6\times[0,\infty)^2\times[0,1]^2\times S^2} e^{-\frac{1}{kT}\left(\frac{m}{2}(|c|^2+|c_*|^2)+I+I_*\right)} \\ &\times \left(\frac{m}{2}|c|^2+I\right)\left\{\left(\frac{m}{2}|c'|^2+I'\right)c'\cdot c+\left(\frac{m}{2}|c'_*|^2+I'_*\right)c'_*\cdot c\right. \\ &- \left.\left(\frac{m}{2}|c|^2+I\right)|c|^2-\left(\frac{m}{2}|c_*|^2+I_*\right)c_*\cdot c\right\} \\ &\times \mathcal{B}H_\delta I^{\delta/2-1}I_*^{\delta/2-1}\,\mathrm{d}\sigma\,\mathrm{d}r\,\mathrm{d}R\,\mathrm{d}I_*\,\mathrm{d}c_*\,\mathrm{d}I\,\mathrm{d}c.\end{aligned}$$

Switching to the center-of-mass framework by means of the change of variables (A.1.3), the term under integral becomes

$$\begin{aligned}&\left(\left(\frac{m}{2}|c'|^2+I'\right)c'\cdot c+\left(\frac{m}{2}|c'_*|^2+I'_*\right)c'_*\cdot c\right. \\ &\qquad\left.-\left(\frac{m}{2}|c|^2+I\right)|c|^2-\left(\frac{m}{2}|c_*|^2+I_*\right)c_*\cdot c\right) \\ &= \frac{m}{2}(u'\cdot V_c)^2-\frac{m}{2}(u\cdot V_c)^2+\frac{m}{4}(u\cdot u')(u'\cdot V_c)-\frac{m}{4}(u\cdot V_c)|u|^2 \\ &\qquad+\frac{1}{2}(I'-I'_*)\left(u'\cdot V_c+\frac{1}{2}u\cdot u'\right)-\frac{1}{2}(I-I_*)\left(u\cdot V_c+\frac{1}{2}|u|^2\right).\end{aligned}$$

The form of the cross section (A.1.5) allows to first integrate with respect to V_c and σ,

$$\begin{aligned}\mathcal{Q}_{rr} &= KL_0^2\left(\frac{\pi kT}{m}\right)^{\frac{3}{2}}4\pi\int_{\mathbb{R}^3\times[0,\infty)^2\times[0,1]^2} e^{-\frac{1}{kT}\left(\frac{m}{4}|u|^2+I+I_*\right)} \\ &\times \left\{-\frac{1}{4}\left(\frac{5}{4}kT+\frac{m}{8}|u|^2+I\right)(I-I_*)|u|^2\right. \\ &+ \frac{mkT}{32}|u|^2\left(\left(\frac{5}{3}R-3\right)|u|^2+\frac{20R}{3m}(I+I_*)\right) \\ &+ \left.\left(\frac{1}{4}I+\frac{5}{16}kT\right)kT\left((R-1)|u|^2+\frac{4R}{m}(I+I_*)\right)\right\} \\ &\times \tilde{B}H_\delta I^{\delta/2-1}I_*^{\delta/2-1}\,\mathrm{d}r\,\mathrm{d}R\,\mathrm{d}I_*\,\mathrm{d}I\,\mathrm{d}u.\end{aligned}$$

Next, passing to the spherical coordinates for the relative velocity u, denoting $|u| = y$, and integrating with respect to R and r we obtain

$$\begin{aligned}
\mathcal{Q}_{rr} &= KL_0^2\left(\frac{\pi kT}{m}\right)^{\frac{3}{2}} 16\pi^2 \int_{[0,\infty)^3} e^{-\frac{1}{kT}\left(\frac{m}{4}y^2+I+I_*\right)} \\
&\times\ y^2\Bigg\{y^\zeta\Bigg[-\frac{1}{4}\left(\frac{5}{4}kT+\frac{m}{8}y^2+I\right)(I-I_*)y^2C_{\left(0,\frac{\zeta}{2},0\right)} \\
&+\ \frac{mkT}{32}y^4\left(\frac{5}{3}C_{\left(0,1+\frac{\zeta}{2},0\right)}-3C_{\left(0,\frac{\zeta}{2},0\right)}\right)-\left(\frac{1}{4}I+\frac{5}{16}kT\right)kTy^2C_{\left(1,\frac{\zeta}{2},0\right)} \\
&+\ \frac{4}{m}(I+I_*)C_{\left(0,\frac{\zeta}{2}+1,0\right)}\left(\frac{5}{96}mkTy^2+\left(\frac{1}{4}I+\frac{5}{16}kT\right)kT\right)\Bigg] \\
&+\ \left(\frac{1}{m}\right)^{\frac{\zeta}{2}}\left(I^{\frac{\zeta}{2}}+I_*^{\frac{\zeta}{2}}\right)\Bigg[-\frac{1}{4}\left(\frac{5}{4}kT+\frac{m}{8}y^2+I\right)(I-I_*)y^2C_{\left(\frac{\zeta}{2},0,\frac{\zeta}{2}\right)} \\
&+\ \frac{mkT}{32}y^4\left(\frac{5}{3}C_{\left(\frac{\zeta}{2},1,\frac{\zeta}{2}\right)}-3C_{\left(\frac{\zeta}{2},0,\frac{\zeta}{2}\right)}\right)-\left(\frac{1}{4}I+\frac{5}{16}kT\right)kTy^2C_{\left(\frac{\zeta}{2}+1,0,\frac{\zeta}{2}\right)} \\
&+\ \frac{4}{m}(I+I_*)C_{\left(\frac{\zeta}{2},1,\frac{\zeta}{2}\right)}\left(\frac{5}{96}mkTy^2+\left(\frac{1}{4}I+\frac{5}{16}kT\right)kT\right)\Bigg]\Bigg\} \\
&\times\ I^{\delta/2-1}I_*^{\delta/2-1}\,\mathrm{d}I_*\,\mathrm{d}I\,\mathrm{d}y,
\end{aligned}$$

where the constants are defined in (A.1.6). Finally, performing integration with respect to I, I_*, y yields

$$\begin{aligned}
\mathcal{Q}_{rr} = -K\rho^2\left(\frac{p}{\rho}\right)^{\frac{\zeta}{2}+3}&\frac{\sqrt{\pi}}{24\Gamma(\frac{2\delta+\zeta+5}{2})} \\
&\times\Bigg\{9((2\delta+\zeta-4)(2(2\delta+\zeta-4)+\zeta^2+38)+7\zeta^2+160)\pi\Gamma\left(\frac{\delta+\zeta}{2}\right)^2 \\
+2^{\zeta+5}((2\delta+\zeta-4)(\frac{3}{2}\delta+\zeta-3)&+\frac{57}{2}\delta+15\zeta+3)\Gamma\left(\frac{\delta}{2}\right)^2\Gamma\left(\frac{\zeta+3}{2}\right)\Gamma\left(\frac{\zeta+5}{2}\right)\Bigg\}.
\end{aligned}$$

Bibliography

[1] The National Institute of Standards and Technology (NIST), U.S. Department of Commerce. `https://webbook.nist.gov`. Accessed: 2022-06.

[2] A. Agrawal, H. M. Kushwaha, and R. S. Jadhav. *Burnett Equations: Derivation and Analysis*, pages 125–188. Springer International Publishing, Cham, 2020.

[3] M. Alnæs, J. Blechta, J. Hake, A. Johansson, B. Kehlet, A. Logg, C. Richardson, J. Ring, M. E. Rognes, and G. N. Wells. The fenics project version 1.5. *Archive of numerical software*, 3(100), 2015.

[4] R. Alonso and M. Čolić. Moment estimates for polyatomic Boltzmann equation with frozen collisions. `https://arxiv.org/abs/2502.08237`, 2025.

[5] F. Auricchio, F. Brezzi, and C. Lovadina. *Mixed Finite Element Methods*, chapter 9. John Wiley & Sons, Ltd, 2004.

[6] G. Bird. *Molecular Gas Dynamics and the Direct Simulation of Gas Flows*. Clarendon Press, 1994.

[7] C. Borgnakke and P. S. Larsen. Statistical collision model for Monte Carlo simulation of polyatomic gas mixture. *J. Comput. Phys.*, 18(4):405–420, 1975.

[8] J.-F. Bourgat, L. Desvillettes, P. Le Tallec, and B. Perthame. Microreversible collisions for polyatomic gases and Boltzmann's theorem. *European J. Mech. B Fluids*, 13(2):237–254, 1994.

[9] D. Bruno, M. Capitelli, C. Catalfamo, R. Celiberto, G. Colonna, P. Diomede, D. Giordano, C. Gorse, A. Laricchiuta, S. Longo, et al. Transport properties of high-temperature Mars-atmosphere components. *ESA Scientific Technical Review*, 256, 2008.

[10] J. Bunger, E. Christhuraj, A. Hanke, and T. Manuel. Structured derivation of moment equations and stable boundary conditions with an introduction to symmetric, trace-free tensors. *Kinet. Relat. Models*, 035, 2022.

[11] Z. Cai, Y. Fan, and R. Li. Hyperbolic model reduction for kinetic equations. In *Recent Advances in Industrial and Applied Mathematics*, pages 137–157, Cham, 2022. Springer International Publishing.

[12] C. Cercignani. *Ludwig Boltzmann: the man who trusted atoms*. Oxford University Press, 1998.

[13] S. Chapman and T. G. Cowling. *The mathematical theory of non-uniform gases. An account of the kinetic theory of viscosity, thermal conduction and diffusion in gases*. Cambridge University Press, London, 1970. Third edition, prepared in co-operation with D. Burnett.

[14] M. S. Cramer. Numerical estimates for the bulk viscosity of ideal gases. *Phys. Fluids*, 24:066102, 2012.

[15] L. Desvillettes. Sur un modèle de type Borgnakke–Larsen conduisant à des lois d'energie non-linéaires en température pour les gaz parfaits polyatomiques. *Ann. Fac. Sci. Toulouse Math.*, 6(0):257–262, 1997.

[16] V. Djordjić, M. Pavić-Čolić, and M. Torrilhon. Explicit evaluation of the polyatomic Boltzmann collision operator. *GitHub*, `/Boltzmann-polyatomic/Supplements2021`, 2021.

[17] V. Djordjić, M. Pavić-Čolić, and M. Torrilhon. Evaluation of the polyatomic Boltzmann collision operator and comparison with experimental data for N_2,O_2,NO, CO,H_2. `https://notebookarchive.org/2025-02-54nhkri`, 2025.

[18] V. Djordjić, M. Pavić-Čolić, and N. Spasojević. Polytropic gas modelling at kinetic and macroscopic levels. *Kinet. Relat. Models*, 14(3):483–522, 2021.

[19] V. Djordjić, M. Pavić-Čolić, and M. Torrilhon. Consistent, Explicit and Accessible Boltzmann Collision Operator for Polyatomic Gases. *Phys. Rev. E*, 104:025309, 2021.

[20] V. Djordjić, M. Pavić-Čolić, and M. Torrilhon. FenicsR17. `https://git.rwth-aachen.de/vladimirdjordjic19/fenicsr17`, 2025.

[21] V. Djordjić, M. Oblapenko, Georgii Pavić-Čolić, and M. Torrilhon. Boltzmann collision operator for polyatomic gases in agreement with experimental data and dsmc method. *Continuum Mech. Thermodyn.*, 35:103–119, 2023.

[22] V. Djordjić, M. Pavić-Čolić, and M. Torrilhon. 14- and 17-moment systems for polytropic gases - comparison regarding transport coefficients. *AIP Conf. Proc.*, 2996(1):040011, 2024.

[23] I. M. Gamba and M. Pavić-Čolić. On the Cauchy problem for Boltzmann equation modeling a polyatomic gas. *J. Math. Phys.*, 64(1):013303, 01 2023.

[24] C. Geuzaine and J.-F. Remacle. Gmsh: A 3-D finite element mesh generator with built-in pre- and post-processing facilities. *Int. J. Numer. Methods Eng.*, 79(11):1309–1331, 2009.

[25] H. Grad. On the kinetic theory of rarefied gases. *Commun. Pure Appl. Math.*, 2(4):331–407, 1949.

[26] M. L. Huber, A. H. Harvey, et al. Thermal conductivity of gases. *CRC Handbook of Chemistry and Physics*, 92, 2011.

[27] S. Kosuge, H.-W. Kuo, and K. Aoki. A kinetic model for a polyatomic gas with temperature-dependent specific heats and its application to shock-wave structure. *J. Stat. Phys.*, 177(2):209–251, 2019.

[28] A. Logg, K.-A. Mardal, and G. Wells. *Automated solution of differential equations by the finite element method: The FEniCS book*, volume 84. Springer Science & Business Media, 2012.

[29] E. Nagnibeda and E. Kustova. *Non-equilibrium reacting gas flows*. Heat and Mass Transfer. Springer-Verlag, Berlin, 2009.

[30] M. Pavić. Mathematical modelling and analysis of polyatomic gases and mixtures in the context of kinetic theory of gases and fluid mechanics. *Hal Theses*, 2014.

[31] M. Pavić, T. Ruggeri, and S. Simić. Maximum entropy principle for rarefied polyatomic gases. *Phys. A*, 392(6):1302–1317, 2013.

[32] M. Pavić-Čolić and S. Simić. Kinetic description of polyatomic gases with temperature-dependent specific heats. *Physical Review Fluids*, 7:083401, 2022.

[33] M. Pavić-Čolić and S. Simić. Moment equations for polyatomic gases. *Acta Appl. Math.*, 132:469–482, 2014.

[34] B. Rahimi and H. Struchtrup. Capturing non-equilibrium phenomena in rarefied polyatomic gases: A high-order macroscopic model. *Phys. Fluids*, 26(5):052001, 2014.

[35] B. Rahimi and H. Struchtrup. Macroscopic and kinetic modelling of rarefied polyatomic gases. *J. Fluid Mech.*, 806:437–505, 2016.

[36] P. Rosenau. Extending hydrodynamics via the regularization of the Chapman-Enskog expansion. *Phys. Rev. A*, 40:7193–7196, Dec 1989.

[37] T. Ruggeri and M. Sugiyama. *Rational Extended Thermodynamics Beyond the Monatomic Gas*. Springer, Cham, 2015.

[38] T. Ruggeri and M. Sugiyama. *Classical and relativistic rational extended thermodynamics of gases*. Springer, 2021.

[39] H. Song, S. Singh, and M. Torrilhon. Non-equilibrium flow simulations based on Grad-14 and Grad-17 moment equations for polytropic gases. *Phys. Fluids.*, 37(3):036140, 03 2025.

[40] H. Struchtrup. Derivation of 13 moment equations for rarefied gas flow to second order accuracy for arbitrary interaction potentials. *Multiscale Modeling & Simulation*, 3(1):221–243, 2005.

[41] H. Struchtrup. *Macroscopic Transport Equations for Rarefied Gas Flows*. Interaction of Mechanics and Mathematics. Springer, Berlin, 2005.

[42] H. Struchtrup and M. Torrilhon. Regularization of Grad's 13 moment equations: Derivation and linear analysis. *Phys. Fluids*, 15(9):2668–2680, 2003.

[43] L. Theisen and M. Torrilhon. FenicsR13: A Tensorial Mixed Finite Element Solver for the Linear R13 Equations Using the FEniCS Computing Platform. *ACM Trans. Math. Softw.*, 47(2), apr 2021.

[44] D. van der Woude, E. van Brummelen, E. Arlemark, and M. Abdelmalik. A φ-divergence based finite element moment method for the polyatomic ES-BGK Boltzmann equation. *J. Comput. Phys.*, 503:112813, 2024.

[45] C. Villani. Chapter 2a - general presentation. volume 1 of *Handbook of Mathematical Fluid Dynamics*, pages 75–139. North-Holland, 2002.

[46] A. Westerkamp and M. Torrilhon. Curvature-induced instability of a Stokes-like problem with non-standard boundary conditions. *Appl. Numer. Math.*, 121:96–114, 2017.

[47] L. C. Woods. Mathematical theory of transport processes in gases. *J. Fluid Mech.*, 61(4):823–825, 1973.

Typeset December 19, 2025